POR-2239(EX)
(WT-2239)(EX)
EXTRACTED VERSION

OPERATION SUN BEAM, SHOT SMALL BOY

Project Officer's Report—Project 7.1.4

Transient Radiation Effects Measurements on Guidance System Circuits

P. J. Sykes, Jr., Project Officer
Air Force Systems Command
Kirtland AFB, NM

20 April 1964

NOTICE:
This is an extract of POR-2239 (WT-2239), Operation SUN BEAM, Shot Small Boy, Project 7.1.4.

Extracted version prepared for
Director
DEFENSE NUCLEAR AGENCY
Washington, DC 20305-1000

1 September 1985

Destroy this report when it is no longer needed. Do not return to sender.

PLEASE NOTIFY THE DEFENSE NUCLEAR AGENCY, ATTN: STTI, WASHINGTON, DC 20305-1000, IF YOUR ADDRESS IS INCORRECT, IF YOU WISH IT DELETED FROM THE DISTRIBUTION LIST, OR IF THE ADDRESSEE IS NO LONGER EMPLOYED BY YOUR ORGANIZATION.

AD-A955 211

REPORT DOCUMENTATION PAGE

1a REPORT SECURITY CLASSIFICATION UNCLASSIFIED	1b RESTRICTIVE MARKINGS
2a SECURITY CLASSIFICATION AUTHORITY N/A since Unclassified	3 DISTRIBUTION/AVAILABILITY OF REPORT Approved for public release; distribution is unlimited.
2b DECLASSIFICATION/DOWNGRADING SCHEDULE N/A since Unclassified	
4 PERFORMING ORGANIZATION REPORT NUMBER(S)	5 MONITORING ORGANIZATION REPORT NUMBER(S) POR-2239(EX) (WT-2239)(EX)
6a NAME OF PERFORMING ORGANIZATION Air Force Special Weapons Center Air Force Systems Command 6b OFFICE SYMBOL (If applicable)	7a NAME OF MONITORING ORGANIZATION Defense Atomic Support Agency
6c ADDRESS (City, State, and ZIP Code) Kirtland AFB, NM	7b ADDRESS (City, State, and ZIP Code) Washington, DC
8a NAME OF FUNDING/SPONSORING ORGANIZATION 8b OFFICE SYMBOL (If applicable)	9 PROCUREMENT INSTRUMENT IDENTIFICATION NUMBER
8c ADDRESS (City, State, and ZIP Code)	10 SOURCE OF FUNDING NUMBERS PROGRAM ELEMENT NO / PROJECT NO / TASK NO. / WORK UNIT ACCESSION NO

11 TITLE (Include Security Classification) OPERATION SUN BEAM, SHOT SMALL BOY, Project Officer's Report—Project 7.1.4, Transient Radiation Effects Measurements on Guidance System Circuits, Extracted Version

12 PERSONAL AUTHOR(S)
P. J. Sykes, Jr.

13a TYPE OF REPORT	13b TIME COVERED FROM ____ TO ____	14 DATE OF REPORT (Year, Month, Day)	15 PAGE COUNT
		640420	117

16 SUPPLEMENTARY NOTATION This report has had sensitive military information removed in order to provide an unclassified version for unlimited distribution. The work was performed by the Defense Nuclear Agency in support of the DoD Nuclear Test Personnel Review Program.

17 COSATI CODES			18 SUBJECT TERMS (Continue on reverse if necessary and identify by block number)	
FIELD	GROUP	SUB-GROUP		
18	3		Sun Beam	Guidance Systems
18	6		Small Boy	Dosimetry
			Radiation Effects	Electromagnetic Shielding

19 ABSTRACT (Continue on reverse if necessary and identify by block number)

This project was conducted to obtain data on the transient response of typical ballistic missile guidance and control systems to the prompt gamma pulse from a nuclear weapon. Self-reading instrumentation was installed at four stations corresponding to four decades of gamma radiation intensity to determine whether the output transients in these circuits exceeded preset threshold levels during the test. Additional diagnostic instrumentation was provided at one location to obtain pulse shape information on the circuits, gamma dose rate time history, and analog data on circuits which exhibited long recovery times. Extensive pre-and post-shot laboratory experiments were performed to determine response in an actual weapon environment.

Results indicated that field test data are consistent with the combined experimental and theoretical predictions.

20 DISTRIBUTION/AVAILABILITY OF ABSTRACT	21 ABSTRACT SECURITY CLASSIFICATION
☒ UNCLASSIFIED/UNLIMITED ☐ SAME AS RPT ☐ DTIC USERS	UNCLASSIFIED
22a NAME OF RESPONSIBLE INDIVIDUAL MARK D. FLOHR	22b TELEPHONE (Include Area Code) 202-325-7559
	22c OFFICE SYMBOL DNA/ISCM

DD FORM 1473, 84 MAR 83 APR edition may be used until exhausted
All other editions are obsolete

OPERATION SUN BEAM

SHOT SMALL BOY

PROJECT OFFICERS REPORT — PROJECT 7.1.4

TRANSIENT RADIATION EFFECTS MEASUREMENTS ON GUIDANCE SYSTEM CIRCUITS

Paul J. Sykes, Jr., T/Sgt, USAF
Project Officer

Research Directorate
Air Force Special Weapons Center
Air Force Systems Command
Kirtland Air Force Base
New Mexico

FOREWORD

Classified material has been removed in order to make the information available on an unclassified, open publication basis, to any interested parties. The effort to declassify this report has been accomplished specifically to support the Department of Defense Nuclear Test Personnel Review (NTPR) Program. The objective is to facilitate studies of the low levels of radiation received by some individuals during the atmospheric nuclear test program by making as much information as possible available to all interested parties.

The material which has been deleted is either currently classified as Restricted Data or Formerly Restricted Data under the provisions of the Atomic Energy Act of 1954 (as amended), or is National Security Information, or has been determined to be critical military information which could reveal system or equipment vulnerabilities and is, therefore, not appropriate for open publication.

The Defense Nuclear Agency (DNA) believes that though all classified material has been deleted, the report accurately portrays the contents of the original. DNA also believes that the deleted material is of little or no significance to studies into the amounts, or types, of radiation received by any individuals during the atmospheric nuclear test program.

ABSTRACT

Project 7.1.4 Small Boy of Operation Sunbeam was conducted to obtain data on the transient response of typical ballistic missile guidance and control systems to the prompt gamma pulse from a nuclear weapon. Self-reading instrumentation was installed at four stations, corresponding to four decades of gamma radiation intensity, to determine whether the output transients in these circuits exceeded preset threshold levels during the test. Additional diagnostic instrumentation was provided at one location to obtain pulse shape information on the circuits, gamma dose rate time history, and analog data on circuits which exhibited long recovery times. Extensive pre-and post-shot laboratory experiments were performed to determine response dynamic ranges and to ascertain the validity of simulation testing for predicting circuit response in an actual weapon environment.

The results of the Small Boy experiment on the five guidance and control circuits and the failure criteria (as established by the manufacturers) are:

These results indicate that field test data are consistent with the combined experimental and theoretical predictions. The extensive pre-and post-laboratory simulation testing conducted by Northrop Ventura, and the circuit response predictions performed by both Boeing and Hughes have supported the validity of the field test results.

PREFACE

This report was prepared by Northrop Corporation, Northrop Ventura Division, under Air Force Special Weapons Center contract AF 29(601)-5214, "Operation **Sun Beam, Shot Small Boy**, Project 7.1.4, Transient Radiation Effects Measurements—Guidance **System Circuits (U)**". The principal contractor personnel who conducted and/or reported the work described herein were: D. A. Hicks, W. E. Crandall, T. M. Hallman, M. S. George, R. G. Saelens, J. Raymond, A. A. O'Dell, L. Malcolm, D. Welch and W. Parker.

The AFSWC Project Officer from February 1962 through August 1962 was Capt. Donald C. Glenn, USAF, and from September 1962 through completion was TSgt. Paul J. Sykes, Jr., USAF, both of the Physics Division, Research Directorate. The Ballistic Systems Division Project Officer was Capt. Kenneth L. Gilbert, USAF, Special Projects Office, Directorate of Guidance and Control.

The contract was formally initiated on 12 March 1962. **The Small Boy** event took place on 14 July 1962 at the Nevada Test Site. The Project Officers Interim Report, POIR-2239, was published in November 1962. Research terminated on 5 March 1963 with the submission of this final report.

Acknowledgement is made of the cooperation and assistance by the following personnel and companies who provided expert advice and/or test sample circuits to the program: W. H. Duerig and Paul Gianas, Kearfott Division, General Precision, Inc.; W. Birnbaum, Max Lawrence and Murray Liss, ARMA Division, American Bosch ARMA Corporation; W. A. Bohan and S. Sedore, Space Guidance Center, Federal Systems Division, International Business Machines Corporation; T. D. Hanscome and J. E. Bell, Ground Systems Group, Hughes Aircraft Company; W. D. Miller, Remington Rand-Univac Division, Sperry Rand Corporation. Particular recognition is due Dr. G. L. Keister and his staff of the Nuclear and Space Physics Department, Aero-Space Division, The Boeing Company; Mr. J. E. Bell and his staff of the Nucleonics Department, Ground Systems Group, Hughes Aircraft Company; and to Dr. V. A. J. Van Lint of the John Jay Hopkins Laboratory, General Atomic Division of General Dynamics Corporation, for their independently-conducted laboratory pulsed-radiation tests and response-predictive analyses of the test circuits exposed by Northrop Ventura at the **Small Boy event.** Test results, circuit analyses and discussions provided by those personnel to the Northrop Ventura staff were invaluable in interpreting and correlating the field results and in producing this final Project Officers Report.

CONTENTS

TABLES

FIGURES

CHAPTER 1

INTRODUCTION

1.1 OBJECTIVE

The objective of this project was to determine the response of typical guidance and control circuits to transients induced by the prompt nuclear radiation pulse from a nuclear detonation. A second objective was to measure and correlate circuit responses to the weapon prompt gamma pulse with those obtained using laboratory pulse radiation facilities (flash X-rays, linacs and pulse reactors).

1.2 BACKGROUND

This experimental project was initiated because the Air Force Ballistic Systems Division required that all guidance systems under development for ballistic systems must survive the transients induced by a peak gamma rate of from a nuclear weapon. The purpose of this project was to determine the threshold of transient effects on basic electronic components and circuits contained in typical ballistic missile systems. Threshold data could then be correlated with circuit transient analysis and laboratory experimental programs.

A peak gamma dose rate of can be achieved with laboratory devices such as flash X-ray systems, linear accelerators, and pulsed reactors. However, these devices cannot simultaneously duplicate the entire time history and energy spectrum of the prompt gamma weapon pulse. Until this program was initiated, no detailed experimental data were available on the effects of actual weapon nuclear radiation environments upon electronic components and circuits.

The guidance system circuits and components selected for testing under this project are contained in one or more of: the General Precision/Kearfott stellar inertial guidance system control unit; the General Motors-A/C Sparkplug guidance computer; the Remington Rand/Univac thin film memory unit for the advanced Titan system; and the GAR-2A and GAR-4A guidance and control systems. The selected guidance systems can be operated from sea level to approximately 100,000 feet altitude. Performance of this experiment on the earth's surface was valid because the prompt gamma pulse shape in the region of the peak dose rate is not appreciably changed by the presence of the atmosphere.

The Air Force (through the Air Force Special Weapons Center) has conducted a growing program to investigate and predict the effects of pulse nuclear radiation on electronic systems and components. Currently AFSWC has the following agencies under continuing contract to investigate the problem: The Boeing Company, Hughes Aircraft Company, General Atomic, and International Business Machines Corporation (IBM). The investigations of these agencies are directed at (1) understanding the basic mechanisms and phenomena of these effects, (2) developing both analog and high-speed automated digital computer techniques to predict the pulse radiation thresholds for vulnerability of electronic systems and components, and (3) providing techniques for designing electronic systems hardened against transient radiation effects.

1.3 THEORY

Gamma or X-radiation incident on an electronic circuit produces excess charge carriers in circuit components and in the surrounding media. The main processes are due to the Compton and photoelectric effects, which produce energetic secondary electrons in and around the irradiated material. Some of the energetic secondaries escape from the irradiated device and in turn some of the energetic secondaries produced in the surrounding media are incident on the device. Thus, the net carrier injection in an irradiated material is the sum of these processes.

The effectiveness (atomic cross section) of the Compton process is a broadly peaked function of photon energy (with its maximum at about 500 kev) and is a linear function of the atomic number of the absorber. The effectiveness of the photoelectric process changes inversely as the photon energy (to some power greater than unity) and increases approximately as the fifth power of the atomic number of the absorber. Thus, the overall photoelectric energy transfer from the photons to the material is greatest at low energies and in materials with large atomic number.

Competing with the charge carrier production are the processes of recombination, trapping, and removal at electrodes connected to the component irradiated. If the injection occurs in a time short compared with the times characteristic of these removal processes, the device will in general exhibit a response proportional to the dose delivered during the injection pulse. If the injection occurs over a time span long compared with the characteristic removal times, the device will achieve a dynamic equilibrium condition, with conductivity increased by an amount

proportional to radiation rate and inversely proportional to carrier removal rate. The responses of devices in cases intermediate to these extremes will depend markedly on the detailed time history of the injecting pulse of radiation, as well as on the characteristics of the particular device. Obviously, these cases are over-simplifications for any real device, but are often useful criteria for classifying responses as "dose" or "dose-rate" dependent in the extreme cases. The combined phenomena are properly termed photoconductivity.

Although capacitors, resistors, vacuum tubes, cables, and other electronic components are affected by gamma irradiation, the largest transient effects generally occur in semiconductor devices.

Most dielectric materials have low atomic number, and the carrier mobilities are low, so that photocurrents per unit dose rate are quite small. Nevertheless, the relative changes in conductivity may be large and may persist for long times because of trapping and polarization. Effects in resistor materials and metals are not as comparably important because of the very short recombination times and large initial carrier densities, even though injection efficiency and carrier mobility are large. Shunt leakage paths are probably the most important factor for large value resistors. In semiconductor materials, on the other hand, carrier injection is efficient, carrier mobilities are large, and recombination is relatively slow. Small minority carrier density changes may produce large changes in the operation of diodes and transistors, and trapping of majority carriers are not allowed to flow off through a low-impedance external circuit.

Although the exchange of energetic secondary electrons with the surroundings was mentioned above as part of the injection process, it should be noted that this is an especially difficult part of the radiation problem to analyze since it depends in a complex manner on environment, sample size, and geometry, as well as on the nature of the incident radiation. It is probable that the main effects in vacuum tubes are due to secondary emission currents.

Neutrons produce permanent changes in electrical and mechanical properties of materials as well as causing ionization, although the latter is appreciable only in materials with low atomic number. Since the main concern in this project was with effects of gamma radiation, neutron effects will not be discussed here except to note that reduction of the integrated flux to less than 10^{11} nvt by proper shielding should prevent significant permanent damage to most, if not all, electronic components.

1.4 DESIGN OF EXPERIMENT

Assuming a (fission) device detonated 10 feet above ground, circuit test locations were selected for dose rates of approximately However, Small Boy was later changed, after the instrumentation pads were installed, to a device of approximately yield. New estimates of the nuclear environment predicted at the station locations were obtained from Major Byron H. Shields, Program 7 Director, and were based on Los Alamos Scientific Laboratory (LASL) predictions for the device as calculated by the Biophysics Division of the Research Directorate, AFSWC.

The burst was treated as a surface detonation for both blast and thermal calculations, since the burst was only ten feet above ground level. In Reference 1 it was estimated that the total thermal radiation could be calculated from the following equation:

$$Q = \frac{2.6 \times 10^{11} \text{Cal/kt} \times \text{yield in kt}}{1.168 \times 10^{4} \text{ cm}^2/\text{ft}^2 \times R^2} \qquad (1.1)$$

$Q =$

Where: Q = thermal exposure, cal/sec

The times of air shock arrival and peak overpressure versus distance were derived by Sachs scaling of the surface burst curves given in Reference 2 to a yield of and to an altitude of 4200 feet (NASA standard atmosphere).

Estimates of the electric and magnetic fields used in subsequent calculations in this Chapter are taken from Reference 3.

For a nuclear weapon, the radius of the ionized region, a, producing the electromagnetic pulse was estimated from the relation

$$W = 4.55 \times 10^{-5} \; a \exp \left\{ 25 \left[1 - \exp (-0.1254a) \right] \right\} \qquad (1.2)$$

Where: W = yield Mt

a = effective radius, kilometers.

For the Small Boy event, a was approximately feet. At distances less than it was expected that there might be large electric fields of sufficient size to produce electrical breakdown in the ionized air. The electric fields for distances outside this region were estimated from the following equations:

$$E_{max} = \frac{3000\ a}{R}\left[1 - \frac{(a)^2}{R} + \frac{(a)^4}{R}\right]^{\frac{1}{2}} \quad (1.3)$$

Where:

E_{max} = peak electric field, volts/meter

a = effective radius, feet

R = distance, feet

Low-frequency magnetic fields could not be predicted reliably. The maximum value for the high-frequency horizontal component was estimated from the equation:

$$H_{\phi} = \left[100\ \frac{W}{R^2}\ \text{exp.}\ (-2.5R)\right]^{0.43} \quad (1.4)$$

Where:

H_{ϕ} = horizontal component, oersteds

R = distance, kilometers

W = yield, **Mt**

The maximum rate of change of the magnetic field was estimated from the relationship:

$$\frac{dH_{Max}}{dt} = 10^6\ H_{max} \quad (1.5)$$

Where:

H_{max} = magnetic field

t = time, seconds

Fallout doses were estimated using TM-23-200 (Reference 4). The ground shock parameters were taken from Brode's report (Reference 5) on protective construction.

Table 1.1 summarizes the predicted environment at each station location.

The blooper and diagnostic stations on this equipment were designed to reduce all associated weapon environments such as thermal, blast and EMP, to below damage-threshold levels for the circuits and instrumentation involved.

Thin aluminum fallout covers were installed at each pad to minimize contamination of the package between H-hour and recovery time. Each diagnostic and blooper package was placed in a 1/4-inch-thick steel box to prevent damage from blast and over-

pressure and minimize EMP effects.

The instrumentation sections of each package were shielded with lead and borated polyethylene to reduce the neutron and gamma flux below threshold levels as discussed in Section 2.3.1.

1.5 ELECTROMAGNETIC SHIELDING

Although precise methods for designing and evaluating the effectiveness of shielding configurations for a transient incident electromagnetic wave are not available, it is possible to justify the reliance on a simple, closed, conducting box for electromagnetic shielding of the test specimens in nuclear device environments of the type considered here. The high-frequency components, both magnetic and electric, are effectively shielded out by a conducting box because the penetration depth (skin depth) is small compared to the wall thickness of the box. In fact, for an iron box ¼ inch thick, the penetration is small for all frequencies above the audio-frequency range. Electric field components at frequencies below this range also should not penetrate (an application of Gauss's theorem); this is especially important in the present case because of the large electric-field values predicted. Very low frequency magnetic fields will not be excluded by a box of the type mentioned above. However, the predicted values for such low-frequency components of magnetic field are small, and as long as no devices especially sensitive to magnetic fields are used, these field components should not cause any difficulty.

page 19 deleted.

CHAPTER 2

PROCEDURE

2.1 TEST SPECIMENS

2.1.1 Guidance and Control Circuits. The five guidance and control circuits selected by the AFSC Ballistic Systems Division for Project 7.1.4 were:

a. IBM Logic Circuit. Used in the General Motors/A.C. guidance computer.

b. Transistor Pre-Pre-Amplifier. Used in the General Precision/Kearfott stellar-inertial guidance unit.

c. Diode Detector Circuit. Typical of circuits used in the GAR-2A and GAR-4A.

d. Azimuth Network. Used for control loop compensation in the General Precision/Kearfott stellar-inertial guidance unit.

e. Miniature Flip-Flop. An American-Bosch-Arma design used in the General Precision/Kearfott guidance computer.

In addition to these five circuits a Remington Rand-Univac Thin Film Memory Unit was exposed to a dose rate of approximately

2.1.2 Remington Rand-Univac Thin Film Memory Unit. A Remington Rand-Univac self-contained package containing a thin film memory unit, with associated monitoring circuitry, was installed at the 4,800-foot pad. A similar memory unit had previously been tested in laboratory simulation experiments, without effects. None of the semiconductor circuitry had been included in the previous laboratory experiments. The package for the Small Boy experiment included semiconductor circuitry, so that (1) the film memory could be tested under actual weapon environments for correlation with laboratory results, and (2) the principles of circuit design for radiation hardening could be evaluated from the results of the performance of the semiconductor circuitry.

The previous laboratory tests mentioned above on Destructive Read Out (DRO) and Non-Destructive Read Out (NDRO) memory tapes, were conducted at the Sandia Pulsed Reactor Facility (SPRF) and at the Ground Test Reactor (GTR) of the USAF Nuclear Aerospace Research Facility (NARF) maintained by General Dynamics/Fort Worth at Fort Worth, Texas.

2.1.3 Expected Circuit Response. Table 2.1 indicates the location of each test specimen for the Small Boy event. Based on test circuit responses during pre-field test laboratory experimentation, the expected circuit response for the Small Boy nuclear environment is given in Table 2.2. The pre-field test experimentation is discussed in the Appendix.

2.2 INSTRUMENTATION

2.2.1 Blooper Stations. Fast pulse measurement of the selected guidance and control circuits on an economically feasible basis required that special instrumentation be developed. The measurement concept required a multichannel system, completely self-contained, which could detect low-level voltage transients produced by pulse gamma radiation in the circuits under test. A permanent record of the transient was necessary because of the access time limitations after the test. Voltage-level sensing on a threshold basis was determined to be the most practical method of detection. The threshold detection system would enable a single channel to detect a transient whose amplitude was equal to or greater than a preset level, or a multichannel arrangement to bracket the transient amplitude within specified limits (300 mv to 8.0 v). To achieve uniform results the channel sensitivity should be almost independent of pulse width.

The blooper channels were required to detect voltage transients from test circuits or components for which output impedances can vary widely between different types. Therefore the first stage of detection was designed to have a high impedance to prevent loading on the test circuits, and a low-output impedance to drive the following detection circuits through a coaxial cable without loss of fidelity. Since the system was battery powered, emitter followers (Figure 2.1) were used for the low-output impedance test circuits, and cathode followers (Figure 2.2) were used only for the high-impedance diode-detector test circuit. Triaxial cable was used between the test-circuit outputs and isolation-circuit inputs. Because the conventional connection of the triax caused unstable operation of the emitter followers, the triax was used with the inner shield floating and connected as a coaxial cable. This eliminated the emitter follower stability problem.

To assure uniform channel sensitivity over a wide range of input pulse widths, pulse-stretching circuits (Figure 2.3) were used. These circuits preserved the voltage level of the input pulse while increasing the pulse width to a minimum of 10 μ sec for input pulses as narrow as 100 ns. The wide-output pulse assured dependable triggering of the threshold detectors. The schematic for the threshold detector is shown in Figure 2.4. When the input pulse exceeded a preset level, regeneration occurred within the comparator circuit which turned on the dynaquad latching

circuit. The dynaquad then blew the fuse. Fuse readout elements were chosen because of their absolute irreversibility.

In a typical blooper channel the minimum detectable pulse was about 300 mv, with almost uniform response for pulse widths of 100 ns or greater. For a 50-ns pulse the sensitivity was typically lower by a factor of two.

Additional circuitry was provided to insure proper sequencing of power application and to protect the dynaquad fuse circuits against false signals after the shot. These are shown in Figures 2.5 and 2.6. The schematics for the Small Boy instrumentation programmer and test circuit programmer are shown in Figures 2.7 and 2.8. The overall blooper instrumentation block diagram is shown in Figure 2.9.

To provide some correlation of the Small Boy event data with data obtained in the Little Feller II event, two blooper packages (Figure 2.10) which had been exposed in the earlier Little Feller II event were installed at the 5,700- and 7,500-foot stations. These packages were similar to the Small Boy packages, except that the test specimens were individual transistors and diodes rather than complete guidance and control circuits. Special circuits were designed around these transistors and diodes to provide operating biases and impedance isolation. The circuits (Figures 2.11 and 2.12) were well-shielded and only the specific transistor or diode test specimen was exposed to significant levels of prompt gamma radiation. These packages contained only six monitoring channels. The samples exposed to radiation in these two packages were 2N2187-PNP silicon transistors, 2N705-PNP germanium transistors, NS480 NPN silicon transistors, 1N457 silicon diodes and NS382 silicon logic diodes.

2.2.2 Remington Rand Experiment. The Remington Rand-Univac package is shown in Figures 2.13 and 2.14. The drive circuits for the two memories (DRO and NDRO), the memories themselves, the sense amplifiers, and a readout register were located above ground in the radiation field. The timing circuits, clock and control circuits, address register and counter, error check device, and a logic matrix for control of the error check device were located below ground in a magnetic- and radiation-shielded well. Design for the well and shielding was the same as that used in the blooper packages.

Error detection was accomplished by blowing fuses connected to appropriate test points, such as the outputs of the current generators, the diverters, the sense amplifiers, and the readout register.

Each fuse blown corresponded to a point of failure in the system. Moreover, the pattern of fuses blown in the array served as a

check on the source of failure in the system. For example, the fuse corresponding to current generator output blew if the output was too low. Too low an output would fail to switch the films at the address being interrogated and would, therefore, also cause the fuses corresponding to the bits in the address to blow, thus pinpointing the current generator as the source of failure and the cause as loss of gain in the generator transistors. In essence, any drive-circuit failure was shown as a failure of all the driven-bit positions in an address, plus a driving-point failure. Any sense-circuit failure was shown as an individual bit-position failure plus an output-point failure.

All circuits to be tested were potted in building-block form and assembled into standard modules. There were two modules, plus the memory pack, above ground. A third module, together with several printed circuit cards and the fuse board, was in the well. The entire system was battery-powered with power turn-on via mechanical timer prior to shot time. The battery pack and timer were also located above ground with the test device.

The circuits in the test system above ground included: (1) Diverter Driver, (2) Diverter, (3) Current Generator, (4) DRO Magnetic Film Memory, (5) NDRO Magnetic Film Memory, (6) Bit Driver, (7) Sense Amplifier, (8) Strobe, (9) Readout Register.

The circuits in the underground control and error checking system included: (1) Clock, (2) Timing, (3) Counter, (4) Address Register, (5) Error Logic Matrix, (6) Error Indicator.

The clock rate was 330 kc. There were two addresses in each memory, with four bits in each address. Each cycle of the clock read out one address of four bits, and cycles were alternated between memories.

The addresses not used for readout were located with information for a static information "disturb" test.

Physically, the radiation test unit was a small memory using advanced digital development (ADD) circuits and magnetic film memory planes plus control and complete error-checking circuitry. The unit was assembled specifically for testing a magnetic film memory and associated circuits for performance in a weapon nuclear radiation environment.

The device contained both a DRO and an NDRO film memory plane. In each memory plane, two four-bit words were operated at a cycle time of 3.5 μ sec. Two "zeros" and two "ones" were stored in each word. The words were interrogated sequentially, alternating from NDRO to DRO, and the output from each bit of

each word was checked for errors. Certain circuits were checked for proper operation.

Included in the memory stack were four NDRO planes which were not operated but contained a preloaded pattern. The contents of these planes were checked in the laboratory after the test was completed.

The unit was divided into four modules as shown by the dotted lines on the block diagram, Figure 2.15. Figure 2.13 shows the physical location of the various modules. The control module was located below ground, shielded from radiation. Not shown on the block diagram is a mechanical timer for turning the unit on and off, and a battery power pack.

Control module circuits included an oscillator, one-shot multivibrators, and inverters. These made up a two-bit counter to provide the memory address, and a timing chain to supply all necessary timing signals. The control modules, which also contained all the circuits used for error checking and indication, are described later.

The word-selection module contained two current generators — one for each memory plane — controlled by the low-order bit of the address register, and two diverters controlled by the high-order bit. These circuits drove a 2 x 2 diode tape-core matrix which supplied current to the selected word.

In the memory stack, the components for the 2 x 2 diode tape-core matrix were located on one end of the memory planes. The magnetic film memory elements and the associated drive and sense conductors made up the remainder of the memory plane. The planes were wired together and installed within a magnetic shield.

In the sense amplifier module, the four sense lines used in each memory plane were connected to four sense amplifiers. Each amplifier had two inputs — one NDRO and one DRO. Each amplifier output set a flip-flop in the readout register if a "one" was read. The two DRO bit drivers located in this module were used for restoring the "ones" in the DRO "one" bit lines. This module also contained several extra sensing circuits whose operation was checked with dummy input signals.

In the error indication circuits, the outputs from the four active bits of the readout register were compared to that expected from the memory. If any flip-flop was not in the proper state, an error signal was generated. This signal turned on one or more transistors on the error side of the transformer diode matrix shown in Figure 2.14. One of the transistors on the address side of the matrix was also turned on, corresponding to the state of the address register. Thus, sixteen intersections

of the matrix each represent a film element in the memory. Should a film element be read incorrectly, the transformer at the corresponding intersection would be energized. The transformer drove a silicon-controlled rectifier (SCR) which had a fuse for an anode load. If an error occurred, the SCR would be turned on, blowing the fuse and giving a permanent record of the error.

The fifth row of the matrix was used to indicate a lack of word current. A current transformer coupled to the two current-generator output lines provided a signal to set a flip-flop if word current was present. The output of this flip-flop was then checked and indicated in the same manner as described above.

In its output line, one DRO bit driver had a current transformer which performed in the same manner as the word-current detection circuit described above. The bit driver functioned independently of address; consequently, its error indicator was fused separately. The necessary circuit is shown in Figure 2.14.

Since the active readout circuits could not be checked directly for proper operation, similar circuits with known inputs were added. If one of the active circuits was affected by radiation, it was probable that one of the dummy circuits would also be affected in a similar way. Included were two complete extra sense amplifiers — one with a dummy "one" input signal and one with no input signal or "zero" — and two extra strobe circuits (output portion of the sense amplifier) also with dummy "one" and "zero" inputs. An extra flip-flop was also included in the readout register and was reset by a timing pulse during each cycle.

The outputs of these five sets of circuits were compared to the state that would be correct if no malfunction occurred. If a malfunction occurred, the proper fuse was blown, as before, using the circuit of Figure 2.14.

All the checks described thus far were checked for improper operation only. One check for proper operation was included and consisted of a circuit to blow a fuse if a particular timing pulse was present. If this particular fuse blew because the timing pulse was present, it was an indication that the power was turned on, that at least part of the unit was operating, and that the unit was ready to indicate errors. Any malfunction which then occurred under these conditions was indicated by the error circuits.

The Remington Rand-Univac package installed in Station **528.13-4 (5,700 feet) is** shown in Figure 2.16.

2.2.3 Diagnostic Station. The diagnostic instrumentation bunker was equipped with an air-conditioning system to maintain adequate interior temperatures. The electrical generator, refrigeration compressor, coolant pumps, and heat exchanger were located in a remote dugout (Figures 2.17 and 2.18). Refrigerated water was circulated to the bunker through plastic pipe. In the bunker the coolant w s circulated through a second heat exchanger. An air-circulation fan drew warm air into the heat exchanger from whence it was exhausted back into the room at a lower temperature.

The power for the diagnostic station was provided as follows: A 50 kw 240 vdc diesel engine generator was connected to a motor generator (MG) set which in turn provided a regulated output of 117 volts, 60 cycles for the diagnostic instrumentation. Prior to the actual test, the diesel engine generator was removed and the MG set (35 kw) connected directly to a bank of batteries which provided dc power to the MG set. The batteries were charged using the 50-kw diesel engine generator.

The battery room shown in Figure 2.34 consisted of 160 batteries, 8 banks of 20 batteries each delivering a total of 240 vdc (~ 35 kw). The batteries were fully charged before final button-up operations. At H + 2 minutes all power was turned off by the programmer.

The diagnostic monitoring equipment consisted of 17 oscilloscopes equipped with cameras to record transient pulses. Tektronix 585 and 555 oscilloscopes were used since they offered the necessary one-shot triggering and the required use-time characteristics. The sweep speeds selected were 50 nanoseconds/cm to 2 msec/cm with sensitivities of less than 5 mv/cm. The rise times of the 585 and 555 oscilloscopes are 3.5 nanoseconds and 12 nanoseconds respectively. The sweep speed and sensitivity for each test-circuit channel were selected so that an overlap in time and amplitude was achieved. The voltage levels and sweep speeds for the oscilloscopes are given in Table 2.3.

Two AMPEX FR-100 magnetic tape recorders were utilized to record slower transient pulses (Figure 2.19). The FR-114 (14 denotes the number of tracks) is capable of both direct record (DR) and frequency modulation (FM) recording by means of interchangeable plug-in amplifiers. The frequency response of the FM amplifier is dc to 20 kc and 100 cps to 120 kc for direct record at a tape speed of 60 inches per second (ips). The minimum signal record levels for FM and DR are 70 mv and 250 mv respectively. The maximum signal level is 50 v by adjusting the input potentiometer on the record amplifiers. The voltage level for the tape recorders is shown in Table 2.4.

2.2.4 Dosimetry

Gamma Dose Rate. Six scintillation-type gamma detectors, each consisting of a Pilot-B plastic scintillator fluor and ITT FW-114 planar photodiode, were used to record gamma time history. A 2500 vdc low-impedance power supply was used as the photo-diode (anode) supply. As shown in Figure 2.20, Detectors 1 and 2 were used for scope triggering. Detector 3 was used to measure the prompt gamma spike. Detectors 4 and 5 were used to measure the dose rate out to 10 μsec and 100 μsec, respectively. Detector 6 was used to determine the time-integrated dose out to about 10 msec.

Gamma Dose. Four types of gamma dosimetry were utilized: Edgerton, Germeshausen and Grier (EG&G) shielded chemical (tetrachloroethylene) dosimeters; EG&G shielded Bausch & Lomb silver phosphate glass rods; EG&G shielded film dosimeters; and unshielded Bausch & Lomb glass rods. The shielding containers used by EG&G were the standard National Bureau of Standards (NBS) tin-lead-polythene configurations. Chemical dosimeters and glass rods measure doses above 25 r and the film dosimeters below 25 r. The chemical dosimeters were designed to cover a factor of 3 on either side of the calculated dose whereas the glass rods had a standard range 25 to 10^4r. The two types were used together to give double data points at most locations. Film alone was used at Pad 528.14 (7,500 feet) where the anticipated dose was below the range of either chemical or glass-rod dosimeters.

Neutron Exposure. Standard EG&G packages of gold foil, cadmium-covered gold foil and sulphur pellets were used for integrated neutron exposure measurements. In addition, EG&G boron-bomb fast-fission foils were used at Pads 528.12 and 528.13, where the neutron dose was sufficient to produce measureable activation. The thresholds for the respective foils were Au - Au Cd, thermal neutrons, E > 0.025 ev; Pu^{239}, E > 10 Kev; Np^{237}, E > 0.75 Mev; U^{238}, E > 1.5 Mev; and S^{32}, E > 3.0 Mev.

2.3 INSTALLATION AND CALIBRATION

2.3.1 Blooper Station Circuits

Installation. The blooper package installation is shown in Figure 2.21. From the viewpoint of packaging and installation features: (1) the test circuits were mounted at the top of the package, the side with the greater area facing the incident radiation; (2) the low-impedance battery pack was installed at the rear of the upper compartment for ease of access and where it could be partially shielded; (3) the semihard isolation circuits were installed below a lead shield to reduce the gamma doses to well below response threshold levels (~ 10^4 r/sec gamma

dose rate) at the pad nearest ground zero; (4) the recording circuits were installed below additional lead and borated polyethylene shielding, since they were more radiation sensitive than the isolation circuits; (5) the electromagnetic shield consisted of the lower steel box above the pad cover plate and the steel lid clamped tightly to the box with a steel-wool gasket to minimize the reluctance of the joint and provide low-resistance electrical connection between the box and lid; (6) the dosimeter cup was located in close proximity to the test circuits; and (7) a gamma trigger unit turned off the power to the recording circuits shortly after the gamma pulse. The power was turned off to preclude fuses being blown by electrical transients after the gamma pulse. Details of the blooper packages and shielding are shown in Figures 2.22 through 2.25.

Calibration. Preshot calibration of blooper packages consisted of checking the electrical performance of each channel and adjusting the channel sensitivity to the desired level. The electrical checkout included checking all power-supply voltages provided by the instrumentation and test-circuit programmers, checking both programmers for the proper turn-off, and turn-off power sequencing, and checking all circuits for satisfactory operation. The performance of each channel was checked covering the input pulse range of 100 mv to 10 volts at a pulse width of 1.0 μsec. After the channel sensitivity was set to the desired level and each channel rechecked, fuses were installed and the blooper cycled on and off. The programmer and the slow gamma trigger were used to simulate actual operation. Fuses were checked after every turn-on and turn-off operation to assure that there had been no malfunction or sporadic triggering.

Postshot calibration consisted of recording the threshold levels on each comparator and rechecking the sensitivity of each channel. A cursory examination of the recorded thresholds before and after the test showed consistency to within voltmeter accuracy. Channel amplitude sensitivity as a function of input pulse width was checked on a sample of 24 channels. The channel performance was essentially uniform for pulses whose width was at least 0.3 μsec as shown in Figures 2.26 through 2.28. Isolation-circuit performance as a function of test-circuit driving impedance was also checked on a sample basis.

From the information determined during blooper calibration, reliable operation was expected for input pulses ranging in amplitude from 300 mv to approximately 9.0 volts depending on the particular channel involved. The lower limit was determined by the noise level and the upper limit was determined by the maximum threshold setting of approximately 5 volts, both limits being at the comparator, and therefore subject to correction by the channel gain to obtain the input levels quoted above. The data obtained during calibration on input level sensitivity as

a function of pulse width showed no particular change in sensitivity for pulses longer than 0.3 μ sec. Successful triggering was obtained at pulse widths as narrow as 40 nanoseconds although the input voltage level required to trigger was considerably increased. No investigation of pulse widths less than 40 nanoseconds was conducted due to limitations in the pulse generator.

2.3.2 Diagnostic Station.

Installation. Cameras were installed on the oscilloscopes to record the data, as shown in Figure 2.29. A trigger generator, in response to a scintillation detector signal, drove the oscilloscope trigger circuits to generate sweep signals at the instant the prompt gamma pulse was received. A programmer (Figure 2.30) installed in the bunker performed all of the functions required to operate the cameras, recorders and power equipment during the shot, since the bunker was unmanned. The program was initiated by either a -30 second or a -5 second range-timing relay. The block diagram for the programmer is shown in Figure 2.31. A timing cable guillotine and retraction system disconnected the timing cables and withdrew them from the bunker upon receipt of the -5 second timing signal, thereby eliminating possible introduction of EMP-induced noise into the bunker by the cables. The timing relays and guillotine control box are shown in Figure 2.32.

A typical coaxial cable installation between the diagnostic package and the bunker instrumentation is shown in Figure 2.33. Additional views of the circuit monitoring equipment and power generator are shown in Figures 2.34 and 2.35. The block diagrams for the diagnostic instrumentation and power supplies are shown in Figure 2.36 and Figure 2.37 respectively.

A ground view of the diagnostic station is shown in Figure 2.38. A detailed cross sectional view of the diagnostic package is shown in Figure 2.39. A closeup view of the installation package shielding is shown in Figure 2.40.

Calibration. Tektronix Type 555 oscilloscopes with Type K or L plug-ins were used for measuring voltage amplitude and waveforms generated by a Rutherford Type B7B pulse generator during the calibration procedures. All voltmeters used during calibration had a sensitivity of at least 10,000 ohms/volt and an accuracy of ± 3 percent.

Diagnostic circuit packages were calibrated in the field laboratory before installation. After installation, pulses were injected at the test-circuit output terminals, and oscilloscope photographs were obtained showing the channel responses. The channel calibration levels are given in Table 2.5.

Bunker instrumentation was calibrated per manufacturer's specification upon installation and periodically checked. Drift calibration was obtained by recording the base lines on the oscilloscopes while on external power, then on battery power at H-3 1/2 hours, and finally while on batteries at D + 2. (No drift was observed during this period).

The two tape recorders were calibrated using methods prescribed by the manufacturer. Voltage calibrations were made with sinusoidal inputs at the maximum frequency response of the record amplifiers.

2.3.3 Dosimetry

Installation, Scintillation Detectors. The six scintillation detectors were installed in diagnostic package hole No. 3, as shown in Figure 2.41. Detectors Nos. 1 and 2 were used for the oscilloscope trigger system; Detectors Nos. 3, 4, and 5 were used to measure the gamma dose rate time history over three ranges of time (0.05 μsec., 10 μsec., 100 μsec.); Detector No. 6 was used to determine the integrated gamma dose as a function of time up to approximately 10 milliseconds.

Gamma Dosimeter. The precoded gamma dosimeters were placed inside small aluminum cans and installed within the blooper and diagnostic packages. Each gamma dosimeter was exposed to the same radiation environment as the test specimens in the package. The film dosimeter film-planes were mounted perpendicular to the line-of-sight to ground zero. The chemical dosimeters and glass rods were mounted with their axes perpendicular to the line-of-sight to ground zero.

Neutron Dosimeter. Neutron dosimeters were installed in the aluminum cans containing the gamma dosimeters. The planes of the sulphur tablets and foils were perpendicular to line-of-sight to ground zero. The gold and gold-cadmium foils were installed on opposite ends of the gamma chemical dosimeters upon EG&G's suggestion.

Calibration, Scintillation Detectors. The gamma detectors and integrating circuit for detector No. 6 were calibrated before the field test in terms of output current versus dose rate at the Northrop Ventura 600-kv Flash X-Ray Facility, using ionization chamber dosimetry. For Detectors Nos. 4 and 5 it was necessary to use cathode followers due to the large photodiode load resistance (4.7 k and 100 k) required to increase detector sensitivity.

At the test site, scintillation detector electronics channels were calibrated using a Rutherford pulser, and where required, a series resistor to simulate the actual source impedance

(4.7 k and 100 k). Subsequently, each detector-electronics chain was calibrated at the test site using a Xenon-tube light flasher incident on the photodiode. By numerically integrating a differential display of the Xenon-flasher pulse (approximately 0.2 μsec wide) the integrating channel (Detector No. 6) could be calibrated directly. Figures 2.42 and 2.43 are representative of the calibration recordings.

After the field test, the scintillation detectors were calibrated at the EG&G, Santa Barbara, Co^{60} Facility. This calibration was used in the final results discussed below.

Gamma Dosimeters. The gamma dosimeters supplied by EG&G, Santa Barbara, were also calibrated and read by EG&G; therefore no calibration procedures were performed by Northrop Ventura.

The unshielded Bausch & Lomb glass rods were supplied, calibrated and read by the Signal Corps (R. G. Saelens). The glass rods were packaged in groups of three in polyethylene containers. Ultrasonic cleaning and extreme care in handling the glass rods gave a readout accuracy of approximately 10 percent.

Neutron Dosimeters. The sulfur pellets, gold foils, and cadmium-covered gold foils were supplied, calibrated, and read by EG&G, Santa Barbara. The fission foils were loaned for use in Project 7.1.4 by Dr. L. J. Deal, Acting Director of the Civil Effects Test Operation of the AEC Division of Biology and Medicine, Washington, D. C. These fission foils were calibrated and read by EG&G.

TABLE 2.1 TEST SPECIMEN LOCATIONS, SHOT SMALL BOY

Station	Package Serial Number	Package Type	Gamma Distance feet	Predicted Gamma Dose Rate r/sec
5.614-1	1	Diagnostic	5700	
5.614-2	2	Diagnostic		
5.614-3	1	Dosimetry		
5.614-4	4	Diagnostic		
5.61 5	5	Diagmostic, MgORAD		
528.12-1	7	Small Boy Blooper	2800	
528.12-2	9	Small Boy Blooper		
528.12-3	8	Small Boy Blooper		
528.13-1	6	Small Boy Blooper	4150	
528.13-2	12	Small Boy Blooper		
528.13-3	4	Small Boy Blooper		
528.13-4	-	Rem-Rand/Univac		
528.14-1	15B	Small Boy Blooper	5700	
528.14-2	14	Small Boy Blooper		
528.14-3	19A	Little Feller II Blooper		
528.15-1	15A	Small Boy Blooper	7500	
528.15-2	10A	Little Feller II 2 Blooper		
528.15-3	11	Small Boy Blooper		

page 33 deleted.

TABLE 2.3 DIAGNOSTIC OSCILLOSCOPE SETTINGS

Scope Number	Channel Number	Horizontal Sweep Speed	Voltage Sensitivity	Base Line Offset	Measurement*	Diagnostic Package Number
		μs /cm	volts/cm	pct		
1	1	10	1.0	25	Ckt. 2(+)	1
1	2	10	1.0	75	Ckt. 2(-)	1
2	3	1.0	0.1	75	Ckt. 3(-)	1
2	4	1.0	0.02	0	Ckt. 5	1
3	5	0.1	0.1	75	Ckt. 1	1
3	6	0.1	0.01	50	Term. C/F	4
4	7	0.1	0.01	50	Term. E/F	2
4	8	0.1	0.02	75	Ckt. 1	2
5	9	1.0×10^3	0.5	75	Ckt. 2(-)	2
5	10	1.0×10^3	0.005	0	Ckt. 4	2
6	11	1.0	0.05	75	Ckt. 3(-)	2
6	12	1.0	0.005	0	Ckt. 5	2
7	13	1.0	0.5	0	Dosim. 4	3
7	14	1.0	1.0	0	Dosim. 2	3
8	15	0.05	5.0	0	Dosim. 3	3
9	16	10	0.5	0	Dosim. 5	3
9	17	10	0.05	0	Dosim. 5	3
10	18	20	1.0	75	Ckt. 1	4
10	19	20	0.01	0	Ckt. 4	1
11	20	20	0.02	75	Ckt. 3(-)	4
11	21	20	0.005	0	Ckt. 5	4
12	22	2×10^3	0.005	0	Ckt. 4	4
12	23	2×10^3	0.005	50	Ckt. 4	5
13	24	1.0	0.02	75	Ckt. 1	5
13	25	1.0	0.01	50	Ckt. 5	5
14	26	0.1	0.05	75	Ckt. 3(-)	5
14	27	0.1	0.005	50	Ckt. h	5
15	28	10	0.1	25	Ckt. 2(+)	4
15	29	10	0.05	75	Ckt. 2(+)	5

* Term. C/F, terminated cathode follower; Term.E/F, terminated emitter follower; Dosim., dosimeter.

TABLE 2.4 DIAGNOSTIC TAPE RECORDER SETTINGS

Recorder Number	Max. Expected Input Voltage	Channel Number	Amplifier Type*	Measurement†	Diagnostic Package Number
1	10	1	DR	Ckt. 2(-)	1
1	2.5	2	DR	Ckt. 3(-)	1
1	2.5	3	DR	Ckt. 5	1
1	2.5	4	DR	Ckt. 4	1
1	2.5	5	DR	Term. E/F	2
1	5.0	6	DR	Ckt. 1	2
1	2.5	7	DR	Ckt. 2(-)	2
1	10	8	DR	Ckt. 2(+)	2
1	2.5	9	DR	Dosim. 5	3
1	1.0	10	FM	10 KC Signal	HP200CD
1	2.5	11	DR	Ckt. 1	4
1	2.5	12	DR	Ckt. 2(+)	4
1	2.5	13	DR	Ckt. 5	4
1	2.5	14	DR	Term. C/F	4
2	2.5	1	DR	Ckt. 1	5
2	2.5	2	DR	Ckt. 5	5
2	2.5	3	DR	Ckt. 3(-)	5
2	2.5	4	DR	Ckt. h	5
2	2.5	5	DR	Ckt. 2(+)	5
2	1.0	9	FM	Dosim. 6	3
2	4.0	10	FM	Dosim. 6	3
2	2.5	11	DR	Dosim. 4	3
2	2.5	12	FM	Ckt. 4	4
2	NA	14	FM	Ckt. 2(+)	5

* DR, direct record; FM, frequency modulated.

† Term. E/V, terminated emitter follower; Dosim., dosimeter; Term. C/F, terminated cathode follower.

TABLE 2.5 DIAGNOSTIC STATION CHANNEL CALIBRATION

Channel	Test Circuit	Package	Scope	Correction Factor
1	2(+)	1	1	2.0
2	2(-)	1	1	2.5
3	3(-)	1	2	3.2
4	5	1	2	2.5
5	1	1	3	2.7
6	Terminated Cath. Follower	4	3	3.34
7	1	2	4	5.0
8	1	2	4	6.66
9	2(-)	2	5	2.5
10	4	2	5	3.45
11	3	2	6	2.84
12	5	2	6	2.22
18	1	4	10	2.47
19	4	1	10	3.33
20	3	4	11	2.85
21	5	4	11	2.35
22	4	4	12	3.64
23	4	5	12	3.33
24	1	5	13	5.71
25	5	5	13	2.22
26	3(-)	5	14	4.0

Channels 27, 28, 29 did not provide reliable calibration factors.

Peak voltage on oscilloscope X correction factor = actual voltage.

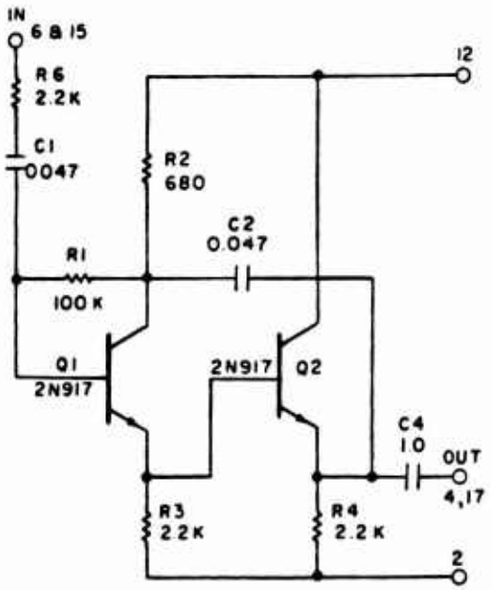

+ EMITTER FOLLOWER

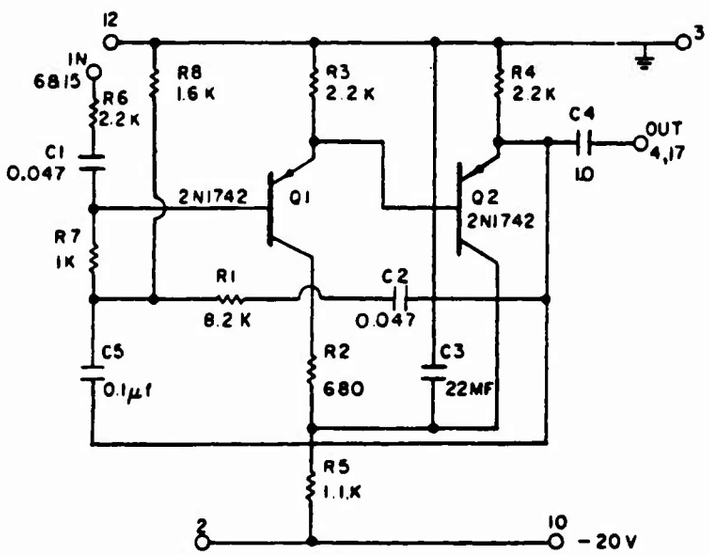

— EMITTER FOLLOWER

Figure 2.1 Emitter follower.

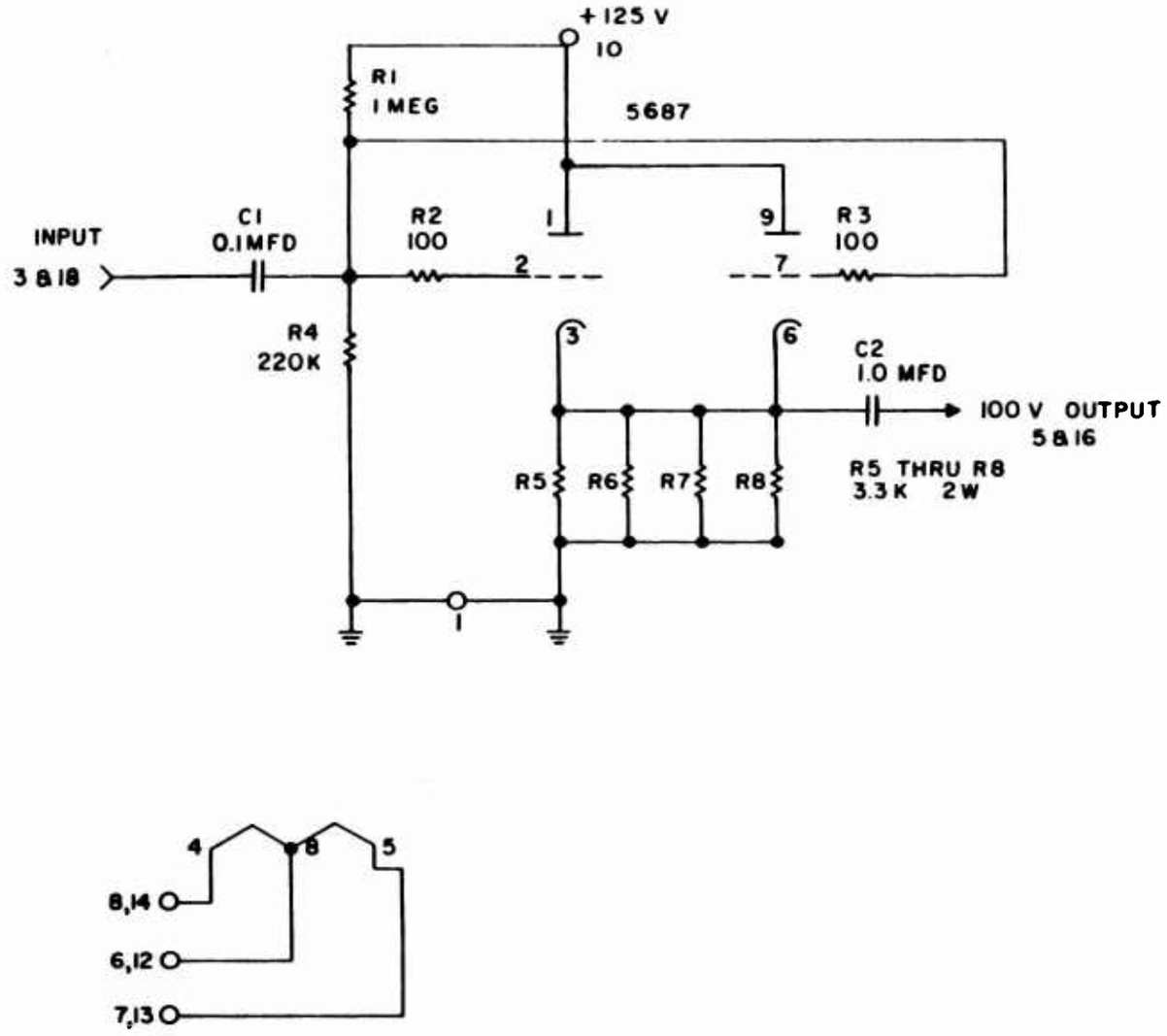

Figure 2.2 Cathode follower.

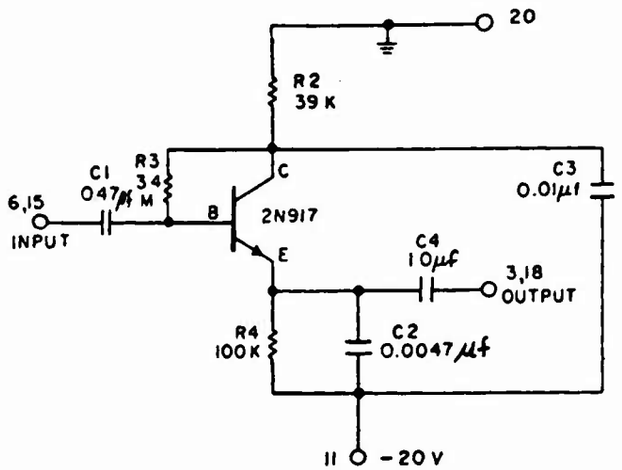

POSITIVE PULSE STRETCHER

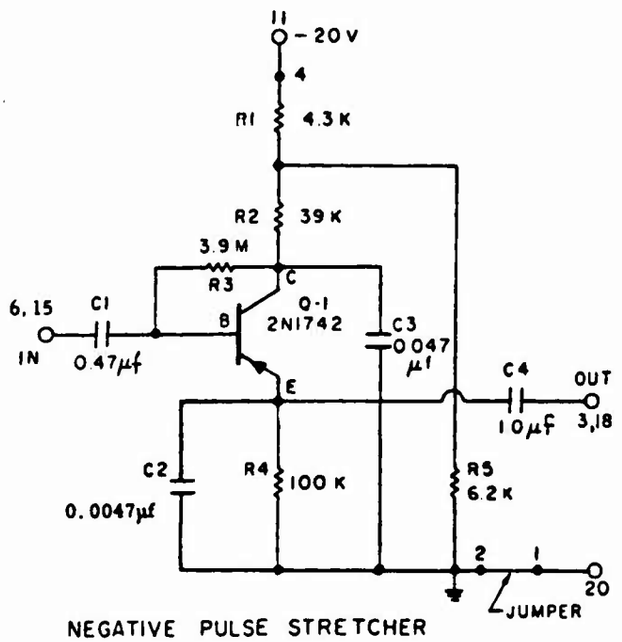

NEGATIVE PULSE STRETCHER

Figure 2.3 Pulse stretching circuits.

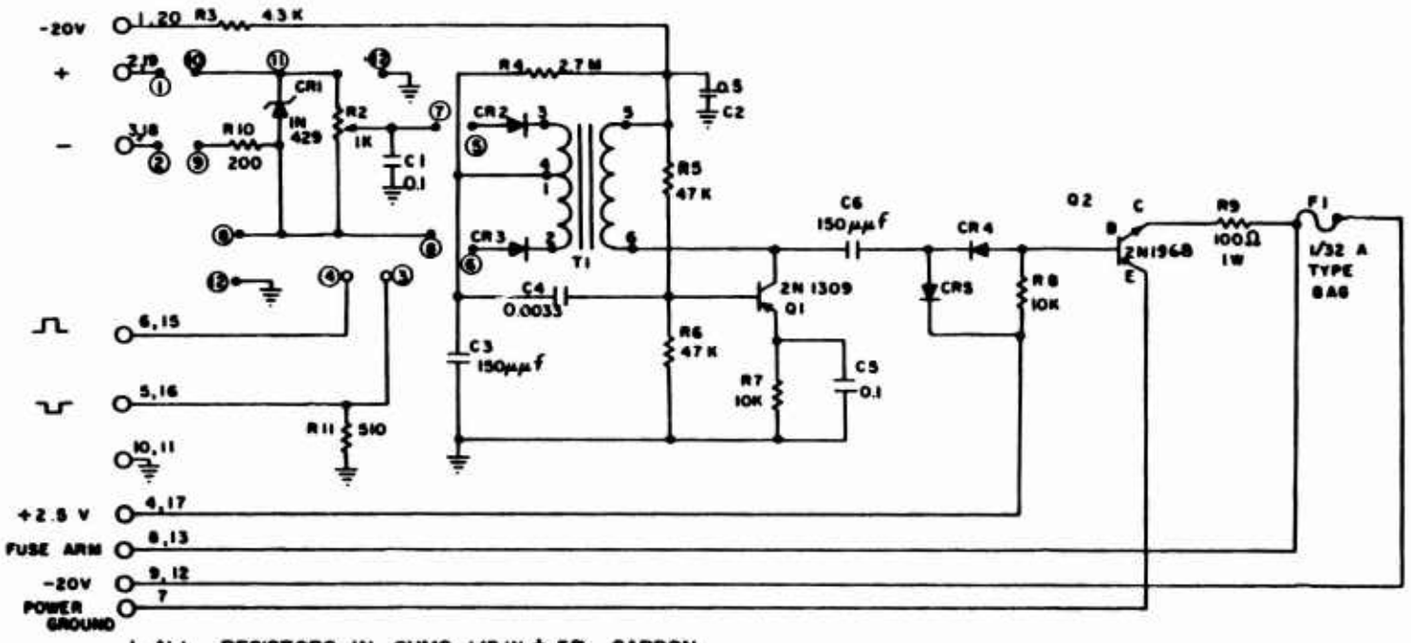

1. ALL RESISTORS IN OHMS, 1/2 W ± 5%, CARBON
2. ALL CAPACITORS IN μf, 100 V UNLESS OTHERWISE SFECIFIED
3. DIODES ARE IN625

Figure 2.4 Schematic for threshold detector.

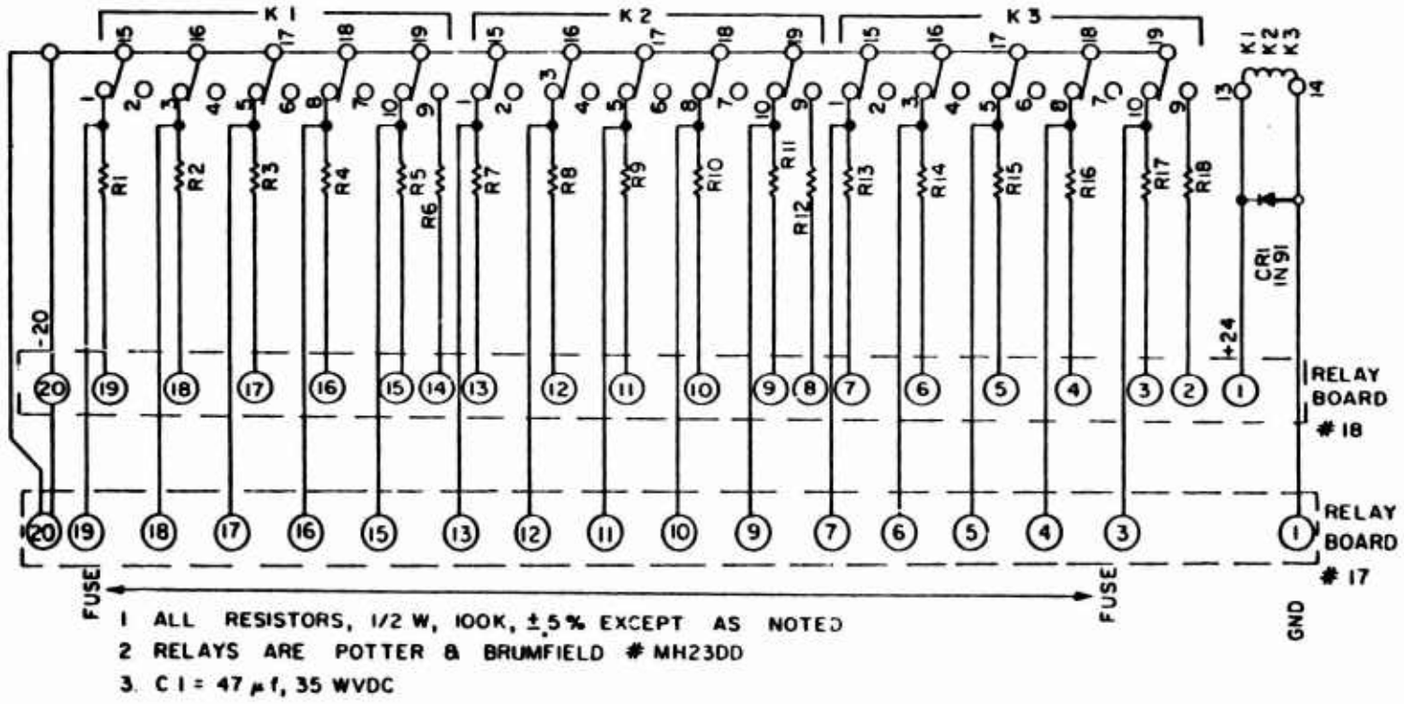

Figure 2.5 Schematic, relay card.

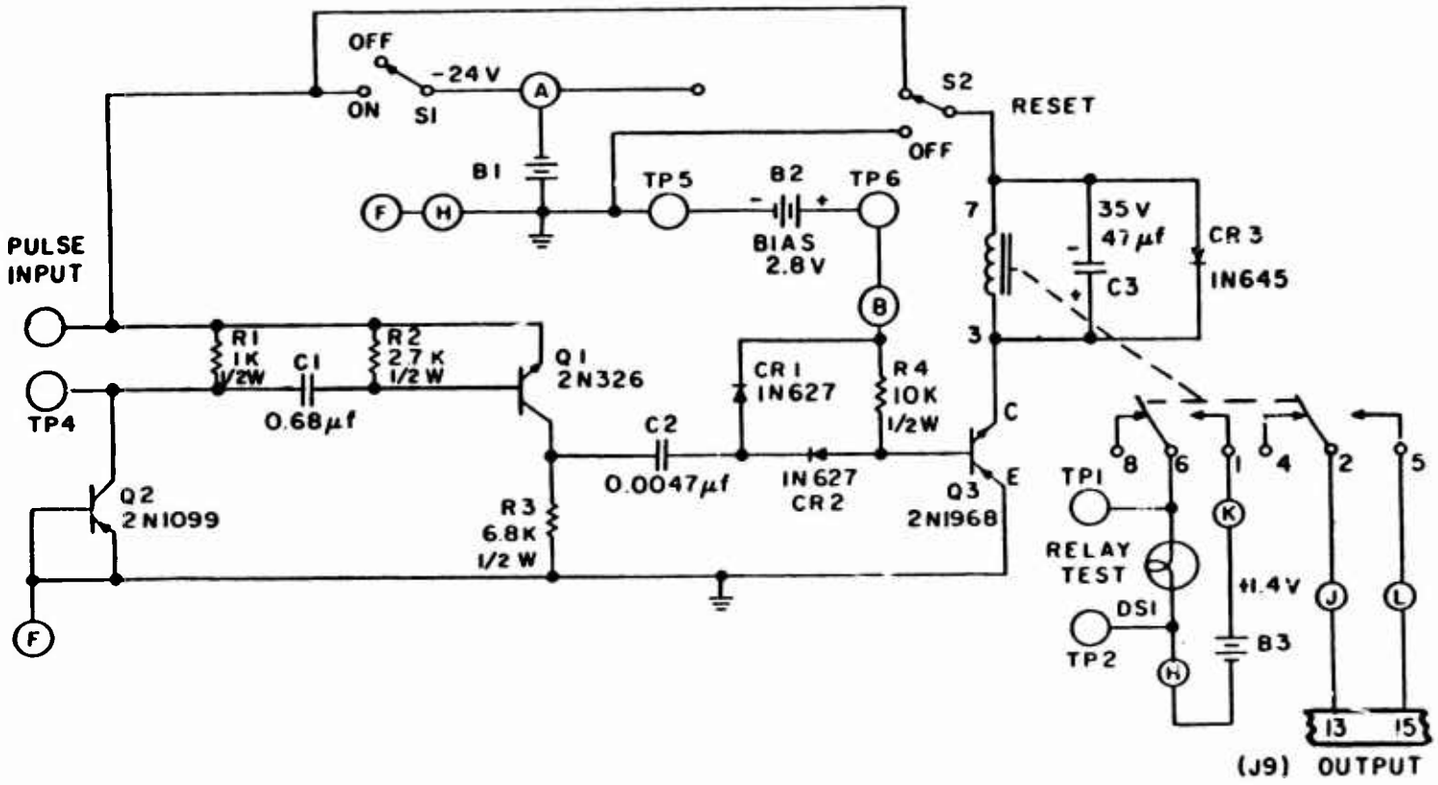

Figure 2.6 Schematic, slow gamma trigger.

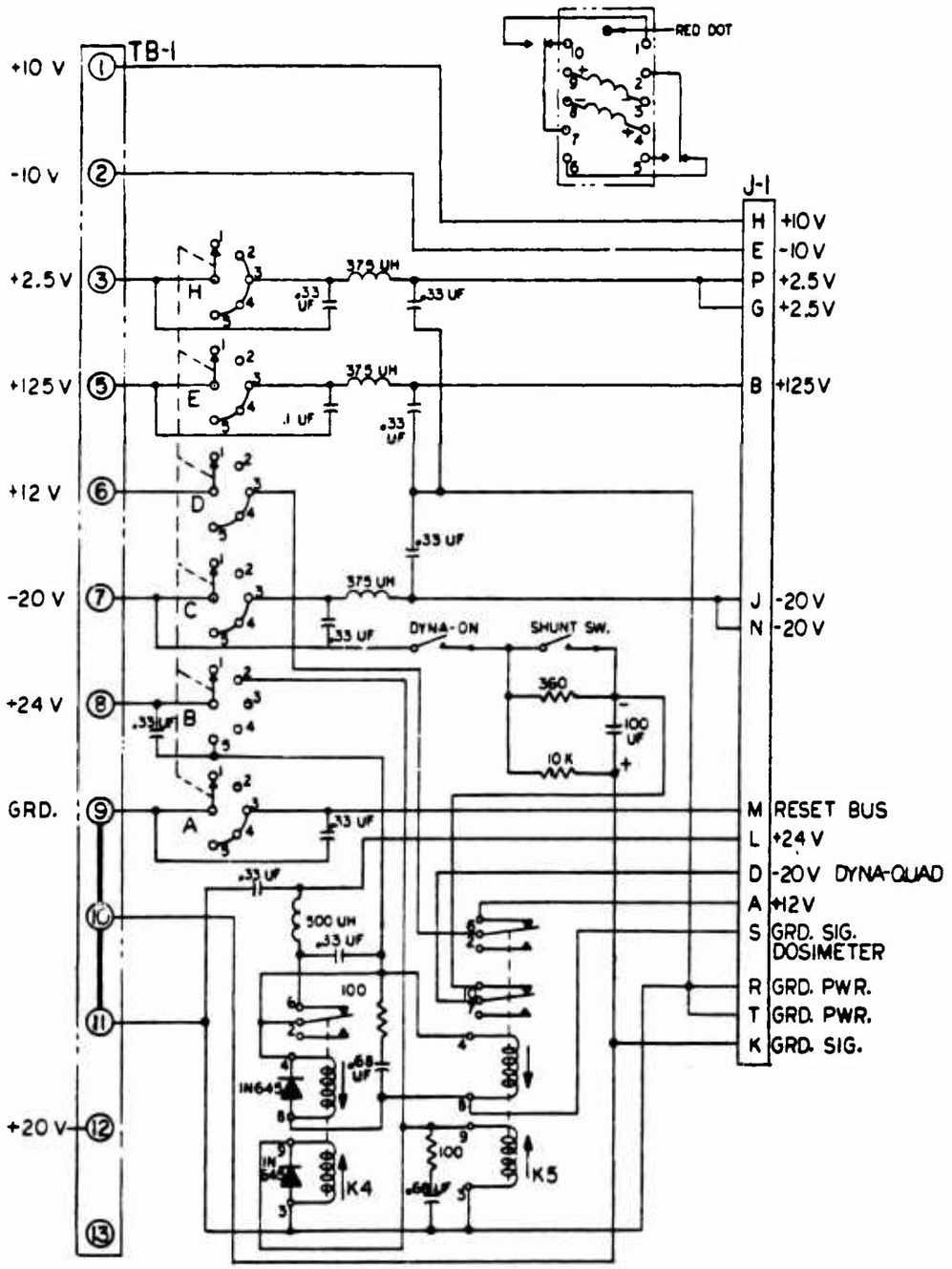

Figure 2.7 Schematic, Small Boy instrumentation programmer.

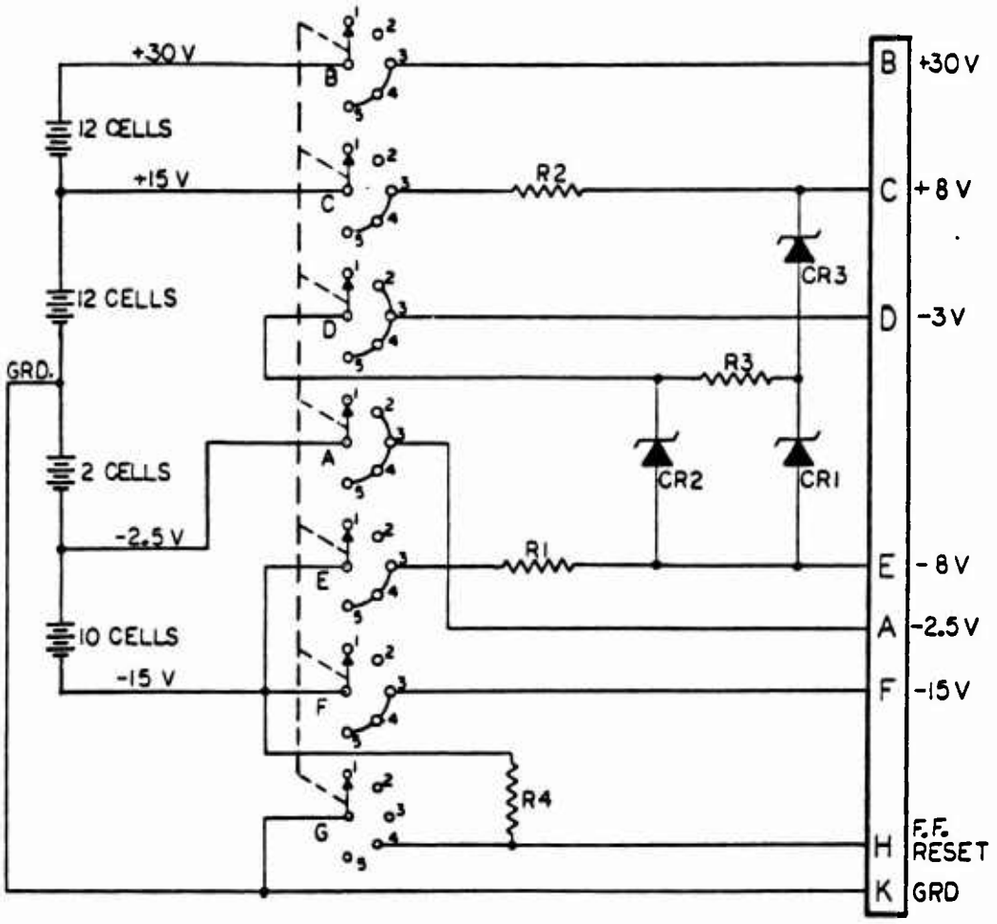

R1 — 330 Ω 1/2W ±5%
R2 — 360 Ω 1/2W ±5%
R3 — 300 Ω 1/2W ±5%
R4 100 KΩ 1/4W ±5%

CR1—IN764-1 ZENER DIODE
CR2—IN761-2 ZENER DIODE
CR3—Z8.0V25 ZENER DIODE

BATTERY CELLS— 42RT2 MALLORY

Figure 2.8 Schematic, test circuit programmer.

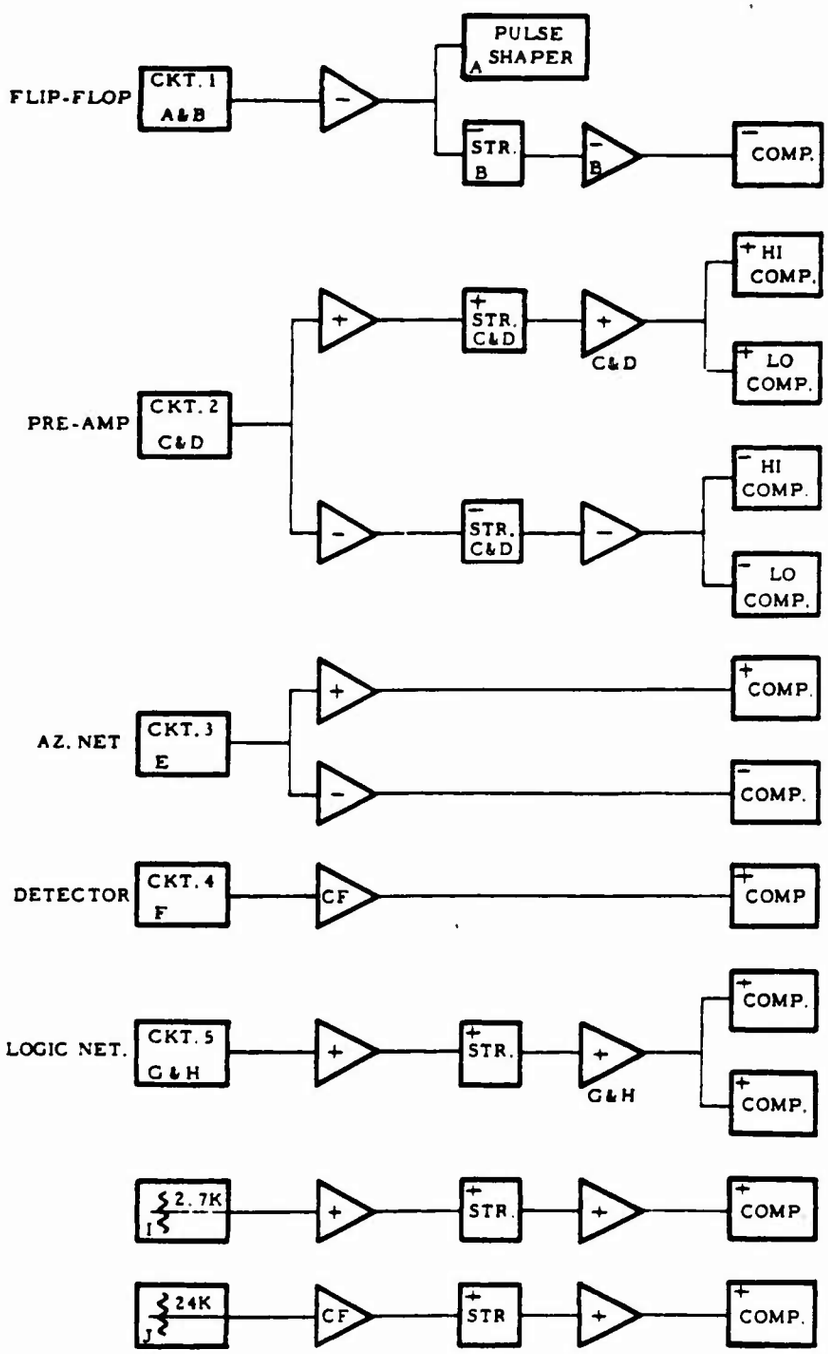

Figure 2.9 Block diagram, blooper instrumentation.

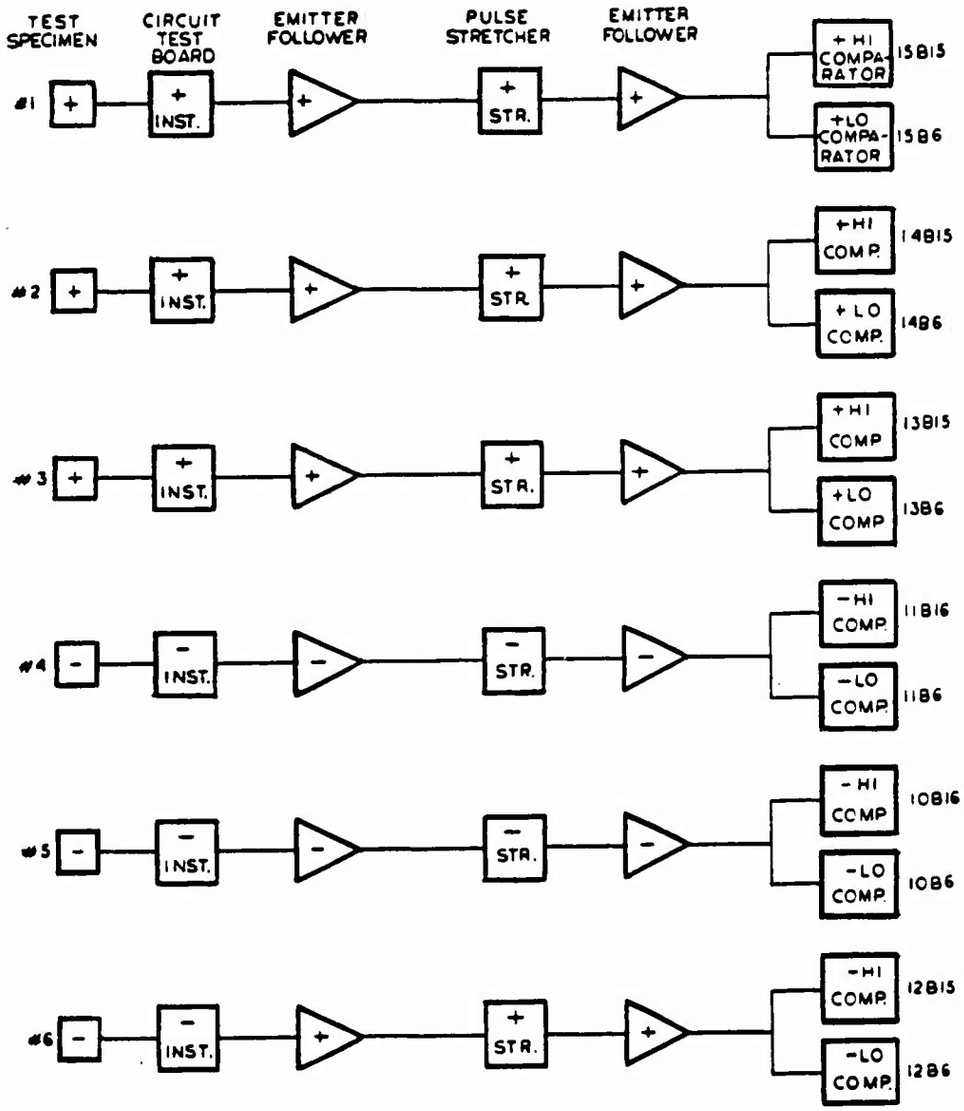

Figure 2.10 Block diagram, Little Feller II blooper instrumentation.

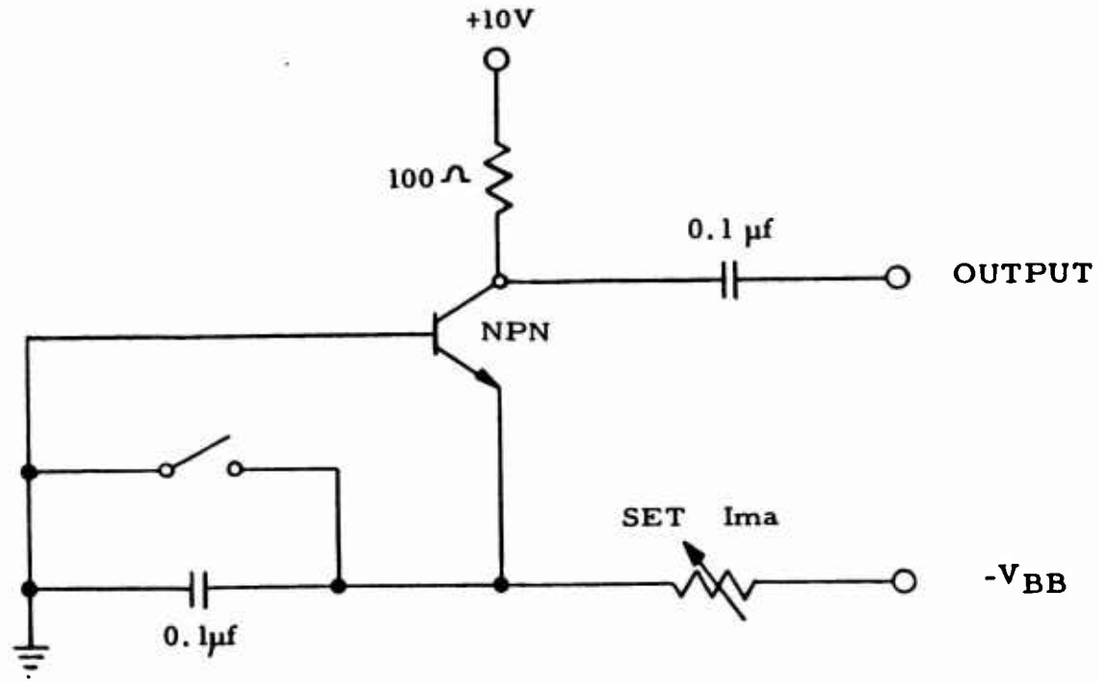

Figure 2.11 Typical transistor circuit, Little Feller II.

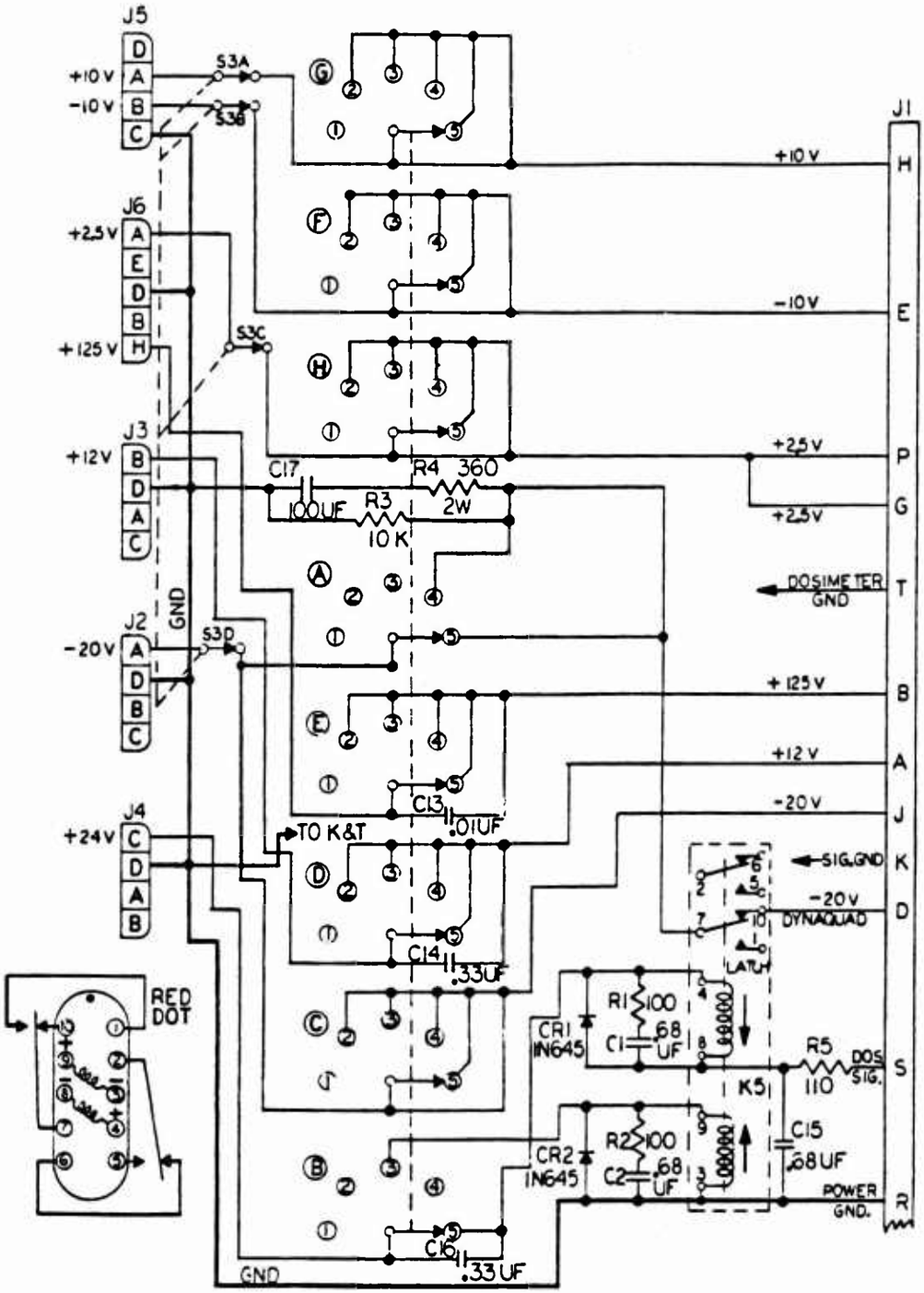

Figure 2.12 Schematic, Little Feller II instrument programmer.

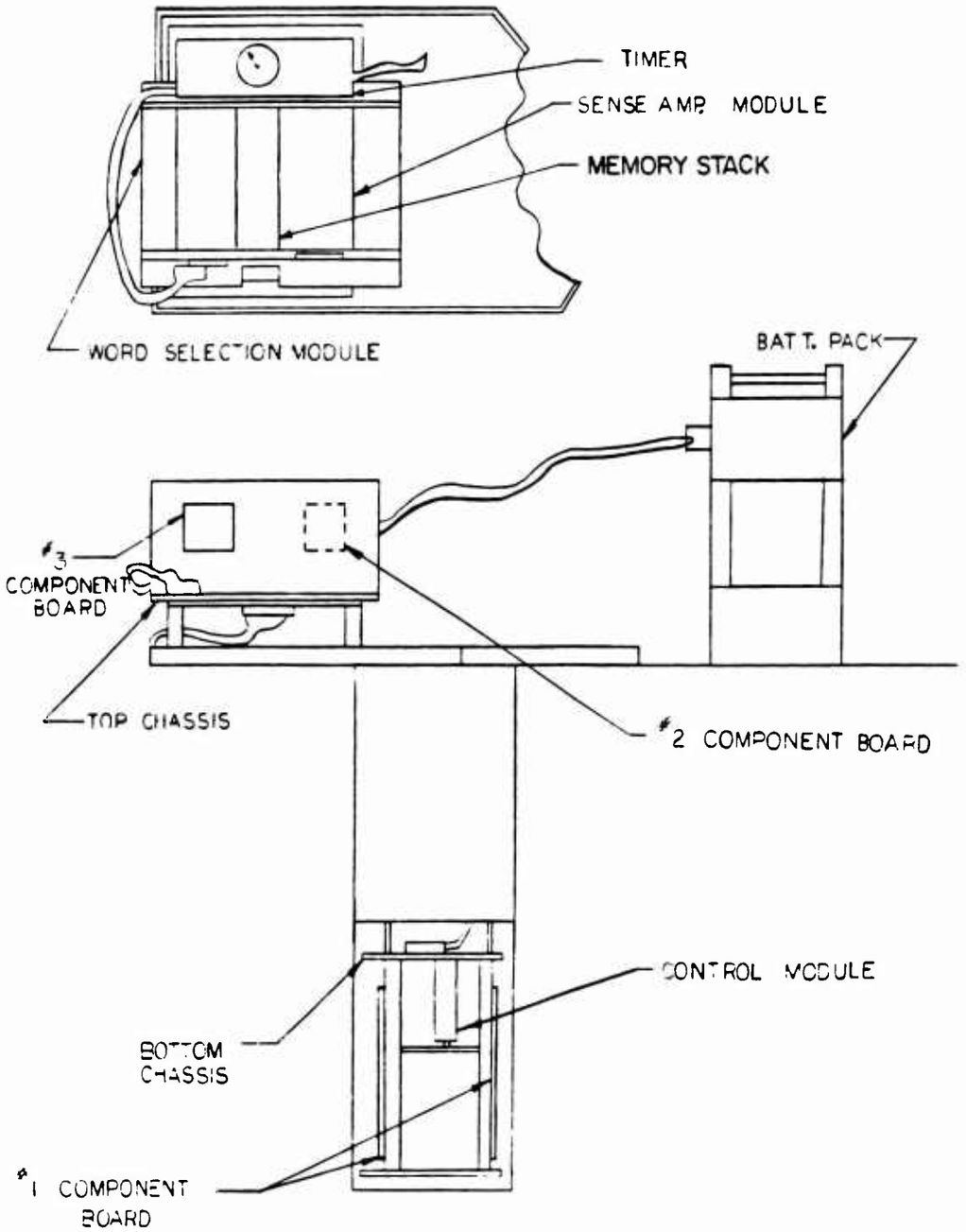

Figure 2.13 Remington Rand package installation.

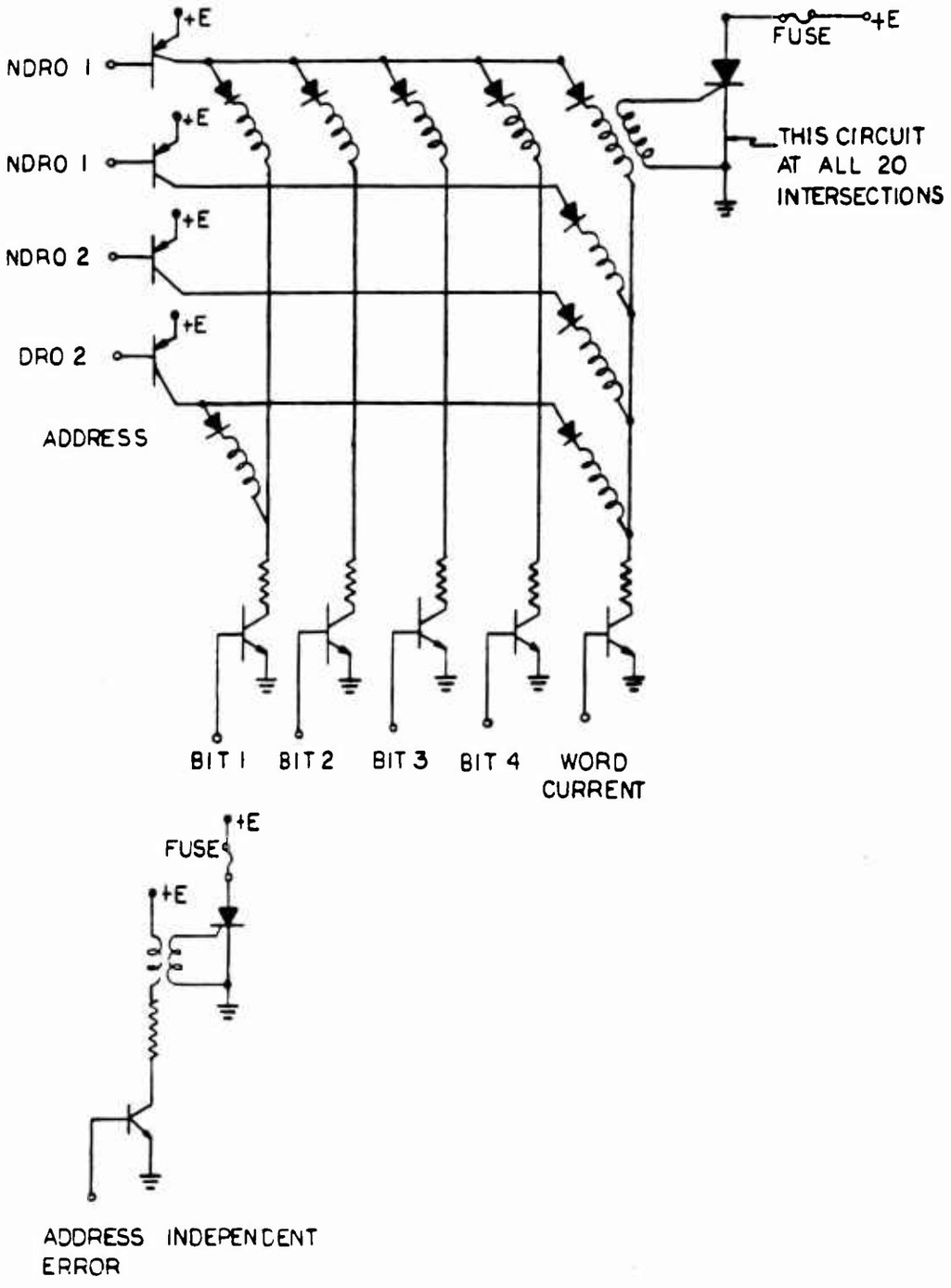

Figure 2.14 Schematic, Remington Rand error circuit.

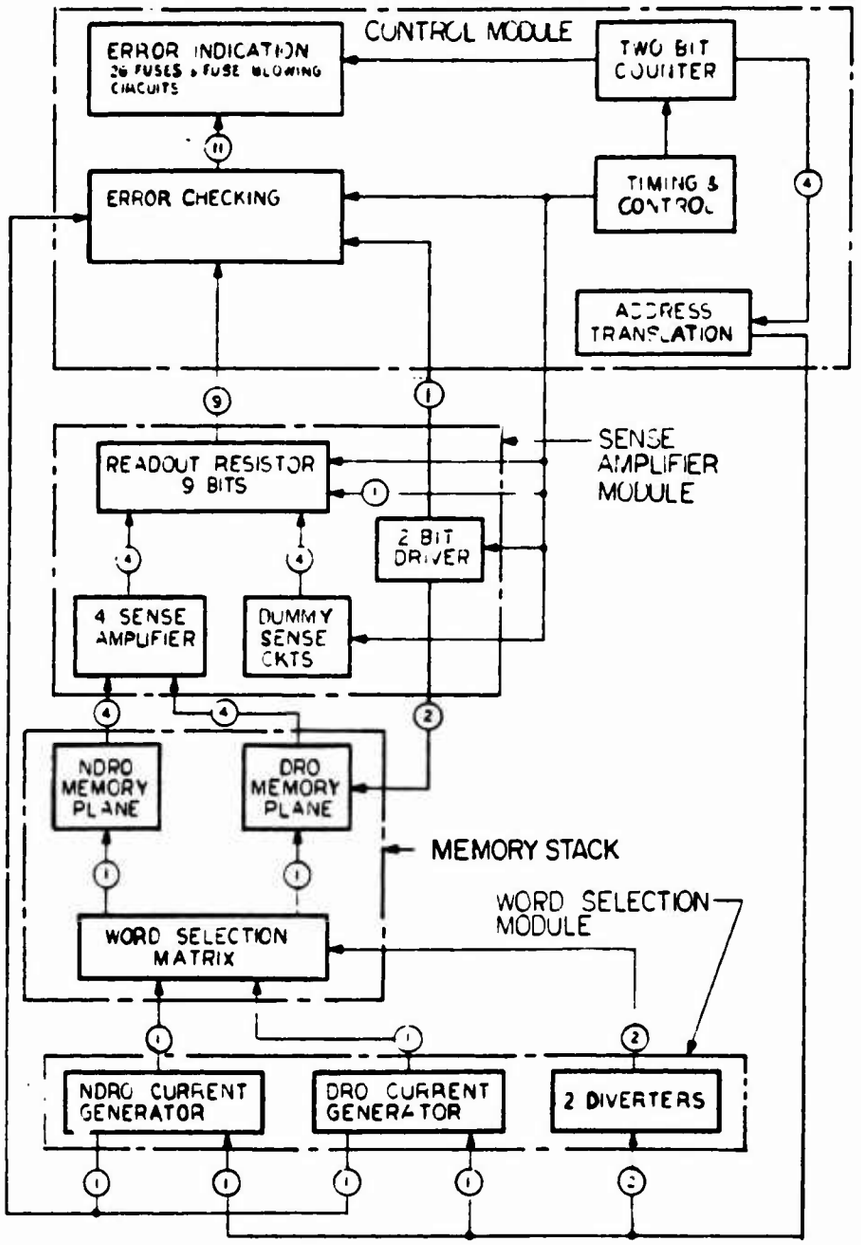

Figure 2.15 Block diagram, Remington Rand instrumentation.

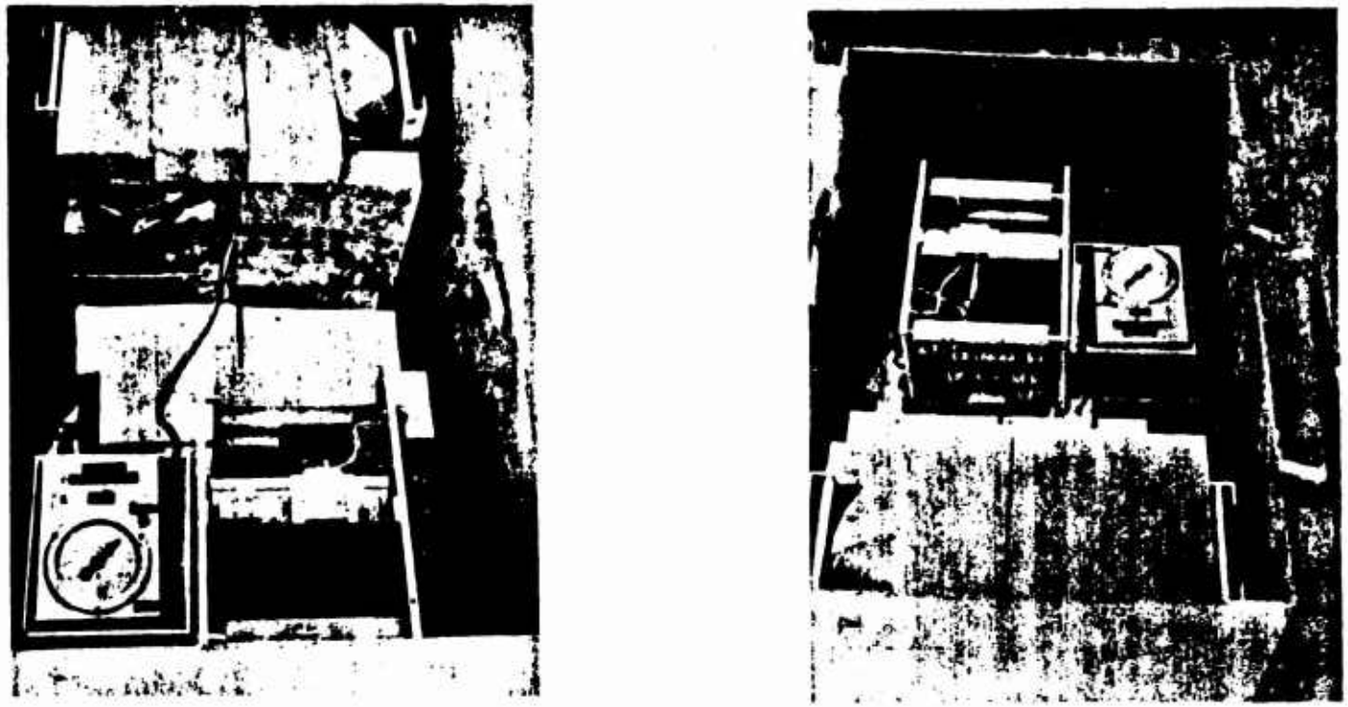

Figure 2.16 Remington Rand-Univac package installation, Station 528.13-4: (Note battery shielding.) (AFSWC photo)

Figure 2.17 Bunker air-conditioning dugout. (AFSWC photo)

Station 5.614 viewed toward GZ across air conditioning dugout.

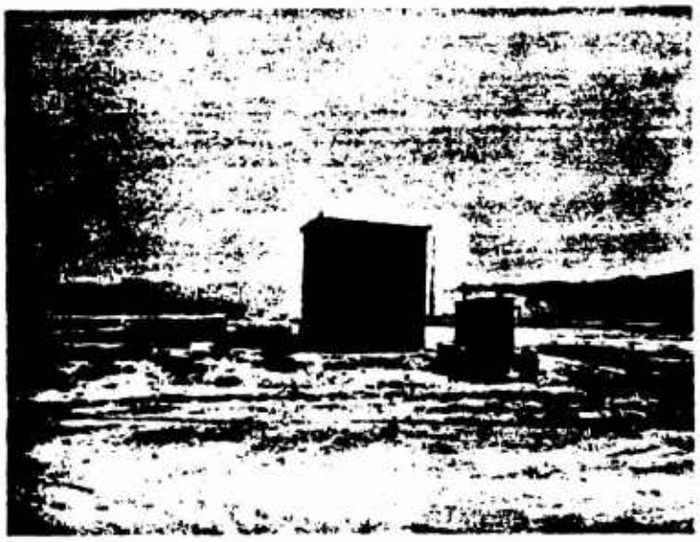

Station 5.614 viewed toward GZ. Note diagnostic boxes on pad, dust shack over bunker entry, and 50 KW dc generator.

Figure 2.18 Diagnostic site and air-conditioning dugout. (AFSWC photos)

Figure 2.19 14-track magnetic tape recorder.
(AFSWC photo)

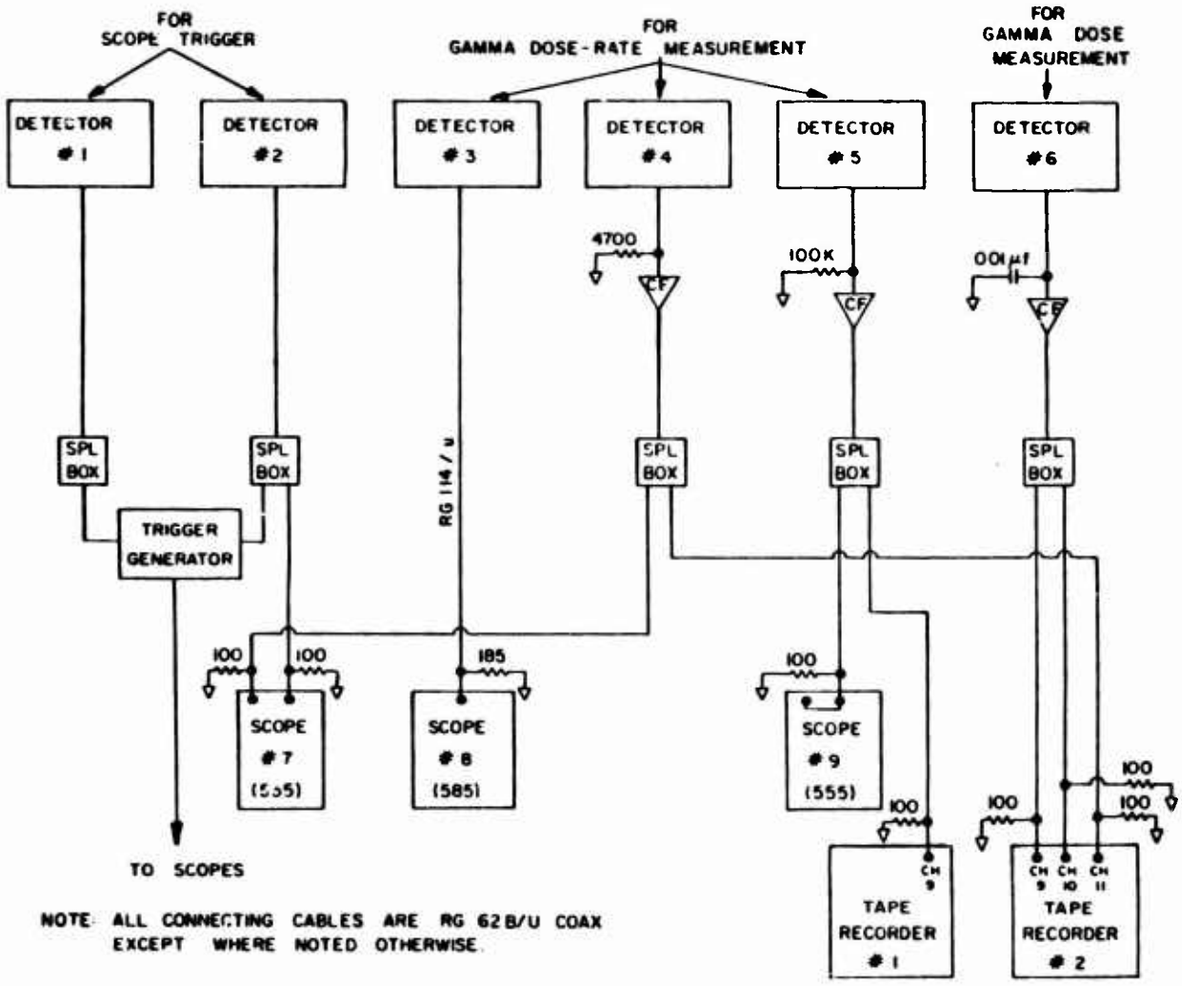

Figure 2.20 Block diagram, bunker dosimetry and scope trigger system.

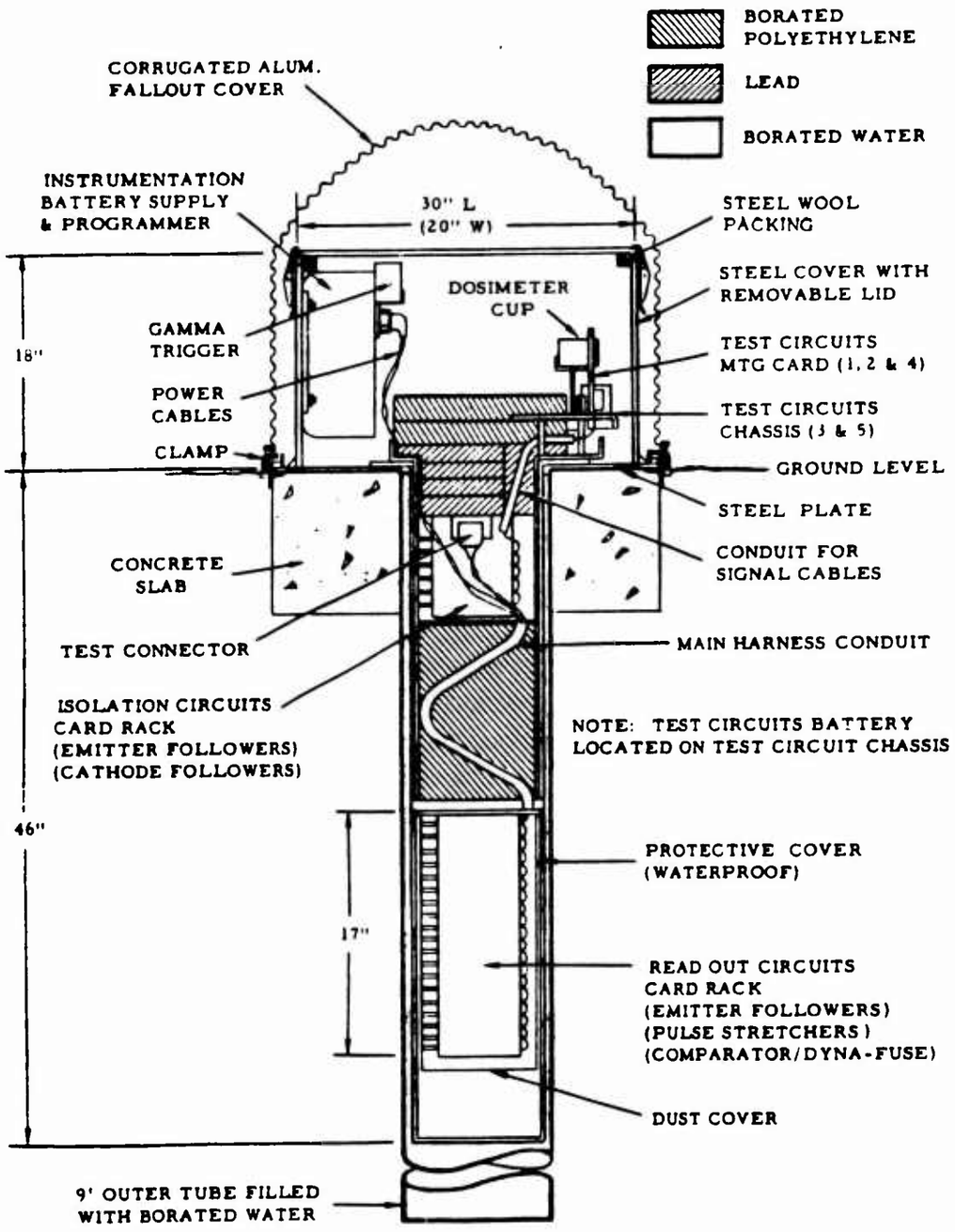

Figure 2.21 Typical blooper package installation.

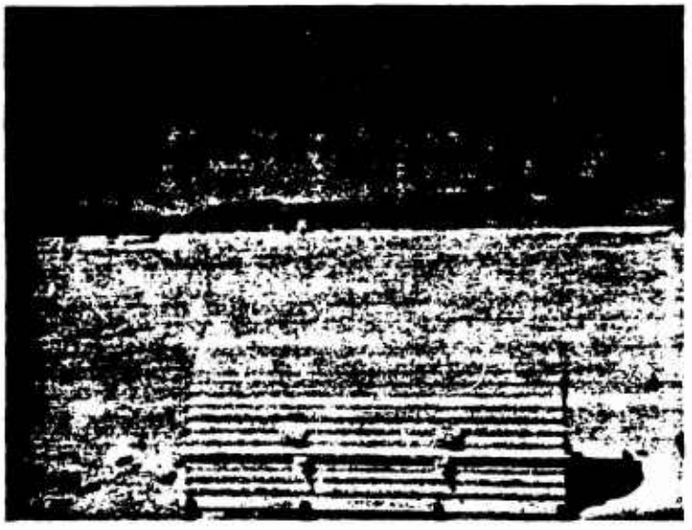

Blooper pad 528.12 viewed toward GZ.

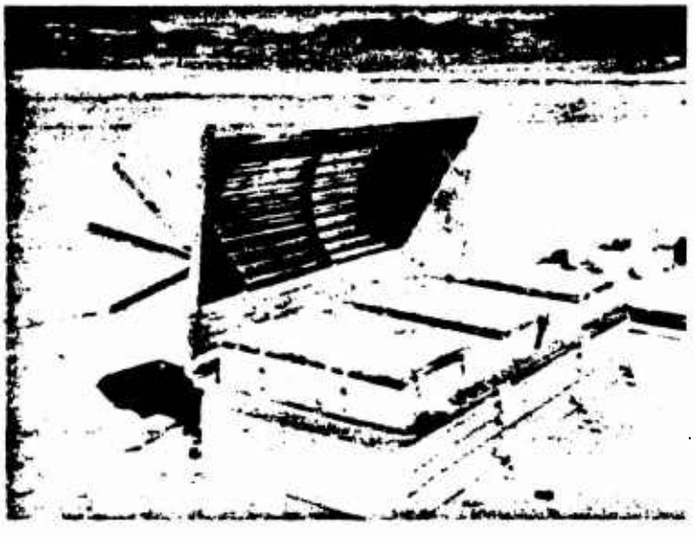

Blooper pad 528.12 with fall-out cover opened.

Figure 2.22 Blooper Pad 528.12.
(AFSWC photos)

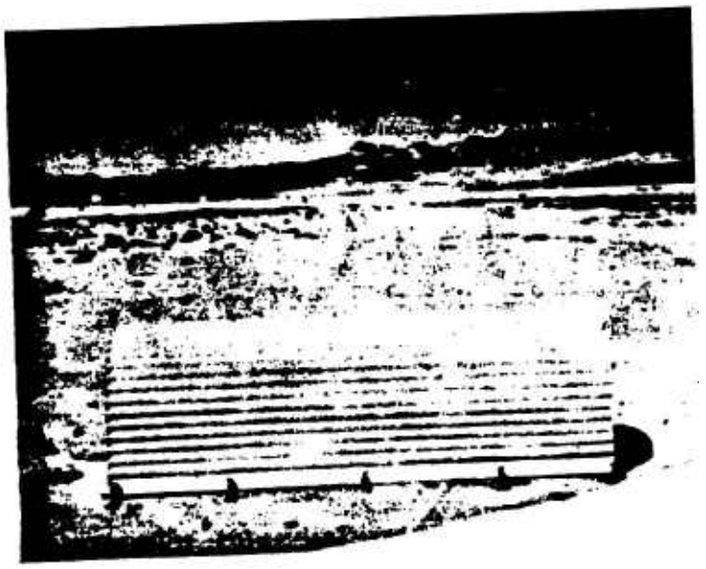

Blooper pad 528.13 viewed toward GZ.

Blooper pad 528.13 with fall-out cover removed.

Figure 2.23 Blooper Pad 528.13.
(AFSWC photos)

Blooper box interior with battery shielding partially removed.

Blooper box interior with blooper package and instrumentation battery removed. Note protective tube floating on borated water.

Figure 2.24 Interior views of typical blooper box. (AFSWC photos)

Figure 2.25 Shielding in typical blooper box. (AFSWC photo)

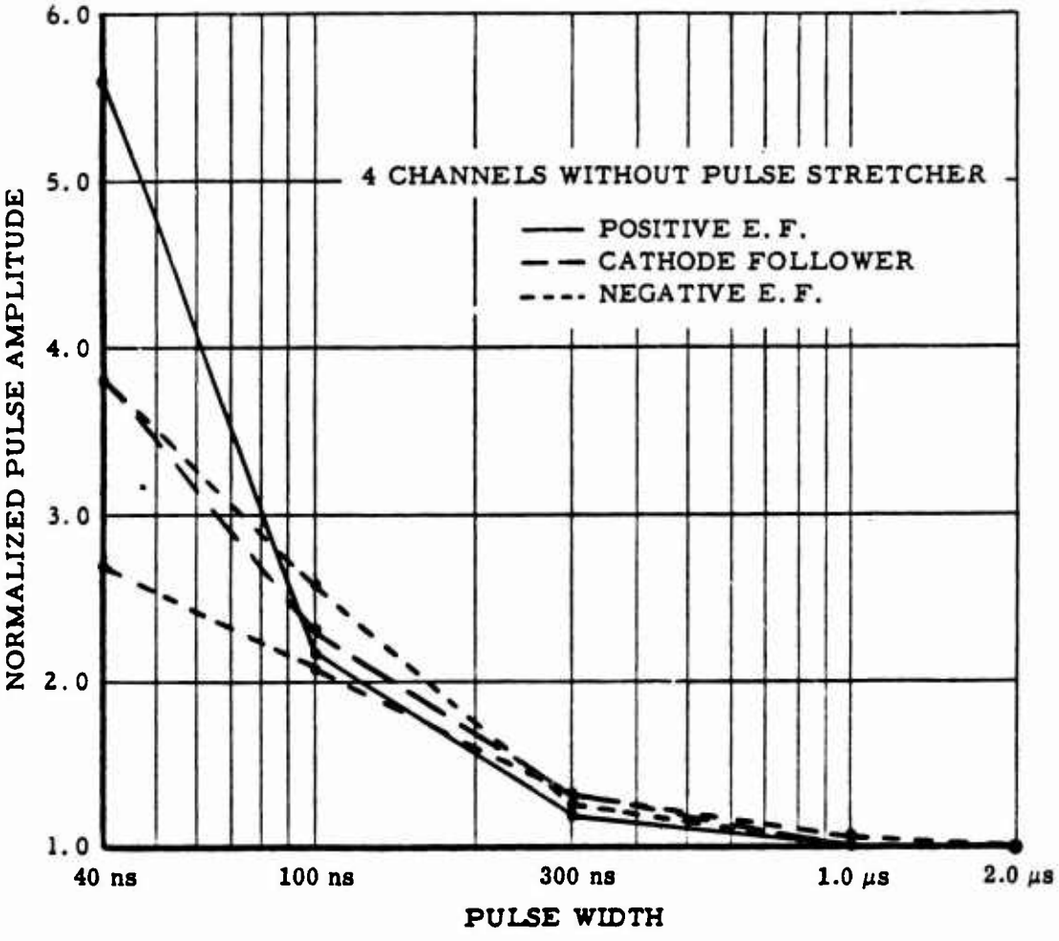

Figure 2.26 Normalized pulse width versus pulse amplitude to trigger (four channels without pulse stretcher).

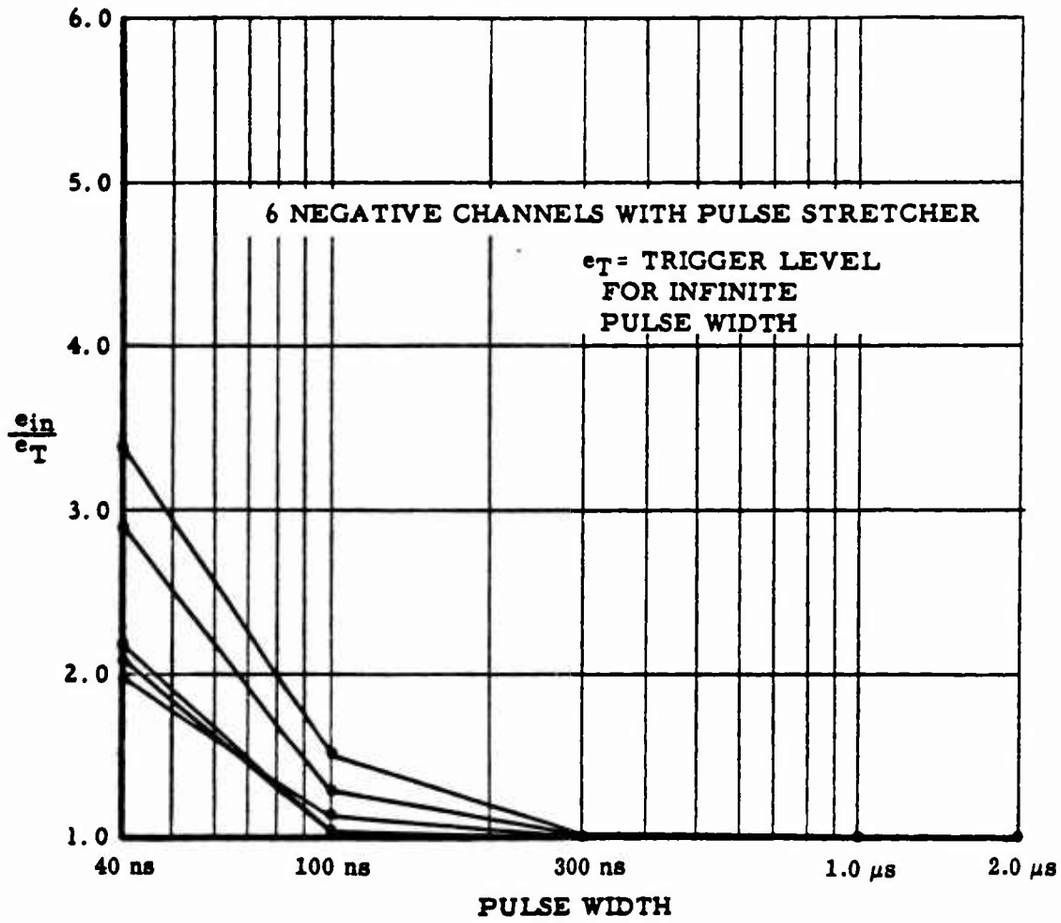

Figure 2.27 Normalized pulse width versus pulse amplitude to trigger (six negative channels with pulse stretcher).

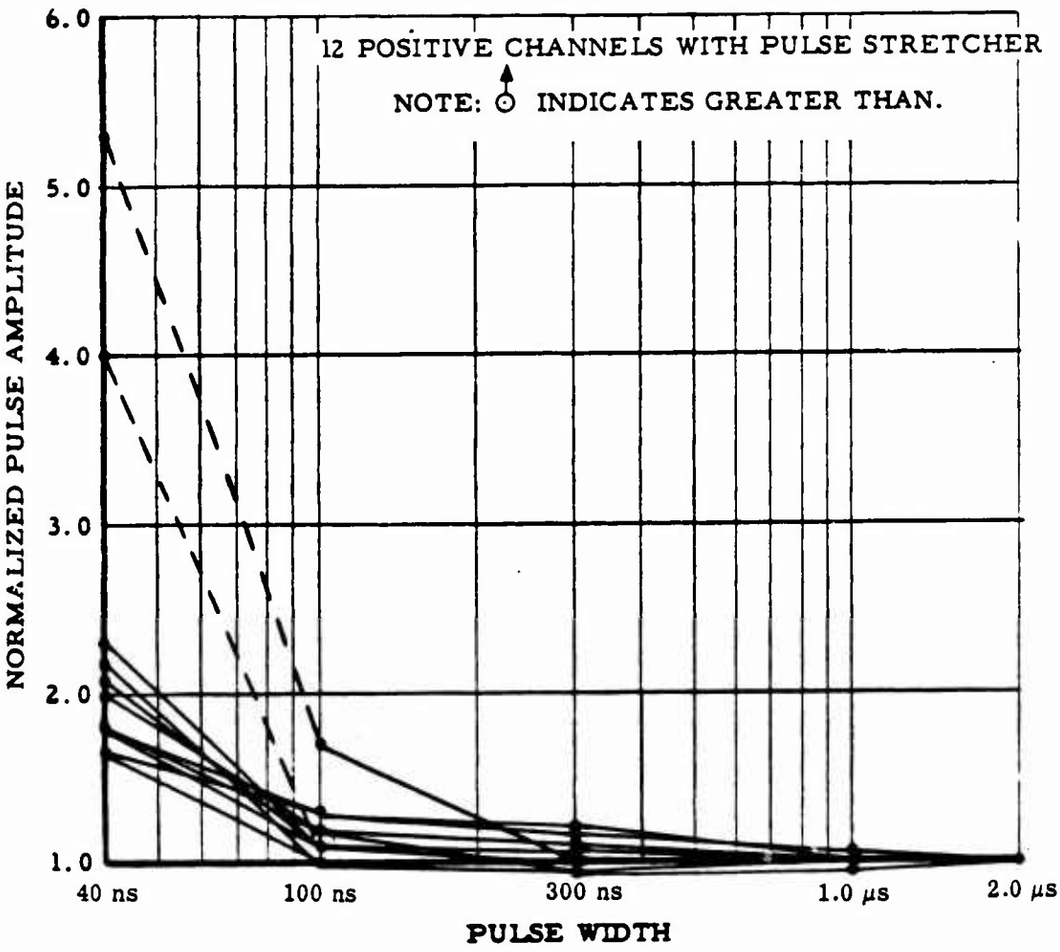

Figure 2.28 Normalized pulse width versus pulse amplitude to trigger (12 positive channels with pulse stretcher).

Interior view of bunker from entry. Note oscilloscope with cameras installed, cable routing, and overhead equipment shelf with temperature recorder and power supplies installed.

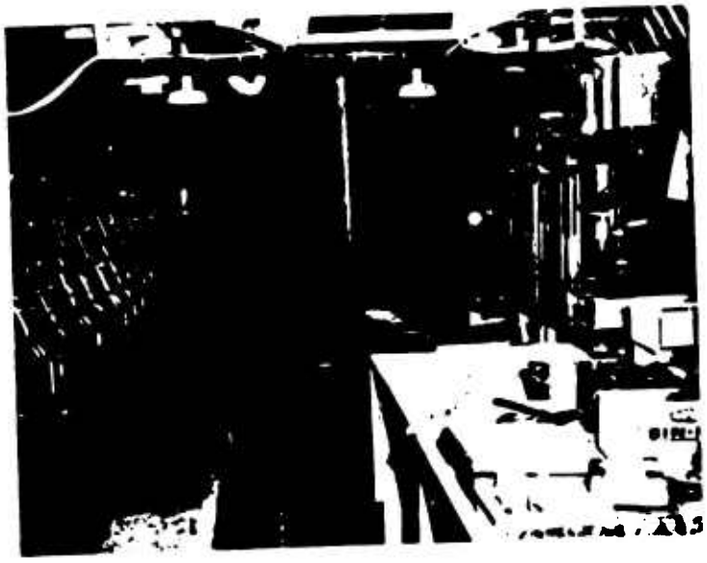

Interior view of bunker toward entry. Note (from foreground to background) acoustic insulation over M-G set, programmer rack, two tape recorders, bench with oscilloscopes installed and entry with ladder in place.

Figure 2.29 Bunker interior. (AFSWC photos)

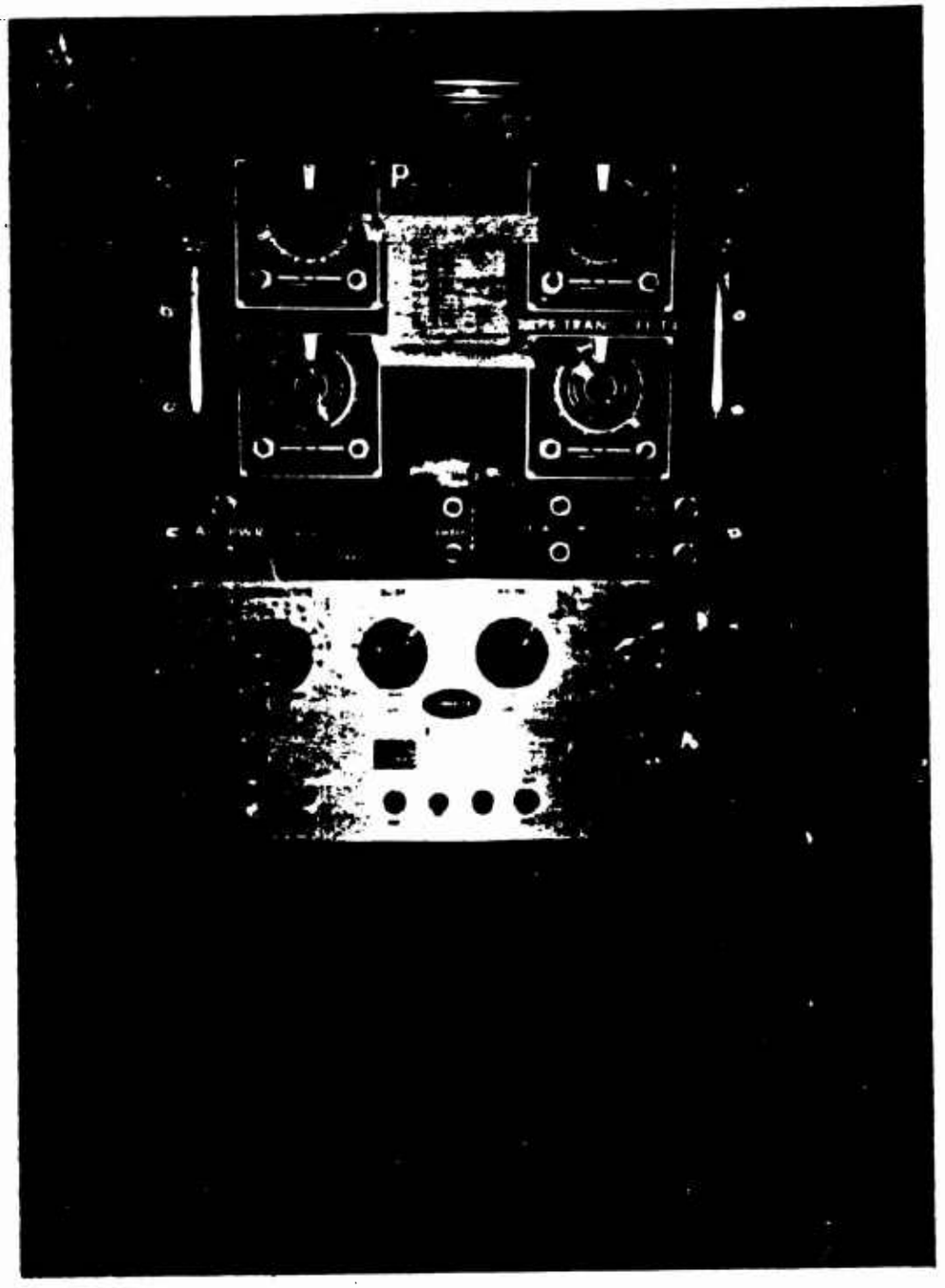

Figure 2.30 Programmer, diagnostic station. (AFSWC photo)

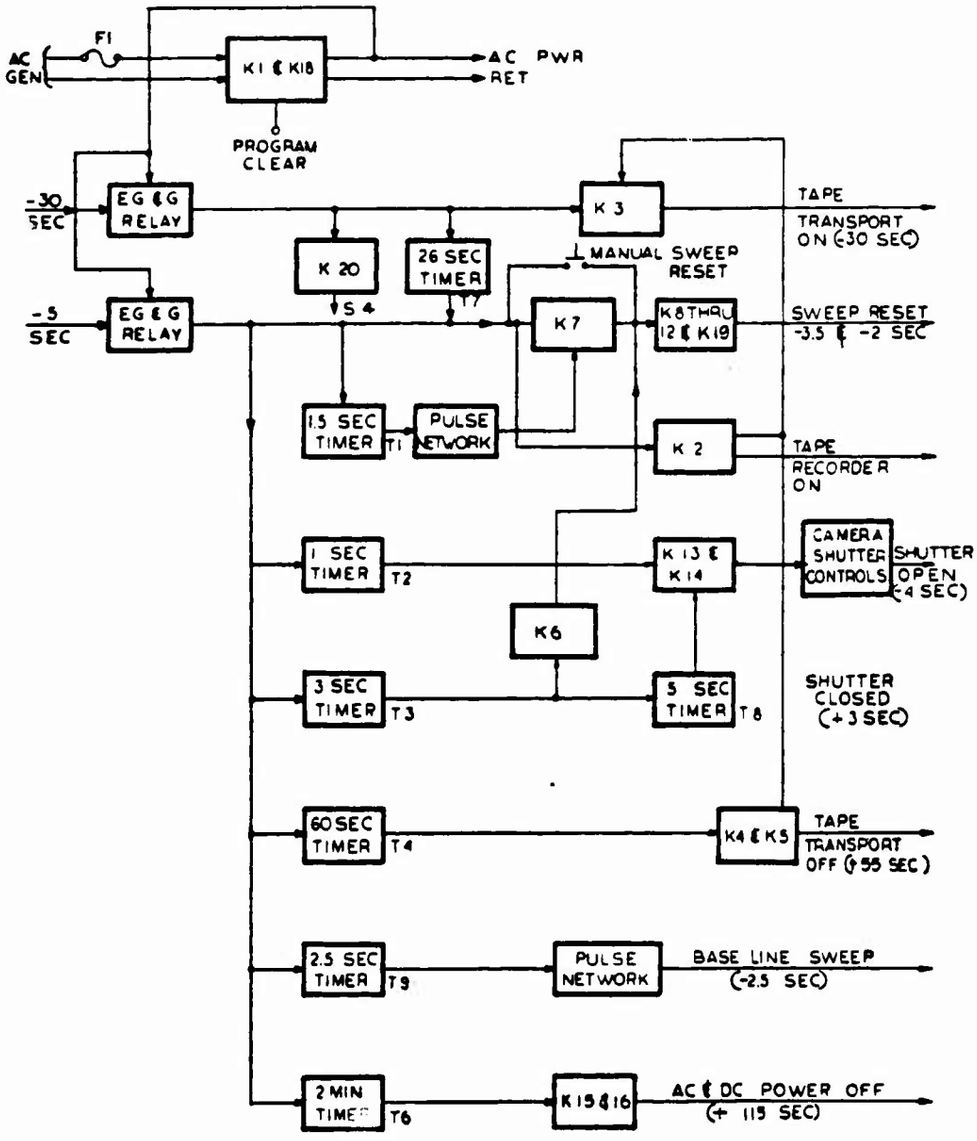

Figure 2.31 Block diagram, programmer.

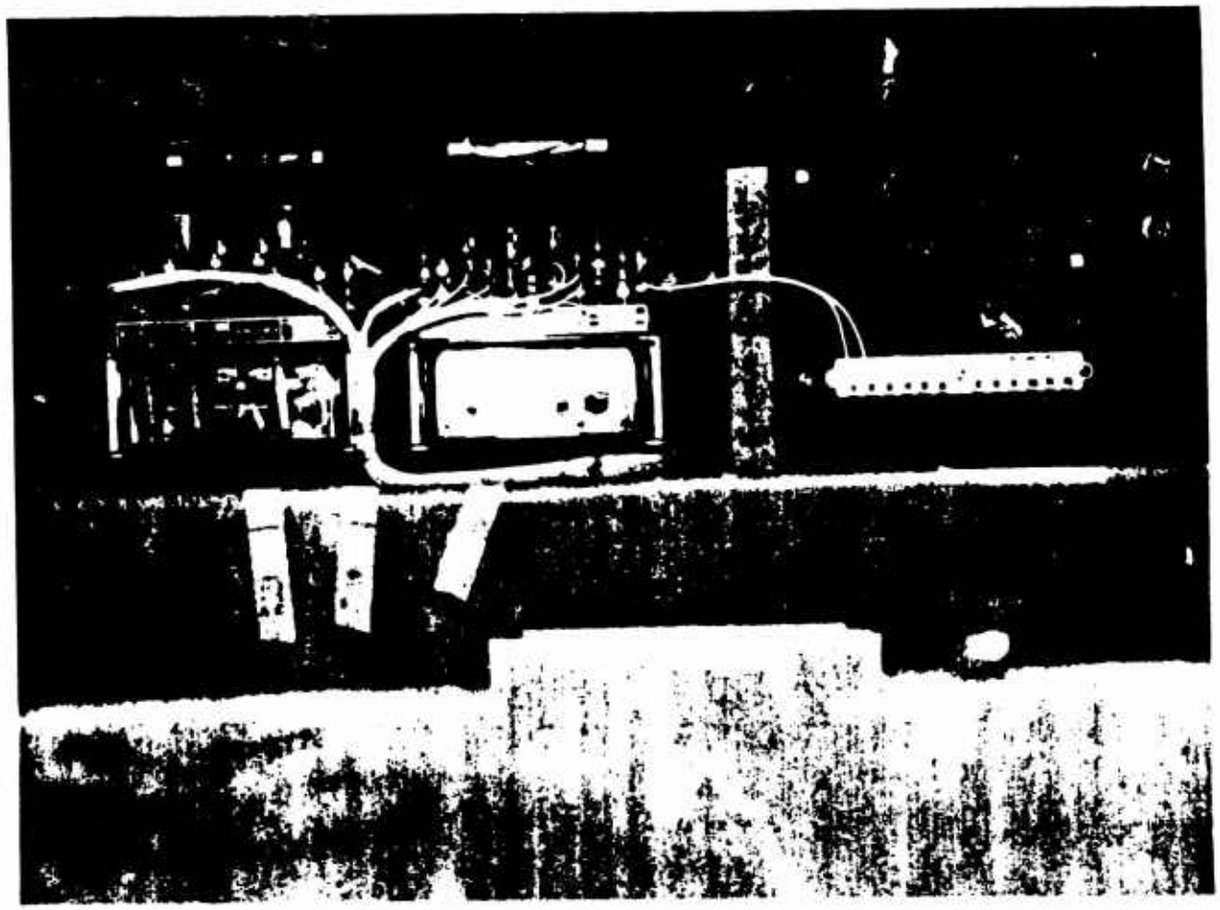

Figure 2.32 Guillotine control box and EG&G timing relays. (AFSWC photo)

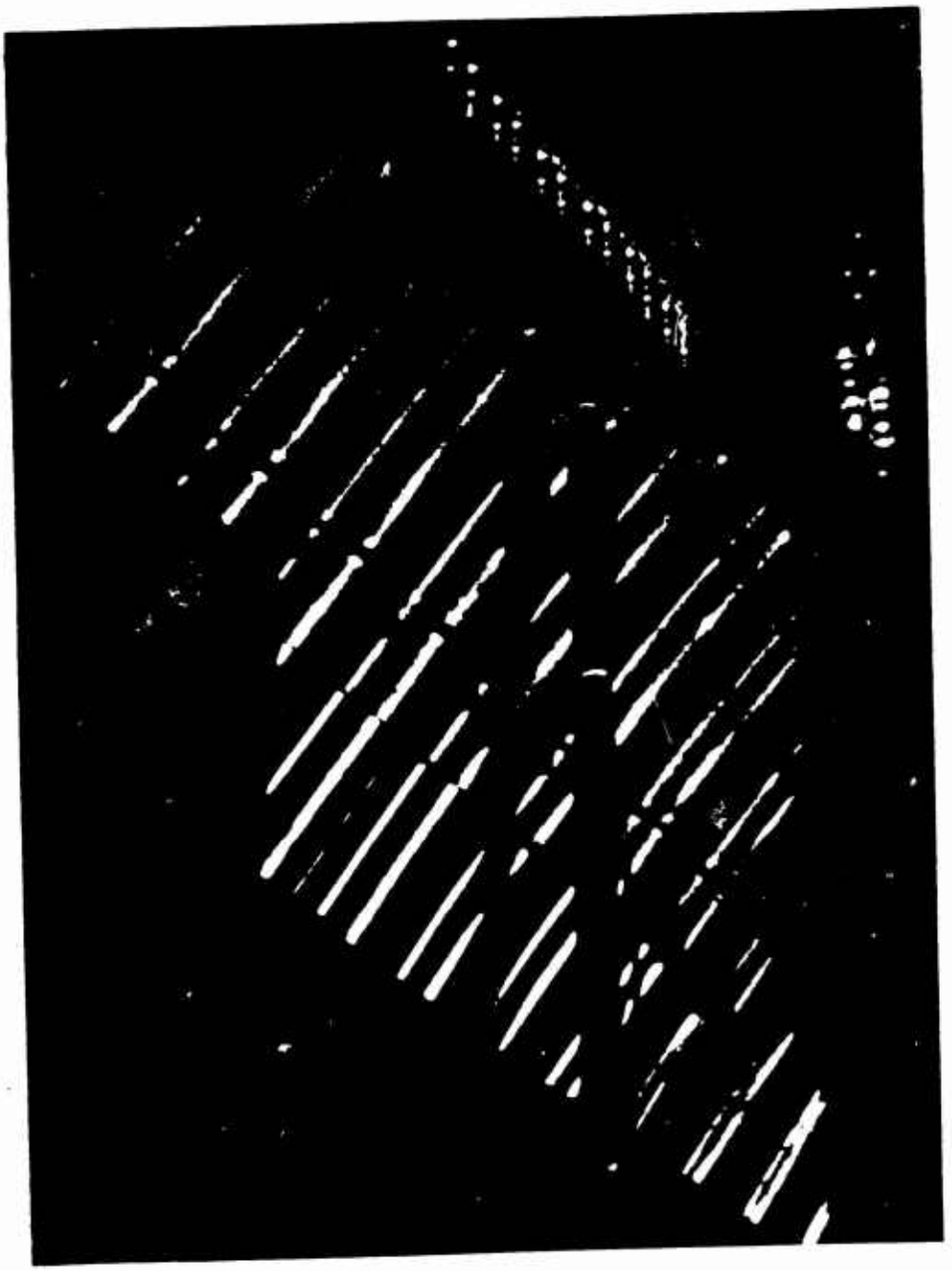

Figure 2.33 Coaxial cable installation in diagnostic station. (AFSWC photo)

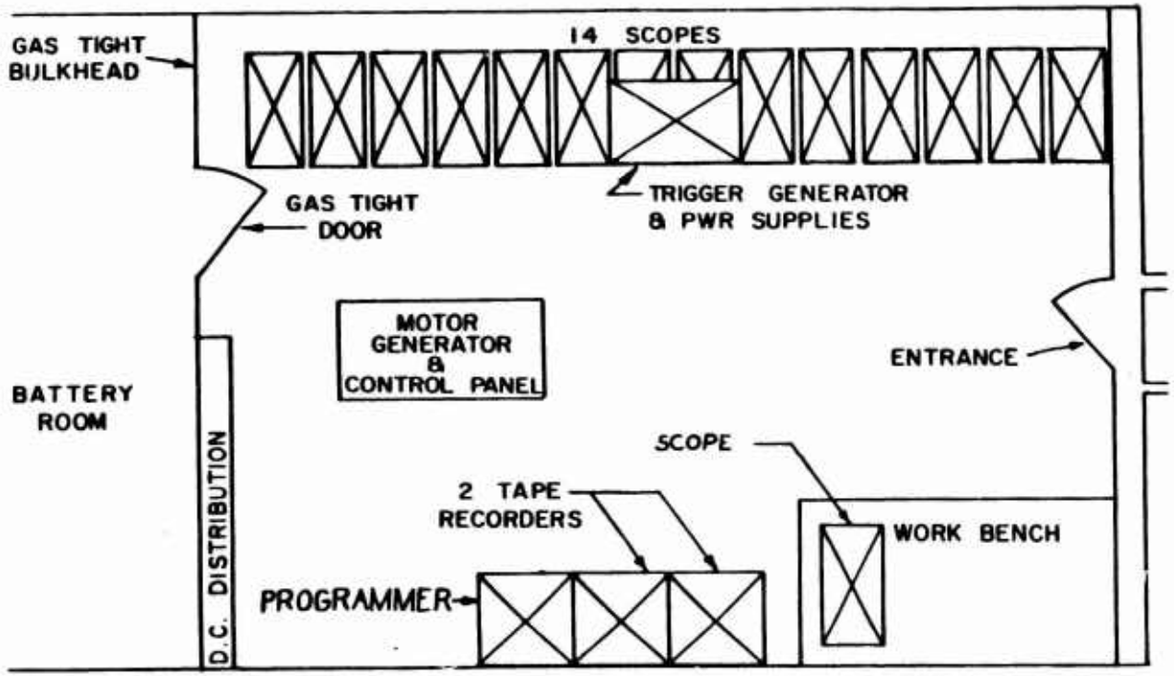

Figure 2.34 Plan view, diagnostic station.

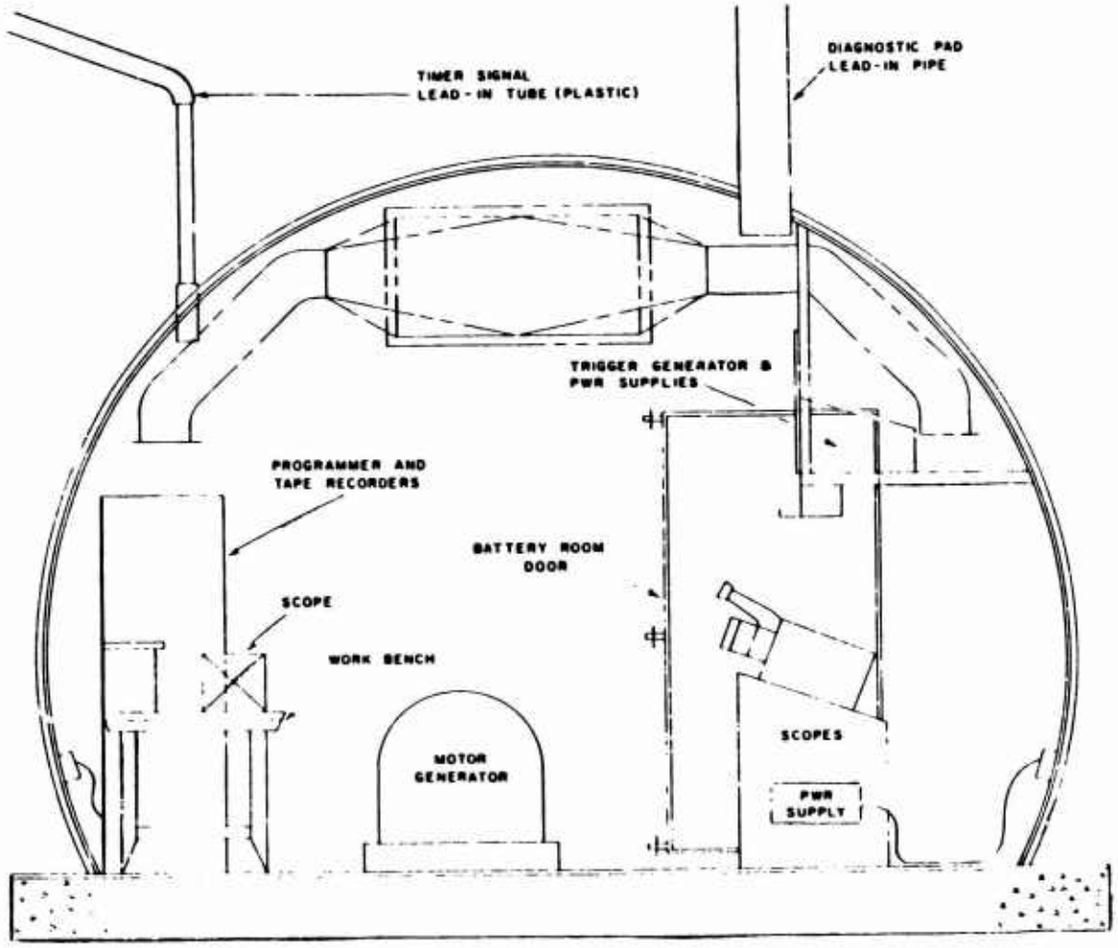

Figure 2.35 End view, diagnostic station.

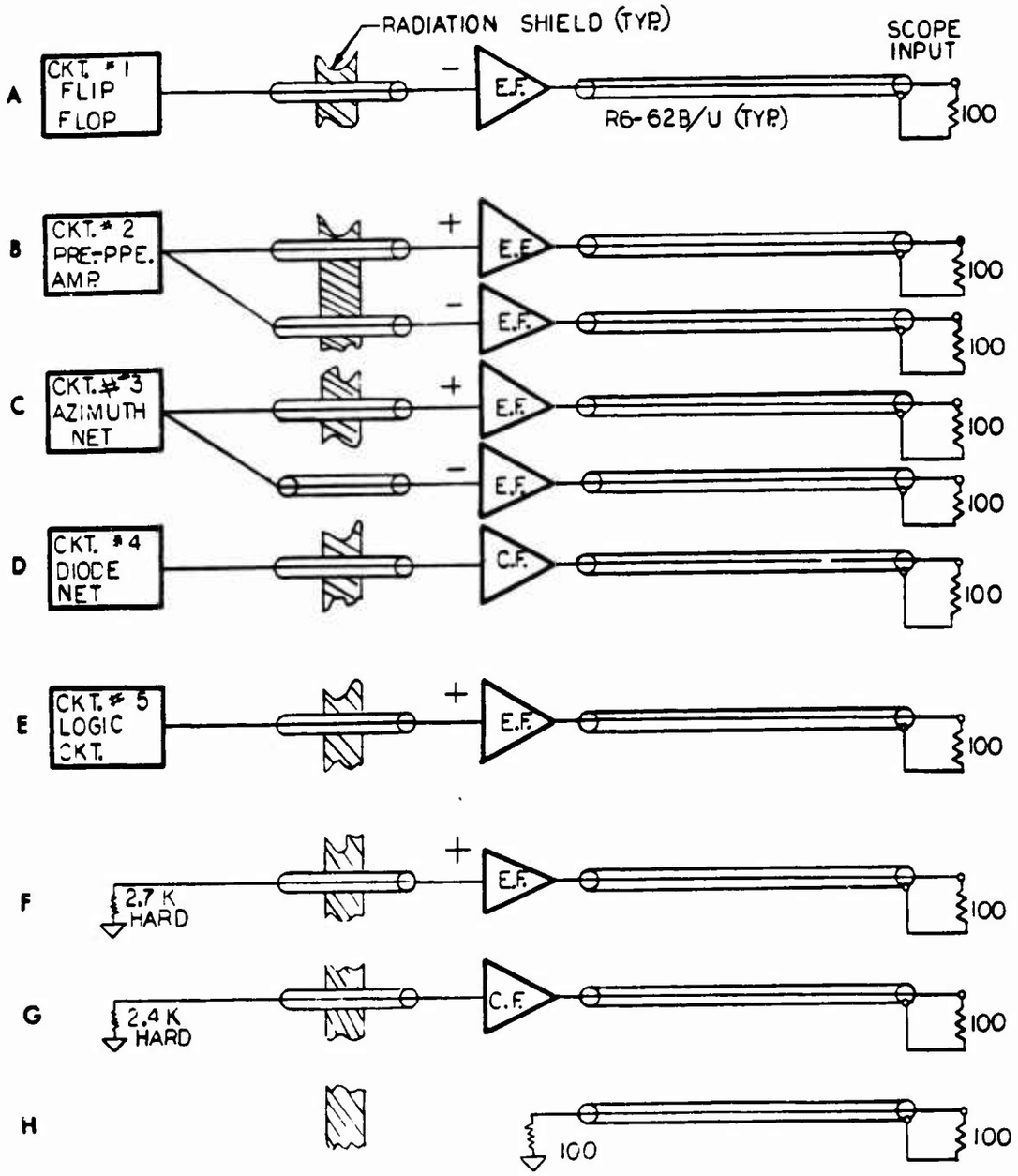

Figure 2.36 Block diagram, diagnostic instrumentation.

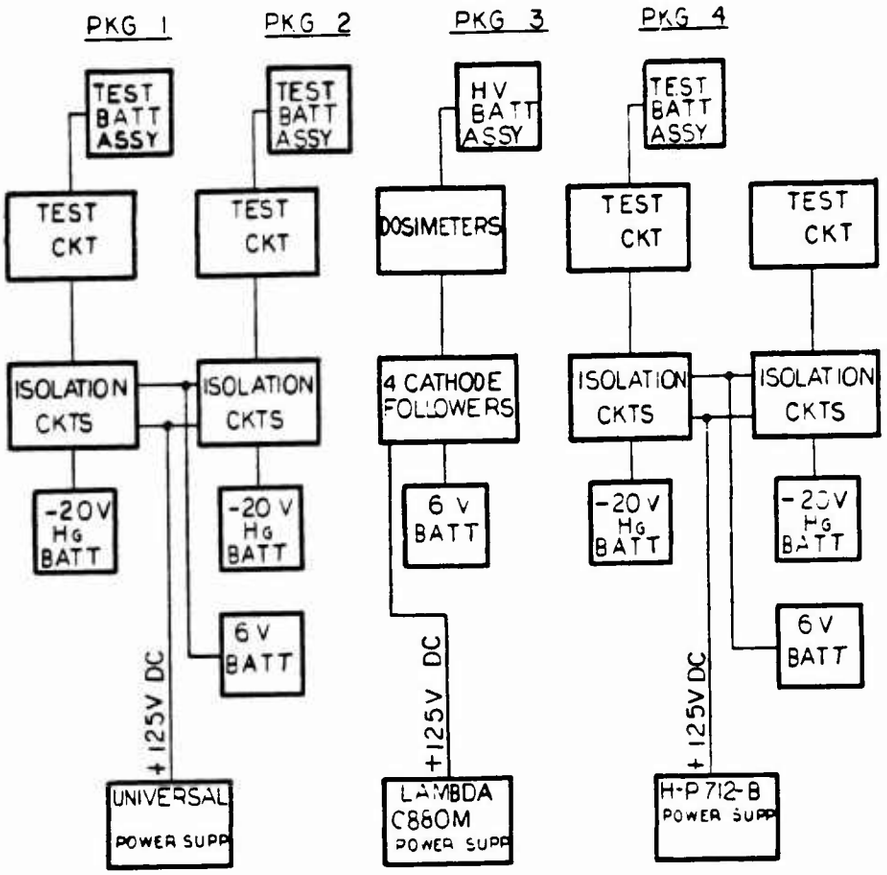

Figure 2.37 Block diagram, diagnostic power supply.

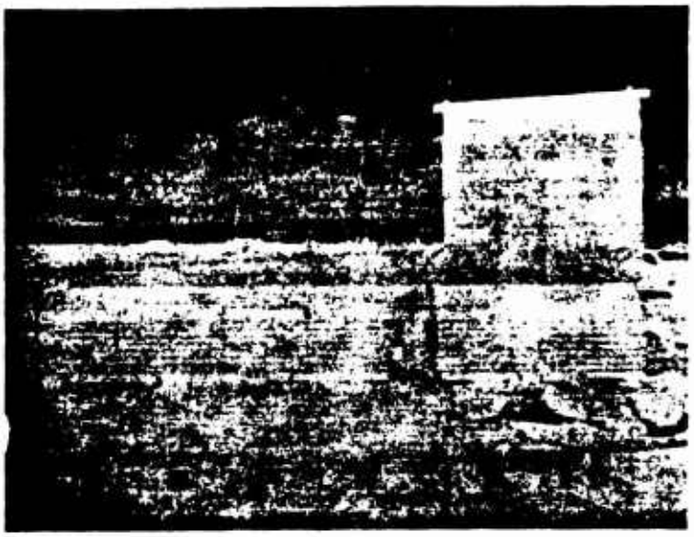

Diagnostic pad 5.614. Dust shack in rear is awaiting placement over bunker entry.

Diagnostic pad 5.614 and bunker entry with wooden cover in place. Sand bags have been removed from entry cover.

Figure 2.38 Diagnostic station, ground view. (AFSWC photos)

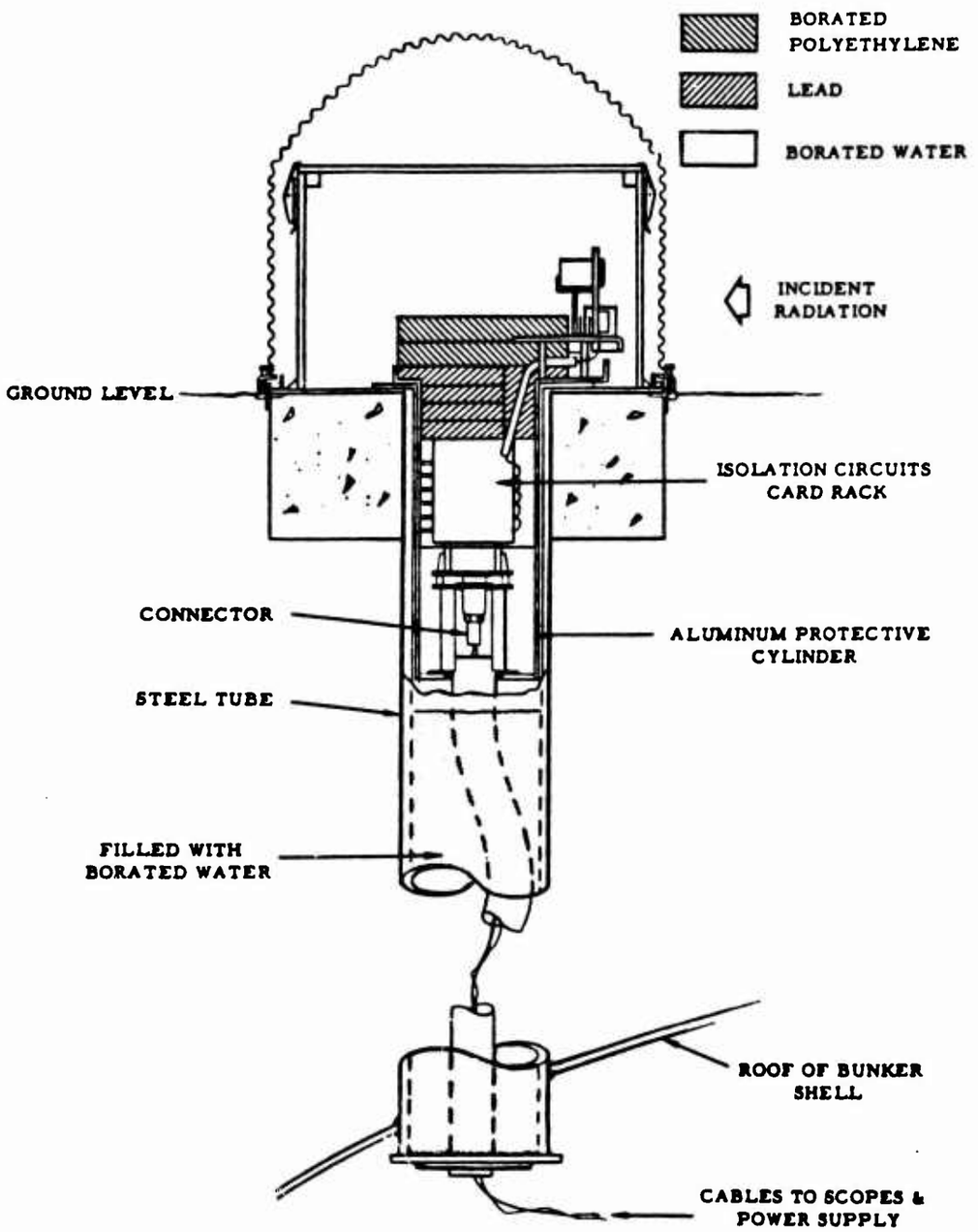

Figure 2.39 Diagnostic package installation

Figure 2.40 Typical diagnostic package installation with shielding in place. (AFSWC photo)

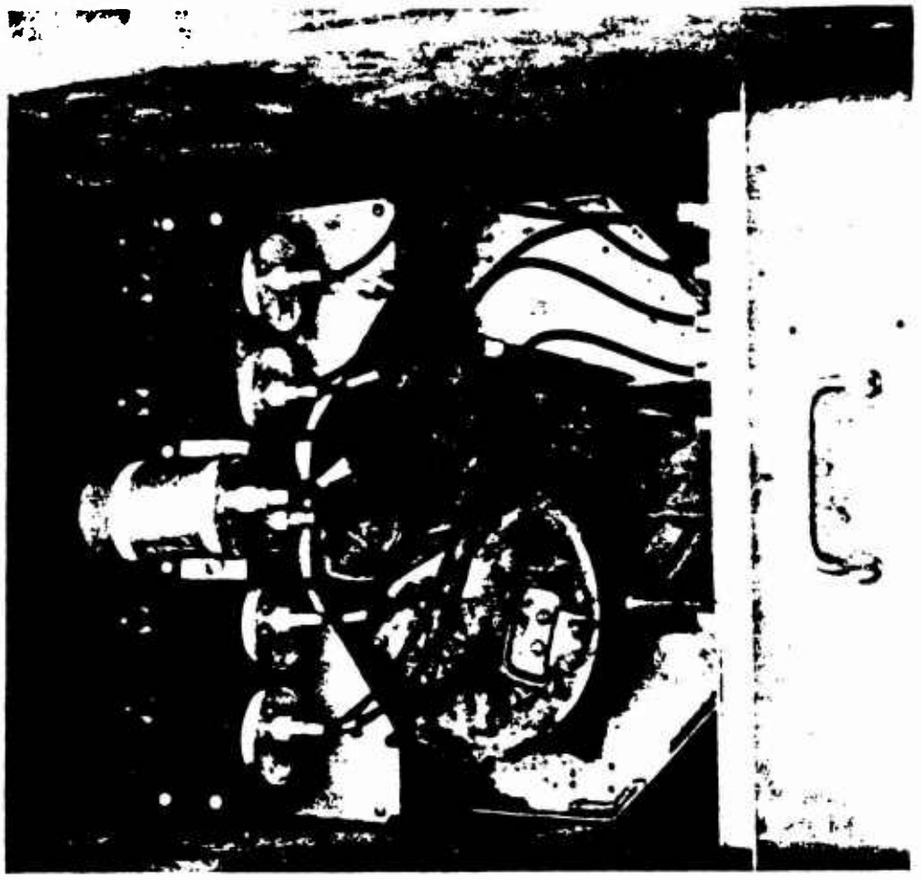

Figure 2.41 Scintillation detectors. (AFSWC photo)

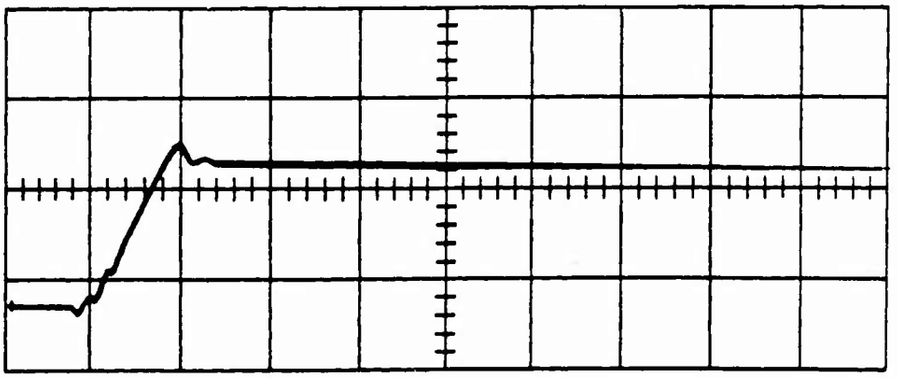

Channel 15, dosimeter 3, package 3, scope 8. Sweep speed 0.05 μsec/cm, vertical sensitivity 1 v/cm. Electronic pulser input.

Figure 2.42 Scintillation detector calibration, Channel 15.

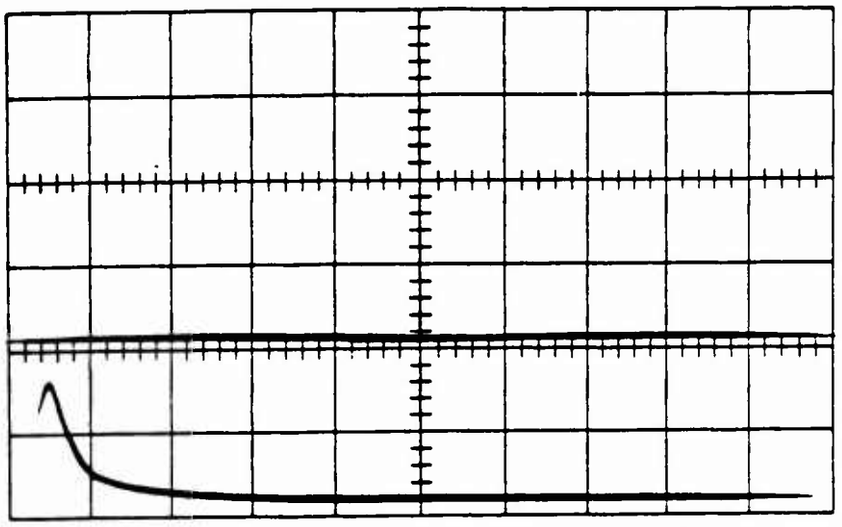

Channel 14, dosimeter 2, package 3, scope 7. Sweep speed 0.5 μsec/cm, vertical sensitivity 1 v/cm. Xenon wink light input.

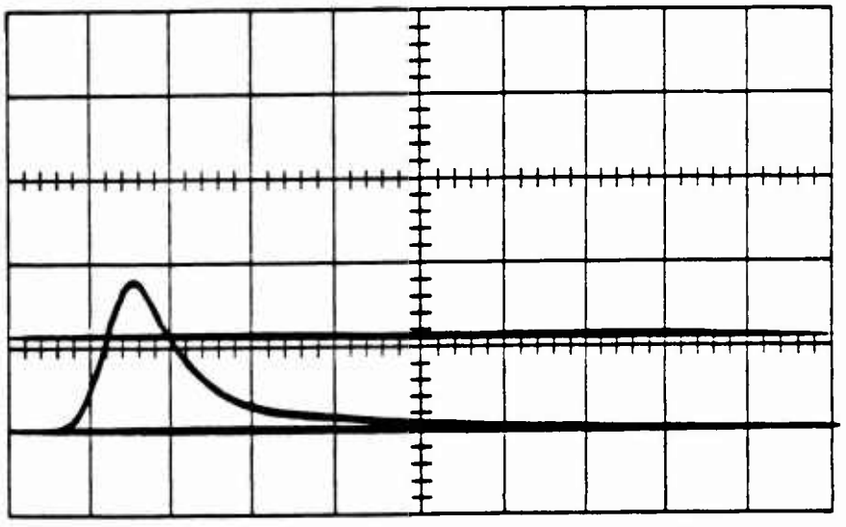

Channel 14, dosimeter 2, package 3, scope 7. Sweep speed 0.2 μsec/cm, vertical sensitivity 1 v/cm. Xenon wink light input.

Figure 2.43 Scintillation detector calibration, Channel 14.

CHAPTER 3

RESULTS AND DISCUSSION

3.1 GENERAL SHOT DATA

A device with a yield of was detonated ten feet above the ground. All instrumentation stations were located in the Frenchman Flat area of the Nevada Test Site. The locations of the four blooper stations and the diagnostic station are shown in Figure 3.1. Field test specimen locations are given in Table 3.1. Detailed information on the Small Boy device is given in Table 3.2.

3.2 DATA RELIABILITY

Eleven of the 144 blooper channels were invalid as a result of malfunctions or incorrect switch sequencing corresponding to a loss of data of approximately 7.5 percent. Although the slow gamma trigger failed to function at the 7,500-ft station (528.14-2), it does not adversely affect the reliability of the data, since the trigger served only to remove power from the instrument pads at H + 3 msec. All packages were removed within 72 hours after the shot. Fuse data were then tabulated and all blooper channels recalibrated. A summary of the fuse data is shown in Table 3.3.

All oscilloscopes at the diagnostic station triggered properly during the test. Polaroid pictures from the oscilloscope cameras were recovered at H + 1.5 hours. The five photodiodes at the diagnostic station functioned correctly during the test. The oscilloscope photographs from the diagnostic station are shown in Figures 3.2 through 3.9. Temperature recordings made at strategic locations in the diagnostic station between H-4 hours and H + 2 minutes indicated no significant temperature increase.

The two magnetic tape recorders operated before, during and after the radiation pulse. However, most of the transient signals from the test circuit specimens were below the voltage levels of the record amplifiers. Data were obtained on the photodiode integrating circuits, as discussed in Section 3.3.

3.3 DOSIMETRY

3.3.1 Gamma Dose Rate Measurements.

The output of Detector 3 is shown in Figure 3.5 (Channel 15). The spot at the left indicates the beginning of the sweep. The sweep photo (before retouching) was very dim and, in fact, the leading edge had to

be dashed-in incorporating the expected delay of about 120 nanoseconds between sweep initiation and signal display. It is not clear, however, why the first 120 nanoseconds of the sweep did not appear as a baseline. The apparent oscillatory behavior on this trace is, at least, in qualitative agreement with similar experiments at the Small Boy event made by Dr. Stanley Kronenberg, USAERDL.

The outputs of Detectors 4 and 5 are shown in Figures 3.5 (Channel 13) and 3.6 (Channels 16 and 17) respectively. The bump in the output of Detector 5 at about 77 microseconds is believed real and could be due to fission neutron arrival. The output of Detector 2 is shown in Figure 3.5 (Channel 14). These data were used to supplement data from Detectors 3, 4, and 5 although the primary function of Detector 2 was for the scope trigger system.

These detector data were analyzed based on a Co^{60} dose rate calibration and combined into a composite graph as shown in Figure 3.10. The output trace from Detector 3 was smoothed for this composite graph. The measured peak dose rate (at the bunker) was which compared favorably with the AFSWC and Northrop Ventura predictions of and respectively, scaled to yield. (These predictions were based on information supplied by Dr. John Malik of LASL.) The measured dose rate for times after the peak is considerably higher than Malik's prediction for a device, and is shown in Figure 3.10. The differences shown in Figure 3.10 for times less than about 5 microseconds, are probably a result of ground and air scattering. The actual measurements reported here were made in uncollimated geometry. The differences shown in Figure 3.10 for times greater than about 5 to 10 microseconds are probably a result of fluor hang-up.

The long decay components (about 10 to 40 microseconds) of plastic scintillators can amount to a few percent of the total light output. It is therefore apparent that fluor hang-up must be considered for times after the occurrence of the initial gamma peak, especially after the dose rate has fallen by a factor of 10 or 20 within about 20 to 100 microseconds. Such corrections are presently being performed.

The output from Detector 6 was monitored by tape recorder channels and is shown in Figure 3.11. Based on the detector-electronics calibration (Chapter 2) the gamma dose is about at 200 microseconds and about at 2 milliseconds. Graphical integration of the composite dose rate plot (Figure 3.10) out to 100 microseconds gives about which indicates fairly good agreement.

3.3.2 Gamma Dose Measurements. In Table 3.4 the results of the gamma dose measurements are compared with AFSWC predictions and with extrapolated/interpolated values from Nuclear Defense Laboratory, Edgewood Arsenal (NDL) measurements. The entries in Table 3.4 are generally averages of several measurements. The EG&G dosimeter results are in very good agreement with the predicted values. The Signal Corps glass rod data are higher than predicted because the sensitivity of the rods increases for low energy gammas (<100 Kev). The NDL measurements were made in a different geometry (and on a different radial field line) and therefore, are expected only to show rough agreement.

3.3.3 Neutron Exposure Measurements. Table 3.5 compares the results of the neutron exposure measurements with interpolated values from NDL measurements. Although the measurement geometries (and radial lines) were different, the results show good agreement.

3.3.4 Supplemental Dosimetry. Additional neutron and gamma dosimetry packages were located near the isolated readout circuitry to eliminate the possibility of radiation effects on the associated monitoring circuits. All dosimetry readout indicated that the radiation levels at these locations were below the thresholds for both transient and permanent damage.

3.4 REMINGTON RAND EXPERIMENT

A detailed analysis of the results obtained on the Remington Rand thin film memory unit is given in Reference 6. The conclusions from the Rand document are:

(2) No additional hardware modifications are necessary to harden to the level quoted in (1) above.

(3) Software (programming) routines may be used effectively as hardening techniques.

(4) Increased hardness can be most economically and rapidly achieved through a combination of hardware and software techniques.

(5) There is at present insufficient real time data from which improved hardware hardness design criteria can be evolved.

(6) It would be highly desirable to perform future experiments with real time instrumentation to gather data usable in improving hardware techniques.

3.5 PIECE PARTS, LITTLE FELLER II PACKAGES

As indicated previously, two Little Feller II type packages were exposed at Small Boy to obtain a possible correlation of piece part response in the two weapon radiation environments.

The fuse data (Table 3.6) at the 7,500-ft station shows that the signal in the 2N2187 exceeded +1.2 v. Laboratory tests required dose rates of approximately to produce signals of this level. Therefore, it is assumed that the fuse blew some time after the final button-up operations and was not caused by effects of the radiation pulse.

Table 3.7 shows a comparison of piece parts data from Small Boy and Little Feller II at respectively. The response data for the NS480, 2N705, and 651C4 show a good agreement between the two weapon radiation environments. On Small Boy, two NS480 fuses were set at -0.9 v; one blew, one did not. This information verifies laboratory test data indicating that various specimens of the same type of semiconductor component will show different response characteristics at the same radiation level. No comparison can be made for the IN457 and 2N2187.

Following the completion of the original Small Boy contract, the scope of the program, under joint Northrop Ventura and AFSWC funding, was expanded to include:

(1) A complete analysis of the field data (including magnetic tape recordings) with efforts concentrated on eliminating data outside the anticipated ranges.

(2) A close liaison with other organizations who made measurements of the initial nuclear radiation pulse, in an effort to provide more detailed information on the radiation environments to which the circuit specimens were exposed.

(3) Additional irradiation experiments and analysis at the peak gamma dose rates measured in the field so that comparison data are available from both field and laboratory experiments.

(4) A comparison of field test results with laboratory results to determine how well the laboratory experiments simulate the weapon environment.

(5) An interpretation of the transient response of each type of specimen circuit on the basis of the particular circuit configuration, to ascertain which components and parameters determine relative hardness. In addition, a determination of design parameters which reduce the vulnerability of the circuits based on experimental results and circuit analysis.

The results of these analyses are given in the following sections.

3.6 IBM LOGIC NETWORK

3.6.1 IBM Logic Network Introduction. The IBM G4-1A inverter is an essential building block in the Titan guidance computer system. Interconnection of this type unit with similar units makes up a large portion of the computer arithmetic capability. Binary signals with associated voltage levels of 0v and -8v are used for intercircuit computer communication. To avoid ambiguity, well-defined non-overlapping tolerances must be assigned both voltage levels. The input conditions for the logic network tested in the field were set to result in a nominal -8v output level. The failure criterion was defined as a +1.8v maximum allowable voltage shift (Reference 7), i. e., the circuit was considered to have failed if the output voltage became more positive than -6.2v.

3.6.2 Normal Circuit Operation. In normal operation, the logic network performs both logical manipulation (Reference 8) of the input signals and logical inversion with power gain, as shown in the block diagram in Figure 3.12. Typical node voltages for the case of all inputs at zero volts and at -8 volts (shown in parenthesis) indicate how the state of the output transistor is manipulated by the input signals (Figure 3.13). Since neither the laboratory tests nor the field test were conducted with dynamic input signals, the only case considered is that resulting with all input terminals grounded. The schematic is repeated in Figure 3.14, showing the current distribution in the circuit with input terminals grounded. The input gating networks are not shown because when diodes CR_5 and CR_6 are reverse biased the transistor and its biasing network are effectively isolated. The primary function of the biasing network is to assure that the emitter-base junction of the transistor remains reverse biased for the worst case of base leakage current. As long as the total current from the +30 volt source is sufficient to supply the base leakage current and a small amount of current through CR_7 and CR_8, the emitter junction will remain reverse biased, and the collector current will be approximately equal to the base leakage current. When

the base leakage currents exceed 360 ma the emitter junction of the transistor will become forward biased. A further increase in the base leakage current will result in a corresponding increase in the collector current multiplied by the transistor common emitter current gain. The output voltage variation as a function of base leakage current is shown in Figure 3.15.

The current from the +30 volt source is called the holdoff current. In normal operation the magnitude of the holdoff current is adjusted to result in an output voltage shift less than failure at the maximum expected leakage current. The leakage current in this case, however, is a result of an elevated ambient temperature.

3.6.3 Radiation Analysis. Assuming a radiation pulse is long compared to the circuit response time, the qualitative analysis of the peak transient output voltage is identical to the analysis of thermal-induced leakage currents just presented. The curve shown in Figure 3.15 should therefore be applicable to the radiation case as well. The relation of the abscissa of the curve to the peak dose rate of the radiation pulse is a slightly nonlinear function. Both this factor and the radiation effects of the other circuit components make the quantitative relationship relatively weak. The transistor effect is certainly predominant.

In a practical radiation environment the pulse width is usually not long compared to the rise time of the circuit when irradiated with a square radiation pulse. If the pulse width is short compared to the circuit rise time and quite nonuniform in shape, (e.g., the weapon radiation pulse), the peak output voltage of the transient will be closely proportional to the total dose integrated over the short radiation pulse time interval. Basically, the only thing that has changed from the steady-state or long-pulse analysis is that the leakage current is now a function of time as well as of radiation intensity. If similarly shaped pulses were compared it would be expected that the curve of Figure 3.15 would again be generally reproduced. The curve now would be a function of the peak dose rate or integrated dose of the radiation environment being investigated.

While the discussion up to this point has considered only the effect of the transistor leakage currents, it is pointed out that the radiation-induced photocurrent of the zener diode will result in a significant circuit effect. The diode photocurrent increases linearly with radiation dose rate. The rise time should be shorter than that of the transistor since conduction is sustained mainly by avalanche multiplication. The magnitude of the effect is somewhat uncertain (Reference 9). The net result of the zener diode photocurrent will be to decrease the reverse bias on the transistor and thus lower the threshold point for

failure. If the diode is irradiated separately from the rest of the circuit, the decrease in bias voltage may cause the transistor to turn on.

A slight improvement in the transient behavior of the logic network could be obtained by reducing the magnitude of the collector supply voltage. The transistor manufacturer states that a significant number of extra carriers contribute to the bias leakage current. This is a result of carrier multiplication in the collector depletion region when the collector is reverse biased by more than 7 volts. The quiescent leakage current can be reduced by about 40 percent by decreasing the collector supply voltage from -8 v to -6 v.

Flash X-ray experiments performed on the logic network after Small Boy showed a response very similar to that observed for a single reverse-biased diode. The results are shown in Figure 3.16a and are consistent provided the emitter junction remains reverse biased and no charge will accumulate in the base region to result in a secondary response. The rise time of the transient response appears to be comparable to the 0.2 μsec radiation pulse width. For experiments in which the radiation pulse width is short compared to the circuit rise time, the peak transient output of the circuit will be closely proportional to the total dose in the pulse. When the radiation pulse is long compared to the circuit rise time the peak output voltage is proportional to dose rate. Since most of the experimental data are for pulses neither long nor short compared to circuit rise time, comparisons must be made carefully to avoid confusion.

When the maximum leakage current exceeds the threshold level, charge accumulation in the transistor base region will result in an additional forward biasing effect which will increase the peak transient output and pulse width. In order to simulate this effect in the flash X-ray, the hold-off current was decreased by reducing the +30 volt source. A typical waveform observed and a summary of the results are shown in Figures 3.16b and 3.16c. The decrease in hold-off current essentially results in a decrease in the threshold level as shown.

Summarizing, it might be expected from experimental and field test results that once the failure criterion has been exceeded, only a slight increase in radiation intensity will cause a significant increase in the transient output. In determining the radiation level necessary to cause failure, the effects of zener diode photocurrent and collector multiplication will tend to decrease the predicted level required.

3.6.4 Discussion of Field Test and Pre/Postshot Experimentation. Data recorded at the diagnostic stations did not determine the peak transient outputs. The photographs shown in Figure 3.2

(Channel 4) are typical of the results on the three powered channels. It can be seen that the peak output was much greater than 50 mv, but an exact estimate is not possible. The long term decay of the output pulse, shown in Figure 3.7 (Channel 21), is much longer than that observed in the laboratory. Since the time involved is long compared to the normal circuit rise time, the trace reflects the response of the circuit to the long, low-level decay of the weapon gamma radiation pulse.

The format for presenting the blooper data, as shown in Figure 3.17, will be generally the same for presenting all the blooper information. An "x" indicates the threshold level at which a fuse was blown; "0" indicates the threshold level corresponding to an unblown fuse. It therefore follows that a peak transient output must be equal to or greater than the threshold level at which the fuse was blown. This voltage range is indicated by a solid line. Conversely, the transient output could not have been greater than an unblown fuse level. The voltage range over which the signal presence cannot be defined is indicated by a dashed line. Separate vertical scales are used for each test circuit for clarity.

Referring to the results shown in Figure 3.17, all samples at Pad A failed, and probably saturated. At Pad B, the blooper results indicate that the logic circuits were close to the threshold levels. It is also reasonable to assume that the variation between thresholds for different units is sufficiently large to allow a 1.0-v signal at Pad A3 and less than 0.7-v signal at Pad B.

[illegible] results at Pad C3 are compatible with other information. [illegible] fuse in the logic network channel in Pad C1 was blown before the shot. The output transient less than 0.4 v at Pad D3 is also [illegible]e consistent. The two blown fuses at Pad D3 resulted from failure of the slow gamma trigger to deactivate power on the package, and the data is unreliable.

Experimental investigation, as well as preliminary circuit analysis (Reference 11) has been performed independently (References 9 and 11). The results of the circuit analysis depend heavily on the assumed value of the zener diode photocurrent. Although the results are preliminary, the analysis indicates the familiar threshold curve. Using a relatively wide pulse (compared to the weapon pulse) of about 0.3 μsec, the failure level was reached at a peak dose rate of from for a radiation pulse corrected to the energy spectrum of the weapon pulse. The variation in level is due to a 10:1 variation in the zener diode photocurrent. As discussed previously, the increase in diode photocurrent corresponds to a decrease in the radiation threshold level. Experimental results obtained using 2-Mev gamma rays (Reference 9) indicates that the radiation threshold occurs at a peak

dose rate of approximately for a 0.15 μsec radiation pulse width. The narrower pulse width corresponds more closely to the weapon pulse shape and agrees quite well with Northrop experimental data and field test results.

A good idea of the steady-state response at low radiation intensities is obtained from the bunker photographs. The 10-millivolt signal measured at t=1.0 μsec should correspond closely to the predicted steady-state response at a dose rate of approximately however, available experimental data must be extrapolated over too great a range for a reliable comparison.

Experimental and analytical predictions are summarized in Figure 3.18. It has been shown that relatively low energy flash X-ray radiation produces ionization in the semiconductor more efficiently than does radiation of a higher energy spectrum such as the weapon pulse, or high energy (2-Mev) gamma rays. Considering the different radiation pulse widths used, the correlation between the field results and laboratory/analytical results appears to be very good.

3.6.5 Conclusions of Small Boy TREE Working Group Meeting. On 7 and 8 November 1962 a TREE (transient radiation effects on electronics) meeting was held at the Aerospace Corporation, El Segundo, California, to discuss and correlate the Small Boy results and predictions on the five test circuits. The groups in attendance were personnel who had actually performed the field experiments, representatives of pertinent military agencies, engineers from the manufacturers of the specific circuits and representatives of organizations who had conducted independent laboratory tests and analyses. The official conclusion of the group concerning the radiation vulnerability of each particular circuit is given following the discussion of field test results in each particular section. The Small Boy TREE Working Group established the most probable radiation level necessary to cause failure of the logic network at an integrated dose of The energy spectrum of the radiation is defined as similar to that of the weapon prompt gamma pulse. The pulse width must be specified, because above the maximum of the integration approximation is not valid.

In the field test the IBM logic network failure level radius from the Small Boy device had been estimated at approximately For comparison with the meeting conclusions, the integrated dose at Pad B

therefore the conclusion of the group appears to be a good approximation.

3.7 PRE-PREAMPLIFIER

3.7.1 Introduction. The Kearfott closed-loop pre-preamplifier is a two-stage Class A transistor feedback amplifier. As the first stage of error signal amplification in the control system feedback loop, the radiation vulnerability of this circuit is an important factor in system vulnerability. Four feedback paths are included in the circuit to increase thermal stability, to provide linear amplification over a wide range of input signal amplitudes, and to stabilize the overall circuit voltage gain. The failure criterion for the pre-preamplifier was defined by Kearfott as a 6-volt signal with a pulse width of at least 1 millisecond.

3.7.2 Normal Circuit Operation. In normal operation the pre-preamplifier is a low-level linear amplifier. Referring to the schematic diagram in Figure 3.19, the dc feedback path through R_5 provides the base current required to maintain Q_1 in the linear region. This method of biasing also allows for variations in the operating point due to temperature variations. Diode CR_1 provides protection for Q_1 in the event of a large negative transient at the input. A reverse bias of more than 8 volts on the emitter junction of Q_1 could cause failure. The function of C_3 is to reduce the circuit gain for all frequencies higher than required, to avoid high-frequency oscillation. The overall gain of the amplifier is closely controlled by the feedback from the collector of Q_2 to the emitter of Q_1. Since the open-loop gain of the amplifier is much greater than the closed-loop gain, the absolute value of the overall voltage gain is determined by the circuit constants rather than by the transistor parameters. The collector load of Q_2 consists of two resistors because of the power limits specified for the miniature resistors used in the circuit assembly.

3.7.3 Radiation Analysis. At radiation levels below 10^8 r/sec the transient behavior of the pre-preamplifier is almost entirely determined by the semiconductor photocurrents. The time-varying charge distribution in the semiconductors, determined by the net result of the photocurrents, controls the amplitude and polarity of the major portion of the transient response. First, consider the photocurrent effect in each semiconductor device separately. The photocurrent of Q_2 alone will cause a negative going output transient. Similarly, the photocurrent of Q_1 will cause a negative going signal at the collector of Q_1. Referred to the output, however, the result of the Q_1 photocurrent is a magnified positive going signal due to amplification in the second stage. The photocurrent of the diode is in the direction to turn Q_1 off. This effect would produce a negatively going transient at the output. Direct linear superposition must be done carefully because of the feedback effects and finite signal propagation times. If one or both of the transistors reaches the limit of its active region, the superposition becomes much more difficult to apply.

Extensive analog computer analysis as well as experimental studies have been done by other investigators (References 10 and 11). The qualitative results of the Boeing computer analysis (Reference 10) generally indicate that the output transient displays three distinct regions. These are: a prompt, relatively narrow negative pulse immediately followed by a larger and wider positive pulse which is followed, in turn, by some sort of long term recovery with a decay time constant of about 25 μsec. It has been shown, both analytically by the Boeing Co. (Reference 10) and experimentally by Hughes Aircraft Co. (Reference 11) that the two pulses are the result of the prompt photocurrents of Q_1 and Q_2, as previously discussed. The secondary response was disturbed as a result of the net charge deposited by the photocurrents of Q_1 and CR_1. Since these currents subtract at the base node of Q_1, the recovery may be either positive or negative, depending on whether the transistor or diode photocurrent predominates. The 25-μsec time constant arises from the discharge of C_1 through the resistance of the parallel combination of R_3 and R_8.

The failure criterion has been defined by the Kearfott Division, General Precision, Inc., in terms of energy required at a frequency of 20 kc, based on system response considerations (Reference 12). Any transient output must therefore have a pulse duration of 25 μsec to have any energy for this frequency component, or 50 μsec to have a significant portion of the transient output appear as a system disturbance. Considering the dynamic output range of the pre-preamplifier as ± 6 volts, a radiation-induced transient must have a minimum pulse width of 1 millisecond to cause system failure. Analytical techniques capable of predicting storage times, which would be necessary to get a 1-millisecond pulse, are not presently available. Experimental data indicate that the required intensity to produce a pulse width much greater than 100 μsec is beyond that conveniently available in a laboratory environment (i.e. $>10^9$ r/sec.).

3.7.4 Discussion of Field Test and Pre/Postshot Experimentation.

The results obtained from the pre-preamplifiers exposed at the 5700-ft diagnostic station are shown in Figures 3.2 and 3.9, corresponding to Channels 2, 28 and 29. The validity of Channels 28 and 29 is questionable. Both signals are negative-going-on-positive channels. Little quantitative data can be inferred, since the response of these channels is not reliable for negative signals greater than 0.3 volts at the input. The character of the recovery, however, is consistent with laboratory observations. On Channel 2 the peak output voltage is approximately -1.3 volts. The time constant of the negative recovery is difficult to measure, but appears to be between 15 and 25 μsec. This corresponds very well to the analytical results already presented (Reference 10).

The results of the positive and negative response channels at the four blooper stations are shown in Figures 3.20 and 3.21. The results at the 2,800-foot station indicate that the peak positive excursions were probably on the order of and the peak negative transients were about This is consistent with postshot testing, but not with the analytical predictions. This point will be discussed later in detail.

At the 4,150-foot station, the variation in unit-to-unit response observed in postshot flash X-ray experiments is apparent. Sample waveforms observed are shown in Figure 3.22. The transient signal levels recorded agree very well with experimentally observed laboratory results and with the analytical predictions. Limitations on blooper channel sensitivity restricted the value of the information. The lack of blown fuses at the 5,700- and 7,500-foot pads is consistent with the diagnostic results and experimental data as well as with the analytical predictions.

Based on the field test results, the postshot experimental program was oriented in two directions. Because of the large variation in response from one sample to another, a large number of the pre-preamps were irradiated in the Northrop Flash X-Ray Facility. A few of the observed responses are reproduced in Figure 3.22. Since the variations between units was in fact very significant, the main characteristics of the unit responses are shown in Table 3.8. The response of the pre-preamp to high-intensity radiation was investigated using direct irradiation with 27-Mev electrons from the General Atomic linear accelerator. A comparison of the results shown in Figures 3.23, 3.24 and 3.25 shows that different pulse widths were used. The main reason for this was to obtain a good signal-to-noise ratio for interpreting the beam monitor signal. The responses of three different units are shown, comparing the flash X-ray response of each unit to the response for increasing radiation intensities using the Linac. There is a very significant shift favoring a negative response at high radiation intensities. This agrees extremely well with the blooper data at Pad A but is not predicted analytically. While an explanation of this effect is not available, the most likely cause would be a decreased charge collection on Capacitor C_1, probably due to charge trapping in C_1. Other possible effects, or contributing effects, are nonproportional increase in the semiconductor photocurrents and/or nonlinear effects in the transistors. However, it is felt definitely that the responses shown are due to the pre-preamplifier transient output, as opposed to radiation effects on the instrumentation or power supply systems. Further work is necessary to determine the cause, especially since no orientation or waveform distortion problems were observed in flash X-ray experiments.

3.7.5 Conclusions of the 7 and 8 November Small Boy TREE Working Group Meeting. Although there was some doubt, the official conclusion of the 7 and 8 November meeting of the Small Boy TREE Working Group was that the pre-preamplifier did not fail in the field test environment. It was firmly agreed that saturation occurred at the maximum radiation level but a transient pulse width long enough to exceed the failure criterion was not reported. It has since been determined that the circuit did not fail at the maximum field intensities.

3.8 DIODE DETECTOR

3.8.1 Introduction. The diode detector is an essential element in the Hughes GAR 4A missile system. In the system, the input to the detector is an amplitude-modulated signal consisting of a 3 to 4 volt, 1600-cps carrier, modulated with a low frequency signal of approximately 200 cps (Reference 13). No failure criterion was supplied, but it would appear that a 1-volt transient output, with a pulse duration of at least 5 milliseconds, would cause a perceptible system disturbance.

3.8.2 Circuit Operation. The circuit consists of a semiconductor diode to rectify and detect the modulating signal plus a low pass filter to allow only the detected signal at the output. The field test configuration of the diode detector is shown in Figure 3.26. In actual circuit operation the input is capacitively coupled. The voltage across the diode, therefore, is zero, since both the anode and the cathode voltage is equal to the supply voltage. With the simulated source impedance directly coupled, the diode cathode voltage is essentially grounded, reverse-biasing the diode with a voltage approximately equal to the supply voltage.

3.8.3 Radiation Analysis. Extensive investigations, using both computer techniques and experimental analysis (References 11 and 14), have shown that the primary cause of the transient signal is ionization and charge trapping in the output Capacitors C_1 and C_2. The capacitor performance is mainly determined by material constants which are not tightly controlled by the manufacturer (Reference 15). Because of the variation between units, the predicted capacitor performance must be specified as a range of values. Diode photocurrent and ionization-induced shunt leakage paths add to the transient output. The diode photocurrent is proportional to the active volume, which is the depletion layer width plus a diffusion length on both sides of the junction. Since the reverse biasing of the diode in the direct coupled input case increases the width of the depletion layer, the resultant photocurrent will be increased. However, at radiation inten-

sities greater than 10^8 r/sec, the effect of the shunt leakage paths will probably become the predominant second-order effect. At this level the effective resistance of Resistors R_1, R_2 and R_3 is significantly reduced, altering the dynamic charge distribution during the radiation pulse.

3.8.4 Discussion of Field Test and Pre/Postshot Experimentation. Based on preshot test data, the predicted waveform from the diode detector during the weapon pulse would be a rounded pulse (Figure 3.27) with a rise time of approximately and a decay constant of approximately The diode detector signal recorded at the diagnostic station (Figure 3.6 Channel 19), while difficult to interpret in detail, indicates a rise time of based on the assumption that the peak occurs at the end of the oscilloscope trace. The signal level was this point.

Before any attempt is made to correlate the flash X-ray results to the field test, two factors must be taken into account. First, the difference in total dose must be considered, including the appropriate integrating time constant for the circuits. Second. the transient response of the diode detector increases as a function of increasing bias supply voltage; however, it is not a linear relationship. At the relatively low dose rates of the flash X-ray, the deviation from linearity may be due to the non-linear variation in diode photocurrent as a function of reverse bias.

Because of the instrumentation sensitivity limitations, the flash X-ray experiments were performed at higher supply voltage levels than the field test.

Figure 3.6, which shows the transient signal from the diode detector, exemplifies the good agreement between flash X-ray and field test. The variation between the peak response at flash X-ray and the field test may be due to the fact that with the flash X-ray the total dose is delivered in whereas, gamma dose from the weapon is still being delivered after

Referring to the blooper data (Figure 3.28), the transient signal was well below the minimum blooper sensitivity at all but the 2,800-foot station (Pad A). At Pad A the estimated total dose, integrated to 100 μsec was approximately two orders of magnitude greater than that at the 5,700-foot diagnostic station. If linear dependence of output for increasing dose is assumed, the transient signal from the diode detector should have been two orders of magnitude greater than the at the diagnostic station. As shown in Table 3.3, two fuses set at + 0.5v and 0.6v did not blow,

whereas the fuse set for + 1.15v did. The fact that the two fuses set at the lower voltages did not blow can be explained by the variations in diode detector response which have been observed for different test circuits during laboratory testing. Variations in capacitor behavior could also explain the firing of the fuse set at 1.15v; however, this data point appears to be anomalous.

The results of postshot linac experiments were inconclusive. However, at a peak dose rate of about
were observed.

3.8.5 Conclusions of the 7 and 8 November Small Boy TREE Working Group Meeting. **It was officially concluded at the 7 and 8 November meeting of the Small Boy TREE Working Group that the diode detector is hard to at least The diode detector, as used in the GAR 2A and GAR 4A systems, would be less vulnerable than the amplifier and IR detector.**

3.9 AZIMUTH NETWORK

3.9.1 Introduction. The azimuth network is an essential element in the Stellar Inertial Guidance system control loop. It consists of an RC filter, used to shape the frequency response of the loop, whose output is fed into a chopping circuit. The chopping circuit simulates a switch which would short out the output signal for every positive half-cycle of the chopping frequency. The low-frequency input signal is therefore transformed into a signal with the original information but in the frequency range of 10 to 40 kc. The advantages in such a transformation allow the design of a more efficient post-amplifier and result in increased loop stability. A block diagram of the azimuth network and a typical output signal are shown in Figure 3.29. The failure criterion for the azimuth network is a
(Reference 12).

3.9.2 Circuit Operation. In normal operation a 19.95-kc square wave, 4.5 volts peak-to-peak, is used for the chopping signal. Referring to the azimuth network schematic in Figure 3.29, with the chopping signal applied to the primary of the transformer, the transistor will be turned off for every positive half-cycle of the chopping signal and will be turned on for every negative half cycle. In the field test the input signal was simulated by a 30-volt battery. Under this condition, if a chopping signal were applied to the transformer, the output voltage would be approximately 1.9 volts when the transistor was turned off and approximately 5 millivolts with the transistor saturated. Since the field test was required to be a static test, however, the chopping signal generator was replaced with a resistor approximately equal to its source impedance (20 ohms). The dc equivalent circuit for the azimuth network under this condition is shown in Figure 3.30. The transistor emitter diode is slightly

forward-biased and the collector diode is reverse-biased. Since the base resistance is large compared to the normal input impedance of the transistor, the leakage current can be approximated by considering the base lead open. On this premise the leakage current will be on the order of I_{CO}. This estimate is probably pessimistic due to the low voltages applied to the junctions. The open-circuit output voltage in this configuration is approximately 0.4 volt. Because of the high source impedance the transistor will saturate when the leakage current increases to about 42 microamps.

3.9.3 Radiation Analysis. On an intuitive basis the primary circuit transient will be due to the transistor photocurrent. In the design of the circuit for normal operation, capacitors C_6 and C_8 were selected to minimize the transient response of the chopping circuit to voltage spikes produced in the chopping process. The transient signal produced due to the transistor photocurrent will therefore be minimized until the intensity of the radiation is sufficient to increase the photocurrent level to saturation.

When saturation occurs the emitter diode will become slightly reverse-biased because of the high source impedance, and rather than operating in the true saturation region, the transistor will be biased essentially in the inverted region. The net result is that almost no storage time results and output voltage will start to return to its original level as soon as the radiation pulse ends.

The effect of the radiation on the passive components must be considered when the radiation intensity increases to about 10^8 rads/sec. The effect is especially important considering the inherently low transistor response (0.4 volt maximum). No analysis based on these effects is available at this time. However, the contribution due to the passive components would be expected to be on the order of hundreds of millivolts superimposed on the transistor response at the maximum dose rate experienced in the field test.

3.9.4 Discussion of Field Test and Pre/Postshot Experimentation. The oscilloscope recordings from the diagnostic station are shown in Figures 3.2, 3.4, 3.7, and 3.8, corresponding to Channels 3, 11, 20, and 26. The only channel which appears to hold any significance is Channel 11. Although the peak amplitude of the transient signal on Channel 11 is not discernible, the duration of the transient pulse appears to be less than 1 μsec. This will be discussed, and is significant because it provides insight into the real time history of the transient in the azimuth network.

The positive and negative response characteristics of the azimuth network at the four blooper stations are shown in Figures 3.31

and 3.32. At Pad A (2,800-feet), two blown fuses were recorded; one indicating a negative 0.6-v pulse and the other a positive 0.3-v pulse. As stated previously, the failure criterion for the azimuth is a
Establishment of voltage amplitude criterion at
and the failure to meet the pulse width criterion, may be determined by referring from the azimuth network of the diagnostic station back to the transient disturbance. It is true that the dose at the 2,800-foot station was approximately two orders of magnitude greater than that of the 5,700-foot station while the azimuth network is dose dependent. However, experiments conducted at Linac (dose 1000r) show that the maximum transient pulse duration from the azimuth network is on the order of microseconds. With these facts, the azimuth network can be considered insensitive to a peak weapon gamma pulse of

Experiments conducted by other investigators with flash X-ray and Linac verify the Northrop conclusion (References 11 and 16).

3.9.5 Conclusions of the Small Boy TREE Working Group Meeting. It was officially concluded at the 7 and 8 November meeting of the Small Boy TREE Working Group that the azimuth network is hard to at least

3.10 ARMA MINIATURE FLIP-FLOP

3.10.1 Introduction. The ARMA flip-flop serves as a storage element for one bit of digital information in a computer system. Two output terminals are available and are used to represent the information stored at one output, and the complement or opposite of the state at the other output. In other words, if the flip-flop is set in the "true" state the output at Terminal A will be at a voltage that corresponds to a logic "true" level, and the voltage at Terminal B will correspond to a logic "false" level. If the flip-flop is set in the "false" state the levels at A and B will correspond to logic "false" and "true" respectively. The definition of true and false as well as the corresponding voltage levels is completely arbitrary and need only be consistent within the total system. The state of the flip-flop is manipulated by applying positive pulses to the trigger input terminals. The failure criterion (Reference 17) for the flip-flop is shown in Figure 3.33.

3.10.2 Circuit Operation. A few definitions will make the discussion of circuit operation considerably easier. Figure 3.34 shows the circuit diagram of the flip-flop connections and additional components used in the field test. The flip-flop state in which Q_1 is on and Q_2 is off will be defined as the "one" state and the complementary state (Q_2 on and Q_1 off) will therefore be the "zero" state. It was assumed that the collector voltage of the off transistor would provide the maximum transient output and

therefore was the node to be monitored in the field test. The turn-on sequence in the test circuit programmer assured that the flip-flop would be set in the "one" state and thus would satisfy this condition. The node voltages and currents for the flip-flop in the "one" state are shown in Figure 3.35.

With the flip-flop in the "one" state, a positive pulse applied to the reset trigger input increases the base voltage of Q_2. Since Q_2 is biased close to the active region, the increase in its base voltage results in an increase in collector current which is coupled as a negative signal to the base of Q_1. C_2 is a speedup capacitor to enable the rapid coupling of the collector voltage changes to the base of Q_1. The quiescent base current of Q_1 is much larger than that required to saturate the transistor. Since Q_1 is saturated, the excess base charge must be removed before the collector voltage will start to rise. Once the collector current of Q_1 starts to decrease, the positive signal will be coupled to the base of Q_2. The process then becomes regenerative and stops only when Q_2 is saturated. If the flip-flop is in the "zero" state and a positive trigger pulse is applied to the set input, the same process will take place, resulting in the flip-flop switching to the "one" state. A trigger pulse applied to the base of a transistor already on (i.e., set input with the flip-flop in the "one" state) will only saturate the transistor a little harder temporarily and will not result in a change of state.

3.10.3 Radiation Analysis. The primary radiation-induced effect on the flip-flop is due to the transistor photocurrents. With the circuit in the "one" state (i.e., Q_1 on , Q_2 off) the effect of Q_2 is much greater than that of Q_1. The collector photocurrent induced in Q_2 will not only appear directly as a transient output, but may cause the flip-flop to change states. A change of state will result only if Q_1 can be pulled out of saturation. If the common emitter current gain of Q_1 is at least 50, less than 100 μa base current is required to keep Q_1 saturated. To drop the base current to this level requires a drop in the collector voltage of Q_2 approximately 2.5 volts, or an increase in collector current of 2.7 ma. Since Q_2 is initially biased close to the active region, the initial photocurrent will cause forward-biasing of the emitter junction such that the peak transient collector current may be several times larger than the initial photocurrent. A hypothetical current distribution in the flip-flop at the verge of transition is shown in Figure 3.35. Before the circuit will become regenerative, however, the excess stored charge in the base of Q_1, due to saturation, must be removed. This requirement establishes a minimum pulse width for transition to occur as well as the amplitude requirement previously established.

Very little is known about radiation effects on an initially saturated transistor. However, it would appear, since only the

magnitude and not the polarity of the emitter and collector junction barrier potentials have been affected, that photocurrents exist and would tend to increase the excess minority carrier concentration in the base. In this case, the amount of charge to be removed from the base of Q_1 is increased, making the requirement for a transition more stringent.

At radiation levels of less than 10^9 r/sec, the contribution of the other components should be small compared to the transistor effects. Photocurrents from the trigger diodes will be in the direction to turn both Q_1 and Q_2 off, but the effect is negligible since the transistor output from the collector will basically determine whether a transition will occur or not.

3.10.4 Discussion of Field Test and Pre/Postshot Experimentation. As shown in Figures 3.3, 3.6, and 3.8 (Channels 8, 18, and 24), no change in state occurred in the flip-flop at the diagnostic station location (5700 feet) at a peak dose rate of The signal on Channel 24 is due to system noise.

Data from the blooper stations are shown in Figure 3.36. Transient signals at the stations corresponding to showed that the levels were below the thresholds for damage or system error (Figure 3.33). The two data points at C and D (Figure 3.36) which indicate the transient signal exceeded respectively are not considered representative of a change in state for the flip-flop for the following reasons: (1) At dose rates as high as during pretest experimentation a change in state was never observed; (2) Stability of the flip-flop has been found to be vulnerable to system noise.

The field test results are consistent with both pre-and postshot laboratory simulation testing. No change in state of the flip-flop occurred which could be attributable to radiation at dose rates as high as during pre-and post-field experimentation. Therefore, the flip-flop should operate without introducing system errors at peak dose rates of at least from a weapon gamma pulse.

3.10.5 Conclusions of the Small Boy TREE Working Group Meeting. It was officially concluded at the 7 and 8 November meeting of the Small Boy TREE Working Group (Ballistic Systems Division, Air Force Systems Command. Los Angeles, California) that the flip-flop is hard somewhat beyond

TABLE 3.1 FIELD TEST SPECIMEN LOCATIONS

PAD	BLOOPER S/N	TEST CIRCUIT CARDS/N
A1	7	14
A2	9	3
A3	8	16
B1	6	22
B2	12	4
B3	4	20
B4	Rem Rand	Not Applicable
C1	15A	10
C2	Little Feller II	Not Applicable
C3	11	2
Bunker 1	1 Diagnostic	7
Bunker 2	2 Diagnostic	19
Bunker 3	Dosimetry	Not Applicable
Bunker 4	4 Diagnostic	6
Bunker 5	5 Diagnostic	1
D1	15B	13
D2	14	11
D3	Little Feller II	Not Applicable

TABLE 3.2 GENERAL SHOT DATA, SHOT SMALL BOY

Device	
Yield	
Date	14 July 1962
Time of detonation	11:30 00.123 PDT
Burst Medium	Air
Actual Height of Burst	10 feet
Placement	Wooden Tower
Nevada State Coordinates	N 747,907.43
	E 717,118.39
Surface Zero	Ground
Air Pressure at Surface GZ(Hg)	26.67
Air Pressure at Surface GZ(Mb)	904
Air Temperature (^{o}C)	31.7
Relative Humidity (%)	16
Dew point (^{o}C)	2.8
Surface wind direction/Velocity$_{o}$/Mph	225/06

pages 100 through 105 deleted.

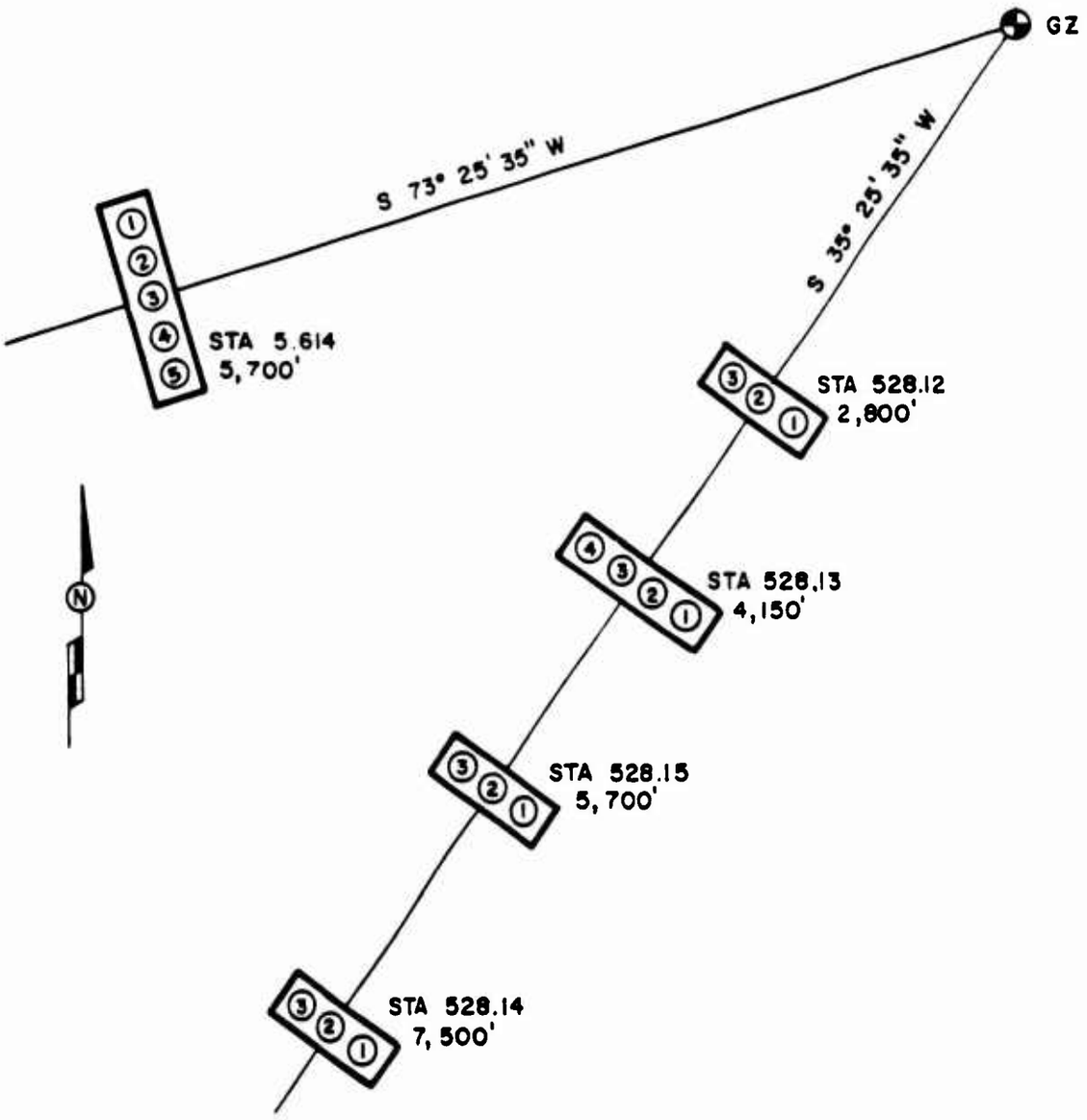

Figure 3.1 Diagnostic and blooper station positions from GZ.

 pages 107 through 116 deleted.

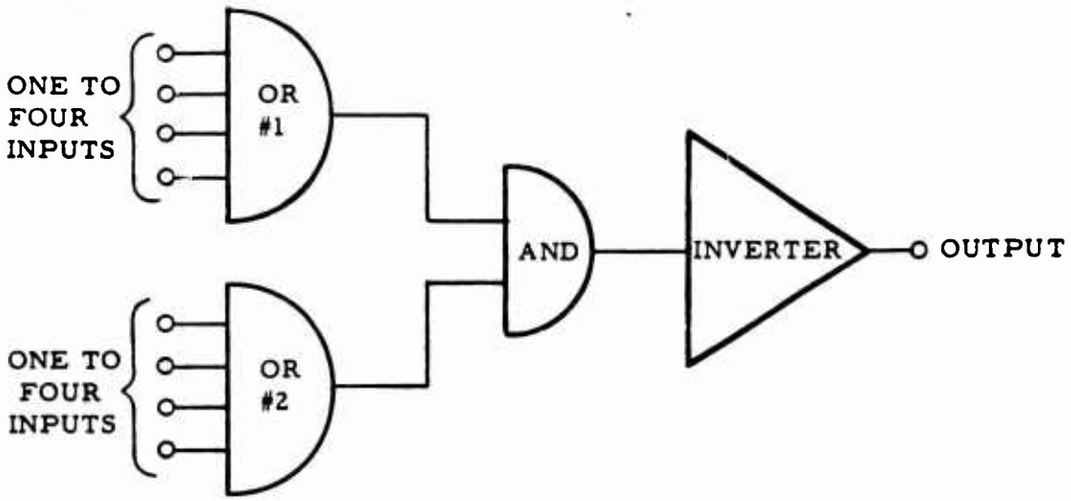

Figure 3.12 Block diagram, IBM logic network.

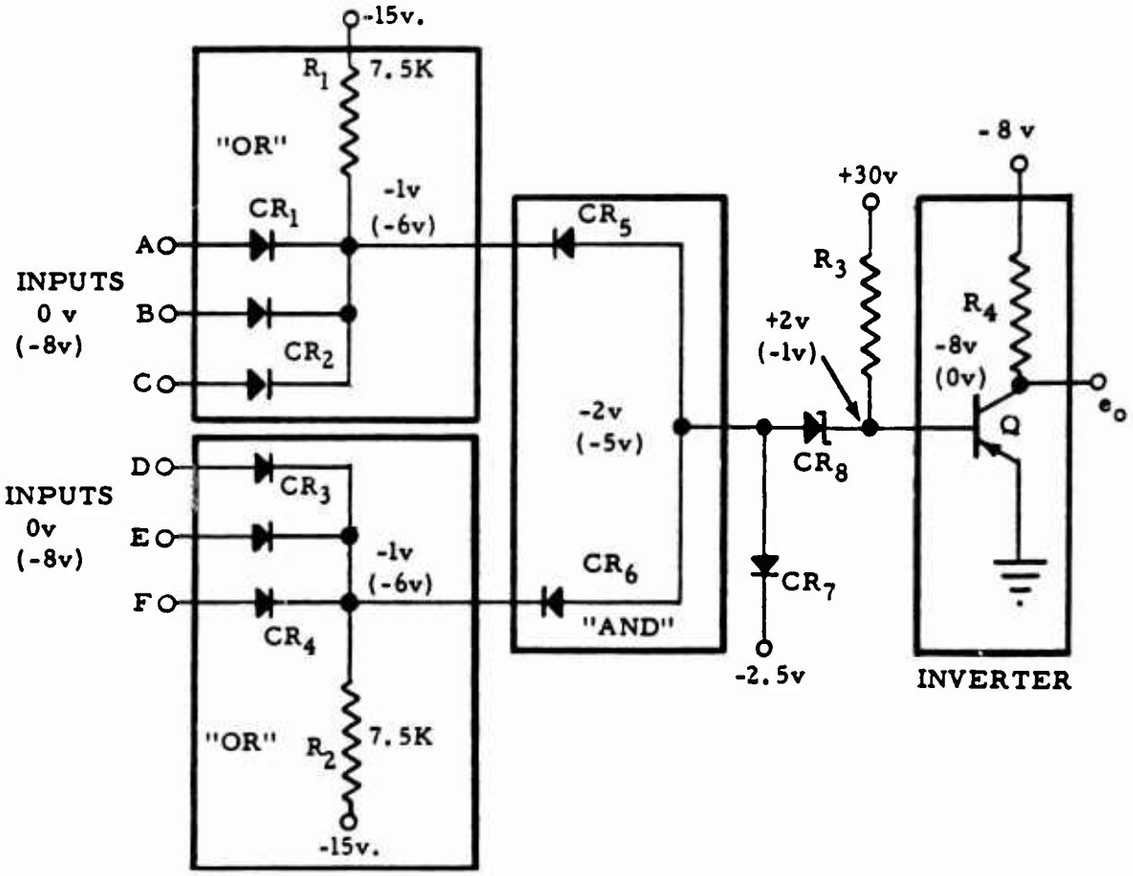

Figure 3.13 Schematic, logic network.

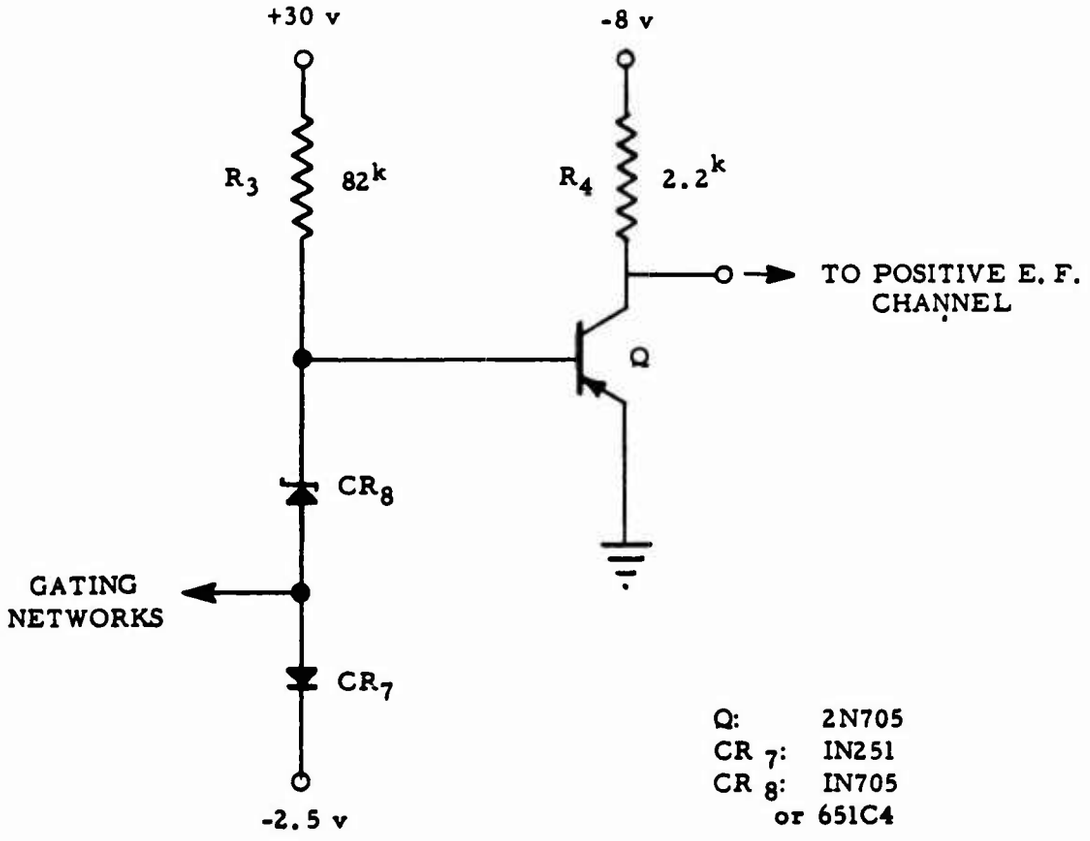

Figure 3.14 Simplified circuit diagram, logic network.

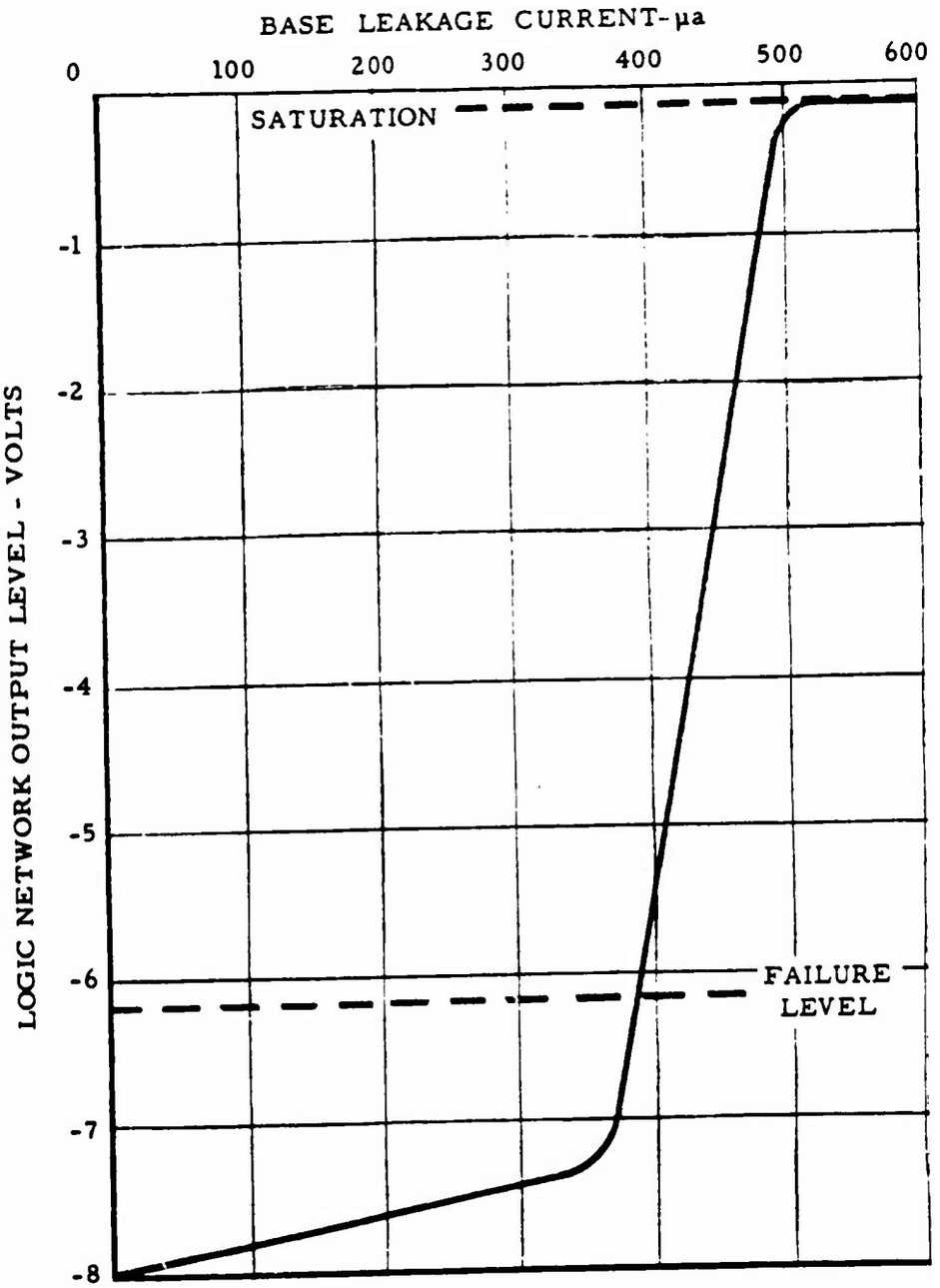

Figure 3.15 Output voltage versus base leakage current, logic network.

pages 120 through
122 deleted.

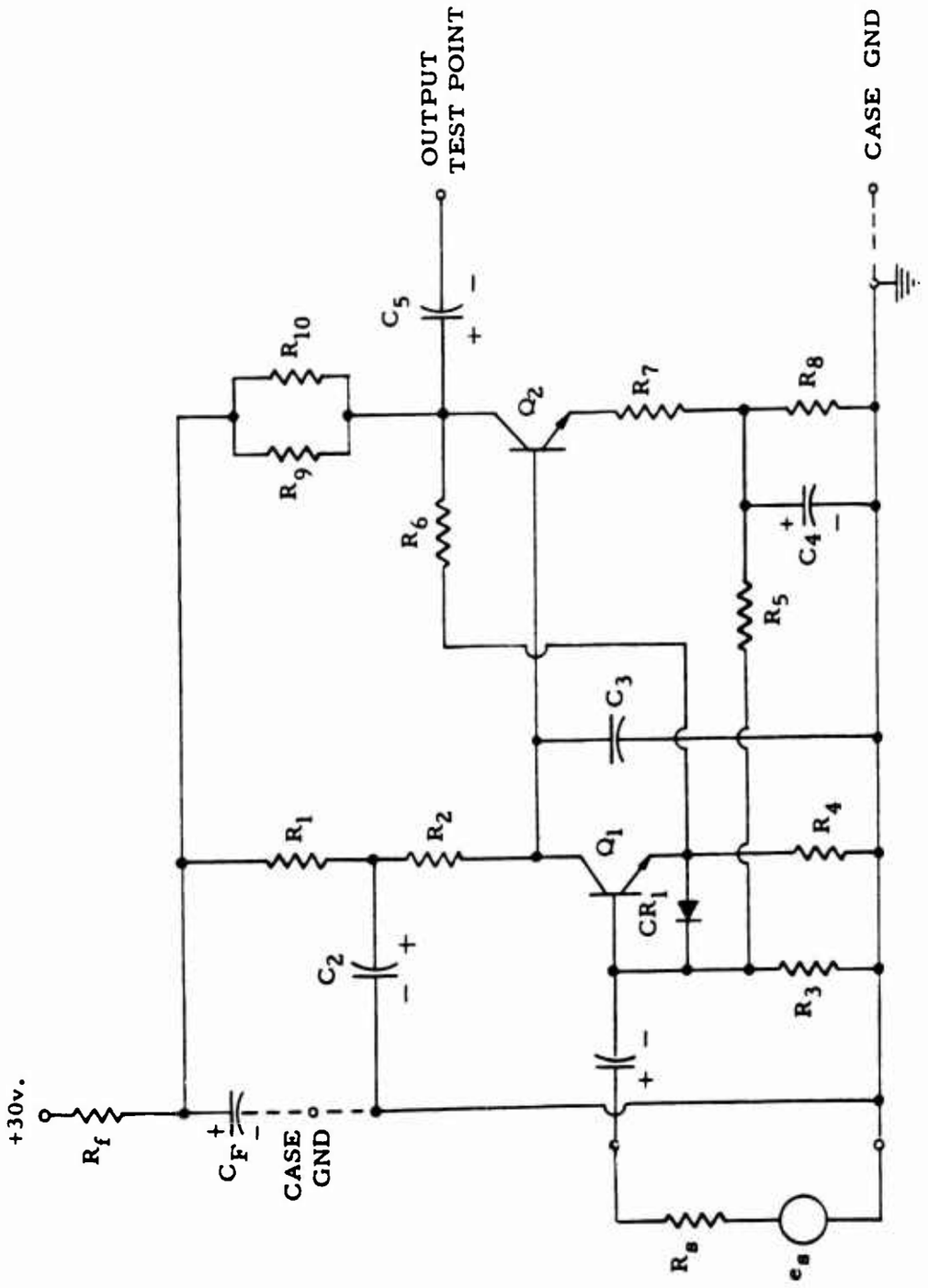

Figure 3.19 Schematic, pre-preamplifier.

pages 124 through 129 deleted.

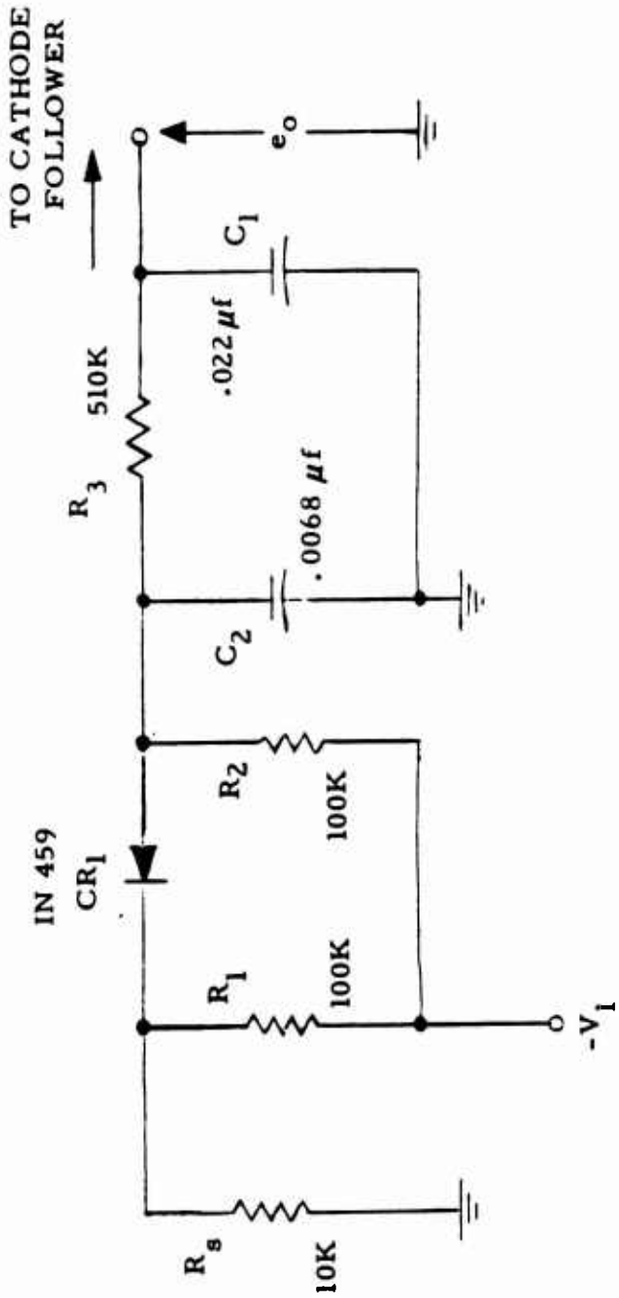

Figure 3.26 Schematic, diode detector.

pages 131 through 132 deleted

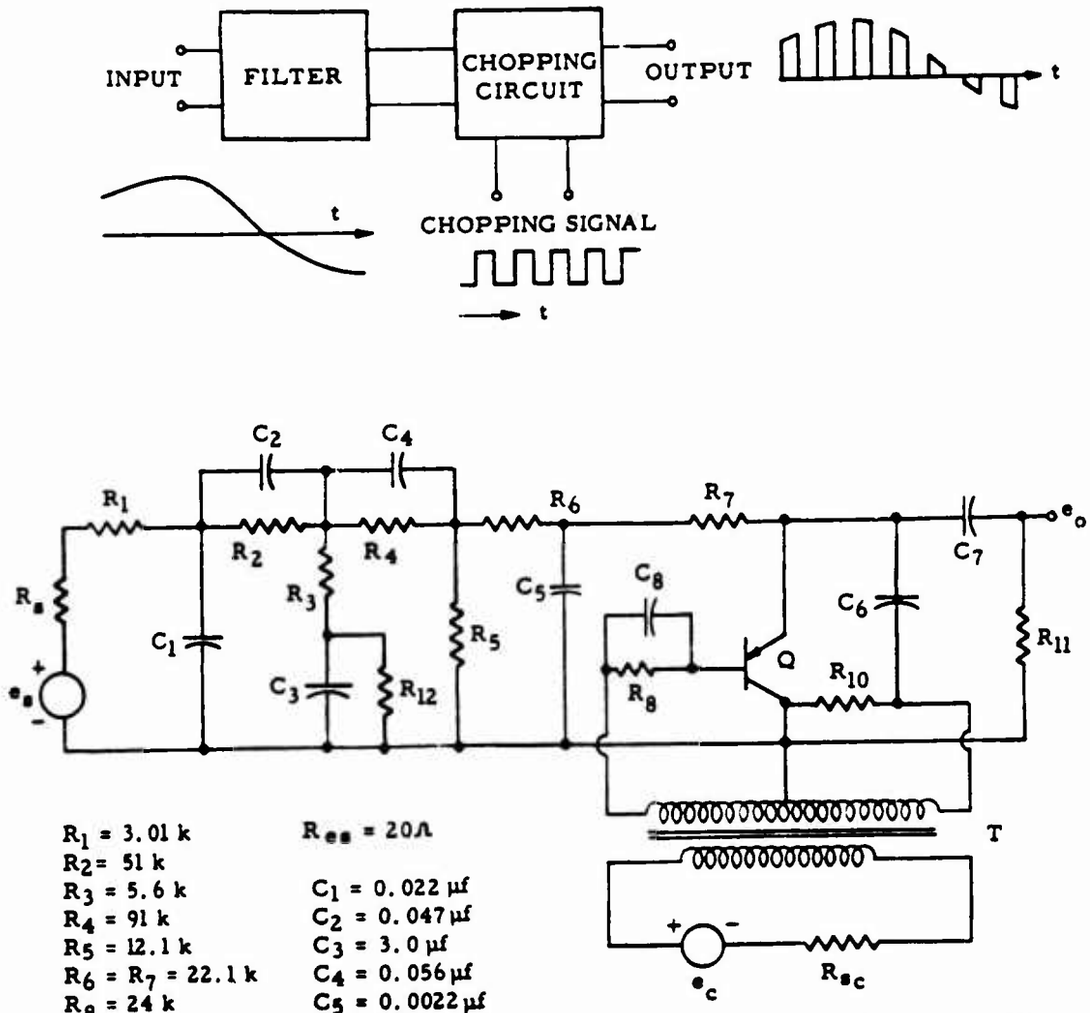

R_1 = 3.01 k
R_2 = 51 k
R_3 = 5.6 k
R_4 = 91 k
R_5 = 12.1 k
$R_6 = R_7$ = 22.1 k
R_8 = 24 k
R_9 = 560
R_{10} = 300
R_{11} = 56 k
R_{12} = 150 k
R_s not specified

R_{ss} = 20Λ

C_1 = 0.022 μf
C_2 = 0.047 μf
C_3 = 3.0 μf
C_4 = 0.056 μf
C_5 = 0.0022 μf
C_6 = 10 pf
C_7 = 1000 pf
C_8 not specified (selected for each circuit)

T: 1 : 1 Transformer (c.t. secondary) assumed
Q: Philco T2357

NOTE: e_s and R_s replaced by 30 v. battery in field test

Figure 3.29 Azimuth network.

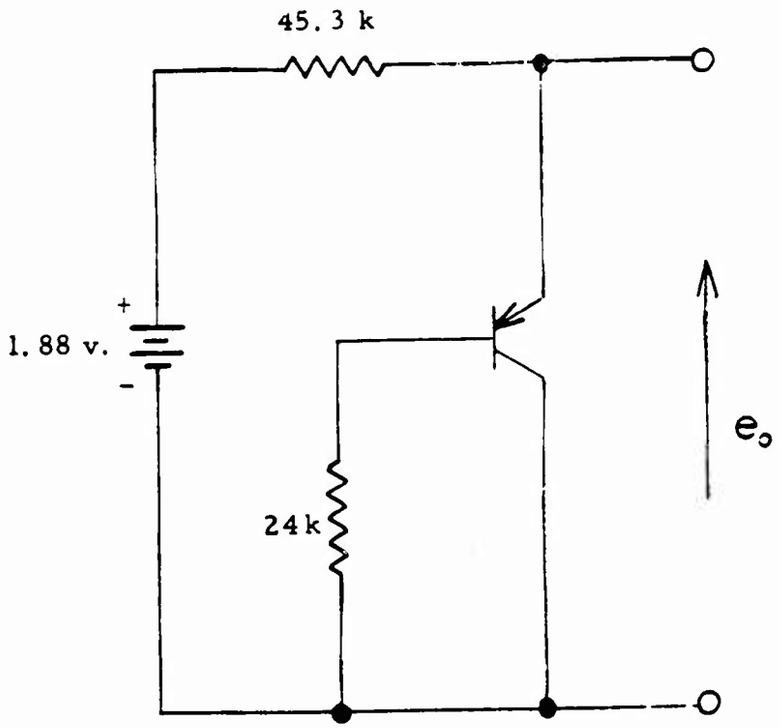

Figure 3.30 Equivalent circuit, azimuth network.

 pages 135 through 137 deleted.

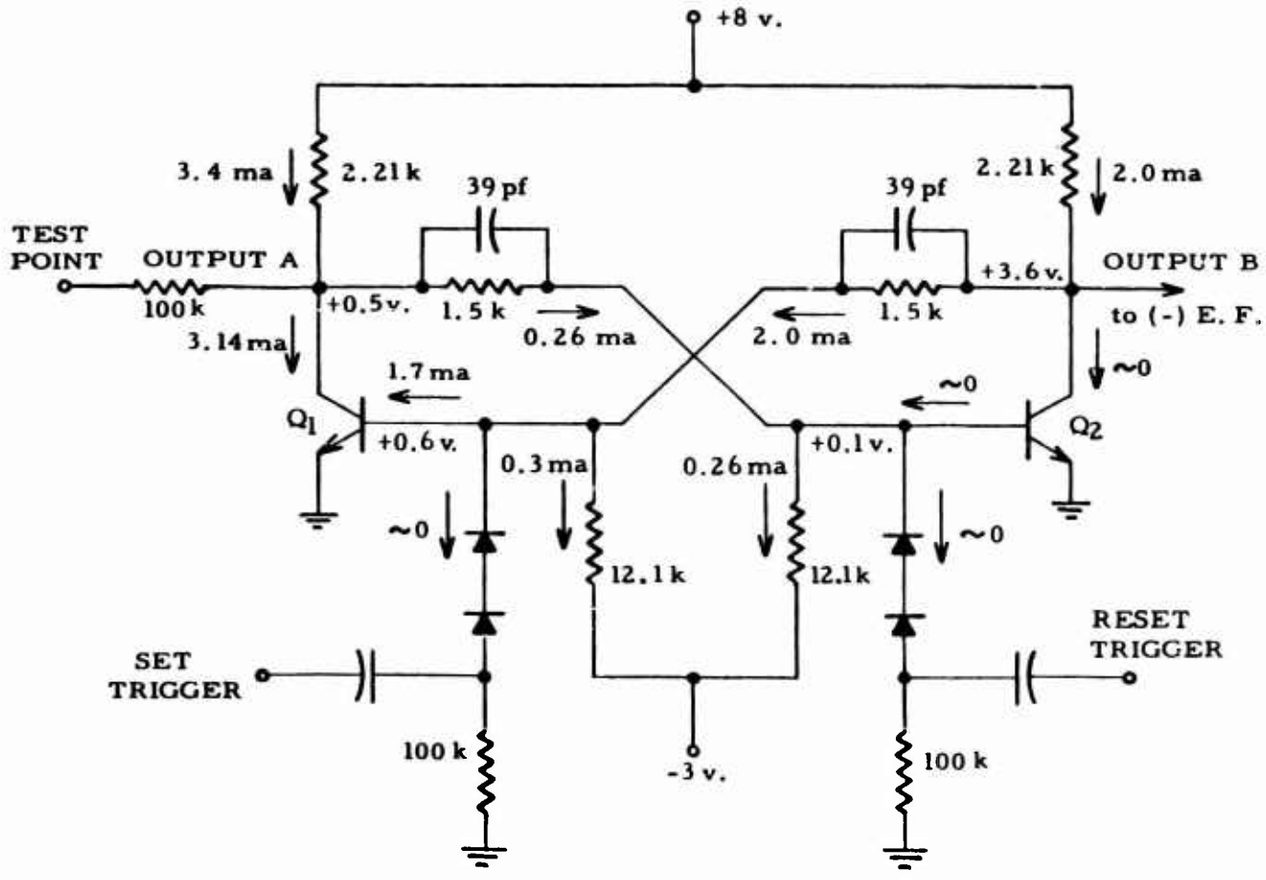

Figure 3.34 Schematic, flip-flop.

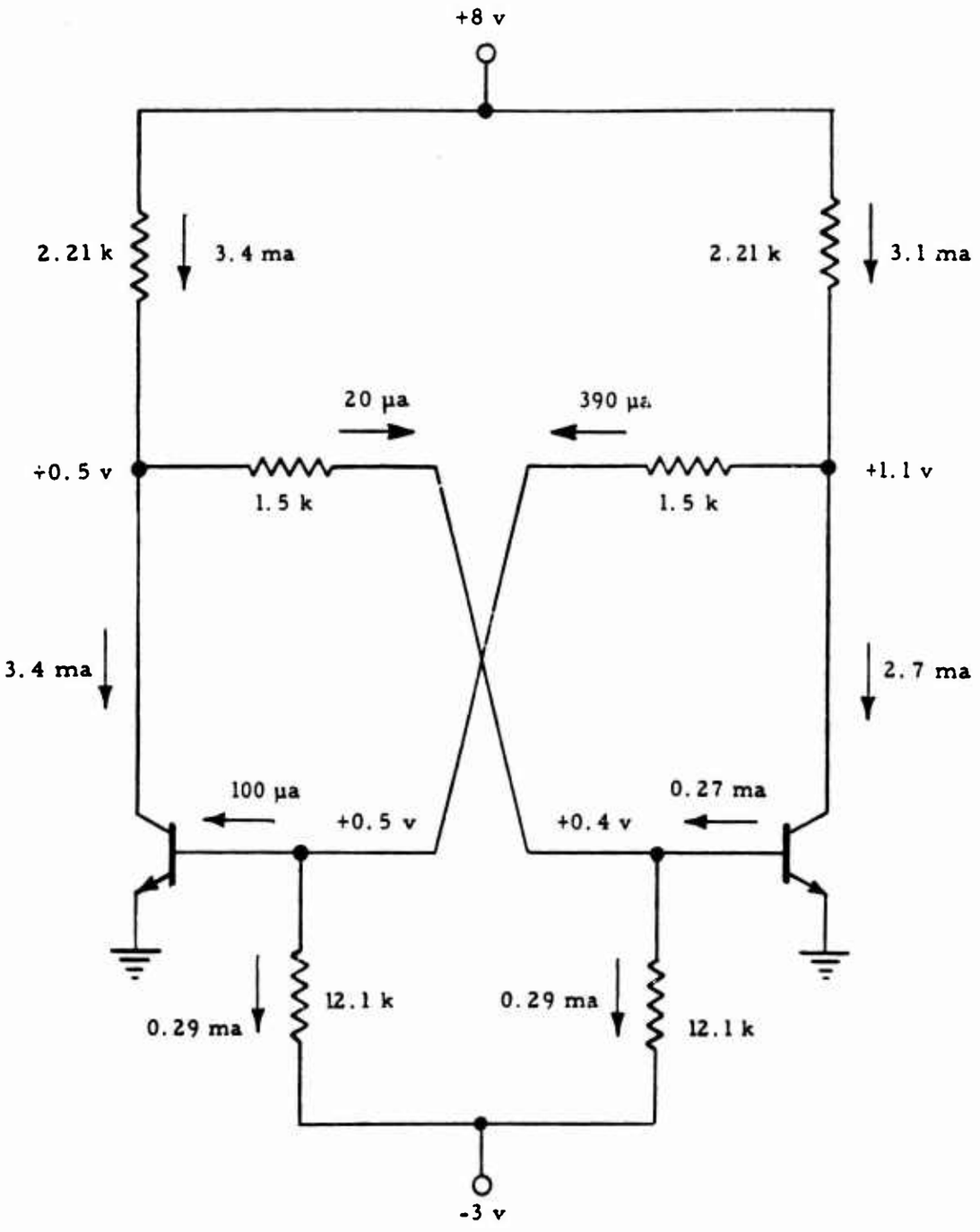

Figure 3.35 Node voltage and current distribution, flip-flop.

 page 140 deleted.

CHAPTER 4

CONCLUSIONS AND RECOMMENDATIONS

4.1 GENERAL

The results of this program prove that with extensive pre-field testing, and by using the instrumentation techniques developed by Northrop Ventura, valid data can be obtained successfully in the field. Correlation between simulation environments and actual weapon environments appears to be valid within state-of-the-art measurement techniques. Improvements in dosimetry and more accurate component models for the radiation environment should provide even better correlation.

4.2 RADIATION VULNERABILITY LEVEL FOR EACH CIRCUIT AND METHOD FOR HARDENING

4.2.1 Logic Circuit. The failure criterion for the logic circuit (1.8-v signal) was exceeded at approximately At higher dose rates, saturation occurs, which would thereby increase the computer "down time." The field test results are in good agreement with laboratory simulation testing and preliminary circuit analysis.

By increasing the compensation current, or by changing to a transistor with a higher collector to base breakdown voltage, the logic network can probably be hardened to without sacrificing circuit performance.

4.2.2 Pre-Preamplifier. The pre-preamplifier is hard to at least Increased radiation hardness could be obtained by matching the diode photocurrent to the transistor photocurrent; however, this may not be effective at higher dose rates. The field test results on the pre-preamplifier are consistent with analytical predictions and experimental data.

4.2.3 Diode Detector. Although no failure criterion was established, the transient output at would cause a system disturbance. However, the system would probably have already failed due to more vulnerable elements. Additional hardening could be achieved by selecting less vulnerable output capacitors.

4.2.4 Azimuth Network. The failure criterion of the azimuth network was not met at a peak weapon gamma dose rate of Laboratory experimentation has proved that the failure criterion was not exceeded at The transistor is the most vulnerable component to consider if additional

hardening is required.

4.2.5 Flip-Flop. The failure criterion for the flip-flop (change-of-state) was not exceeded at No transition attributable to gamma radiation has been observed in the laboratory at dose rates of

4.2.6 Remington Rand Thin Film Memory Unit. No permanent damage or system failure is expected in this type of electronics as a result of peak gamma weapon pulse of

4.3 DOSIMETRY

The Northrop Ventura gamma dose rate measurement from the scintillation detectors compares favorably with the predictions of John Malik of LASL and with other measurements made in the field. Dose rates indicated (with the NV scintillation detector) to be higher than those predicted (after the prompt gamma spike) are largely attributable to fluor hang-up. Investigations on the fluor hang-up are currently being performed. Neutron and gamma dose measurements conducted by other groups in the field are in good agreement with Northrop Ventura.

4.4 DIAGNOSTIC VERSUS BLOOPER TYPE INSTRUMENTATION

Although both types of instrumentation proved to be successful during the field test, most data were obtained from the blooper packages. However, this is attributable mainly to the fact that the dose rate at the diagnostic station was near the threshold level for most circuits involved. Probably the most distinct advantage derived from diagnostic type measurements is that both the amplitude and time history characteristics of the test specimens are obtained. State-of-the-art blooper techniques at the time of the Small Boy event provided only amplitude type readout; however, both amplitude and time readout techniques now appear to be feasible.

In order to make a selection between the two recording techniques, the purpose of the particular experiment must be examined. If failure criteria, in terms of amplitude and time, can be established for the particular test specimen, and if the sole requirement is to know if these criteria were exceeded, then blooper readout techniques are more practical. If, however, exact characterization of the time and amplitude response of a test specimen is a prime requirement, and the number and/or complexity of blooper readout circuits required to bracket these requirements becomes prohibitive, then the diagnostic or analog type recording is more feasible.

It would appear however, that if analog techniques are to be

pursued in any future weapon test, small, self-contained multi-channel recording stations should be utilized, rather than one large permanent installation such as the diagnostic station. By utilizing self-contained packages, they could be placed at strategic locations corresponding to several radiation levels, and of more significance, the package could be recovered and used for experiments in different areas.

4.5 RECOMMENDATIONS

It has been shown that reasonable correlation can be attained between weapon results and laboratory results. Therefore, as more fundamental information on circuit behavior is obtained, it can be applied directly to the circuit behavior in a weapon environment.

Based on data obtained on the vulnerability of the logic circuit, it appears probable that transient radiation effects on additional circuits in the Titan digital computer could introduce system errors, e.g., in timing circuits and in low-level amplifiers.

Future tests should be directed toward engendering and substantiating present correlation factors for the weapon environment and simulation environments.

A more realistic estimate of the vulnerability of the Arma flip-flop in a radiation environment would be obtained from an evaluation in a subsystem employing this circuit.

APPENDIX

PRE-FIELD TEST EXPERIMENTATION

A.1 SCOPE OF LABORATORY TESTING

Extensive laboratory testing was conducted at the Northrop Ventura 600-kJ Flash X-ray facility, the General Atomic Linear Accelerator and the Sandia Pulsed Reactor Facility. The objectives of these experiments were:

(1) To determine the threshold of radiation response of the associated test circuitry incorporated in the blooper and diagnostic packages.

(2) To determine the expected responses of the circuit test specimens in the nuclear field environment, and thereby establish required dynamic ranges for diagnostic and blooper instrumentation.

(3) To determine the ability of the above simulation facilities to provide TREE response results by comparison with actual weapon pulse radiation field test data.

(4) To determine the influence of weapon neutrons on the transient response of the test circuits.

(5) To determine whether the test sample circuits were sensitive to gamma dose, dose rate, or both at gamma dose rate levels characteristic of a nuclear detonation.

Three Linac experiments, one SPRF experiment, and several Flash X-ray experiments were performed. Efforts were concentrated on minimizing extraneous cable and air ionization effects from both the test circuits and associated monitoring equipment. Characteristic input and output terminations were connected and cathode or emitter followers were utilized in some cases. The radiation tolerance levels for the associated blooper circuitry were determined, to ascertain the shielding requirements.

It should be reiterated that the primary purpose of these experiments was to obtain qualitative data on the response of the test specimens so that voltage levels for the blooper packages and diagnostic station could be set. Although the data spread was large for some circuits, it did provide the basis for predicting the test circuit response in the field with reasonable confidence. Wide variations in the response of the individual test circuits of the same type (due to actual differences in "identical" components) accounted for some of the spread in data points.

A.2 EXPERIMENTAL FACILITIES

A.2.1 Linac Experiments.

Linac experiments were performed to determine the test-sample circuit response at dose rates between The high dose rates were achieved by direct exposure to pulses of 27-Mev electrons. Lower dose rate measurements were made with 6-Mev X-rays. Pulse widths for all experiments were between

The dose rates were generally calculated from the calorimeter data provided by General Atomic. During the second Linac experiment (6.0-Mev X-rays) the dose rate calculated from the calorimeter temperature rise was an order of magnitude higher than calculated from an NV photodiode A subsequent experiment was performed under essentially identical conditions to resolve this discrepancy. The dose rate measured with the photodiode was consistent with the previous experiment within experimental uncertainties. The calorimeter (copper block and thermistor) measurements in this subsequent experiment indicated approximately an order of magnitude lower dose rate than for the previous experiment, and thus agreed with the photodiode results.

The specific test specimens and experimental conditions for the three Linac tests were:

Linac 1a. Irradiation (28-Mev electrons) of mercury cells, cathode followers, emitter followers, and the pre-preamplifier at dose rates from

Linac 1b. Irradiation (6-Mev X-rays) of cathode followers, emitter followers, and pre-preamplifier at dose rates from

Linac 2. Irradiation (6-Mev X-rays) of the azimuth network, pre-preamplifier, diode detector, and flip-flop at peak dose rates of

Linac 3. Irradiation (28-Mev electrons) of cables, logic network, azimuth network, pre-preamplifier, and diode detector at dose rates between

A.2.2 SPRF Experiments.

Experiments were performed at SPRF to determine the transient response of the test circuits in a mixed neutron and gamma envi-

ronment. Variations in the neutron-to-gamma ratio (lead and paraffin shielding) were used in an attempt to differentiate between the relative transient effects due to the neutron and gamma components. Qualitative data were obtained on most of the test circuits evaluated.

An experiment was performed to determine the relative sensitivity of the NV scintillation detector to neutrons and gamma radiation. Although the fast-neutron sensitivity was found to be important, the detector could be used for the field test measurements at 5700 feet because of the 25 μsec neutron time of flight. The scintillation detector was also used to monitor the shape of the SPRF radiation pulse.

Four significant phenomena were observed during the SPRF experiment: (1) the positive and negative response of the pre-preamplifier was observed for the first time; (2) the transient response of some test circuits was found to decrease with increased neutron dose; (3) dose dependence of the azimuth network and the diode detector responses was confirmed; (4) transient signals induced in the cables changed polarity by varying the neutron-to-gamma ratio.

A.2.3 Flash X-Ray Experiments.

Several experiments were performed on the test circuits, cables, and blooper packages at the NV flash X-ray. The maximum dose rate was Dose rate measurements were made with the NV photo-diode.

A.3 EXPERIMENTAL RESULTS

A.4 CONCLUSIONS

The results of the pre-field test experimentation show that even within the short time frame involved, qualitative data were obtained. The validity of the data was verified during the field test as discussed under Chapter 3. Had additional time been available, more refined experiments could have been performed, thereby reducing the spread in data. However, most of the spread in data is probably attributable to dosimetry and to the normal experimental errors encountered during radiation testing.

 pages 148 through 157 deleted.

REFERENCES

1. R.W. Hillendahl; "Characteristics of the Thermal Radiation from Nuclear Detonations"; AFSWP 902, 30 June 1959; U.S. Naval Radiological Defense Laboratory, San Francisco, California; Secret Restricted Data.

2. James F. Moulton, Jr.; "Nuclear Weapons Blast Phenomena"; DASA-1200, March 1960; U.S. Naval Ordnance Laboratory, White Oak, Maryland; Secret Restricted Data.

3. Conclusions and Recommendations of the Ad Hoc Panel of EM Radiation. STL Report 6101-6055-GQ000, 28 December 1961; Space Technology Laboratories, Inc., Redondo Beach, California; Secret Restricted Data.

4. "Capabilities of Atomic Weapons"; Department of the Army Technical Manual TM 23-200, Department of the Navy OPNAV Instruction 03400.1B, Department of the Air Force AFL 136-1, Marine Corps Publications NAVMC 1104 Rev; Revised Edition, November 1957; Prepared by Armed Forces Special Weapons Project, Washington, D.C.; Confidential.

5. "Weapons Effects for Protective Designs—Ground Support System Weapon Effects"; RC Report P-1951, March 1960; The RAND Corporation, Santa Monica, California; Unclassified.

6. "Transient Radiation Effects Tests"; Final Report PX 2643, 1 January 1963; UNIVAC Division of Sperry Rand Corporation, 4th Ave. and 23d Street, New York; Secret Restricted Data.

7. "Final Report on Small Boy Project for Northrop Ventura"; IBM Report 62-521-9, 2 May 1962; IBM Corporation, New York; Unclassified.

8. Montgomery Phister; "Logical Design of Digital Computers"; 1958; McGraw-Hill Publishing Company, Inc., New York; Unclassified.

9. Personal Correspondence with R.S. Caldwell; The Boeing Co., Seattle, Washington.

10. Boeing Internal Report 2-5471-5-94 (revised), dated 17 October 1962; The Boeing Company, Seattle, Washington.

11. Hughes Aircraft Co. Report FR 63-17-32, "Transient Radiation Effects on Missile Electronic Circuits"; Hughes Aircraft Company, Fullerton, California.

12. P. Gianas, Kearfott Division, General Precision Equipment, Inc., 90 Gold Street, New York; Letter to: Capt K. Gilbert, Ballistic Systems Division, Air Force Systems Command, AF Unit P.O., Los Angeles 45, California; 29 May 1962.

13. Personal Communication with J.E. Bell, Hughes Aircraft Company, Fullerton, California.

14. Boeing Presentation at 7 and 8 November 1962 Small Boy TREE Working Group Meeting at Aerospace Corporation, El Segundo, California.

15. Personal Communication with H.W. Wicklein, The Boeing Company, Seattle, Washington.

16. Boeing Internal Report 2-5471-3-157 (Revised), dated 6 November 1962; The Boeing Company, Seattle, Washington.

17. Arma Division, American Bosch ARMA Corporation, Roosevelt Field, Garden City, Long Island, New York; Letter to: Northrop Ventura Division, Northrop Corporation, Newbury Park, California; BSCA 431-C4526, 5 June 1962.

159—160 page 161 deleted.